Dynamics of Three-Degree-of-Freedom Systems With Quadratic Nonlinearities

by

Tariq Ali Nayfeh

Thesis submitted to the Faculty of the

Virginia Polytechnic Institute and State University

in partial fulfillment of the requirements for the degree of

Master of Science

in

Engineering Mechanics

APPROVED:

Ali H. Nayfeh

Dr. A. H. Nayfeh, Co-chairperson

Dean T. Mook

Dr. D. T. Mook, Co-chairperson

L. Glenn Kraige

Dr. L. G. Kraige

May, 1991

Blacksburg, Virginia

Dynamics of Three-Degree-of-Freedom Systems With Quadratic Nonlinearities

by

Tariq Ali Nayfeh

Dr. A. H. Nayfeh, Co-chairperson

Dr. D. T. Mook, Co-chairperson

Engineering Science and Mechanics

(ABSTRACT)

The dynamics of two three-degree-of-freedom systems with quadratic nonlinearities are studied. The first system has two simultaneous two-to-one internal resonances. The second has a combination internal resonance. In both cases the response to a primary resonant excitation of the third mode is studied. The method of multiple time scales is used to obtain the equations that govern the amplitudes and phases of the first system. Then the fixed points of these equations are obtained and their stability is determined. The fixed points undergo Hopf bifurcations, and the overall system response can be periodic or periodically, quasiperiodically, or chaotically modulated. The method of the time-averaged Lagrangian is used to obtain the equations that govern the amplitudes and phases of the second system. The fixed points of these equations are obtained and their stability is determined. These fixed points undergo Hopf bifurcations, and the overall system response can be periodic or a two- or three-torus.

Acknowledgements

I wish to express my appreciation and gratitude to University Distinguished Professor Ali. H. Nayfeh for his support, guidance, and advice both as an advisor and a father throughout my career. Next, I would like to thank Professor Dean T. Mook whose valuable advice, guidance, and rich humor kept my spirits up.

I would also like to thank Professor L. Glenn Kraige who not only served on my Master's committee but served as my invaluable and knowledgeable undergraduate course advisor. I wish to express my thanks to all the professors who taught me at VPI & SU.

I thank Perng-Jin (Frank) Pai, Samir Nayfeh, Mahir Nayfeh, Marwan Bikdash, Kyoyul Oh, Balakumar Balachandran, Tony Anderson, and Jafar Hadian for their insightful discussions, forceful debates, and friendship. I would also like to thank Jamal Masad and Charn-ming Chin for their friendship. Finally, a special thanks goes to Sally Shrader; her patience and expert typing skills were of great help.

I wish to express my special deep gratitude to my mother Inam Nayfeh for her incredible patience. Her insistence on excellence helped me achieve all that I have. She patiently sat countless times at the dinner table while my father, my brothers, and I discussed nonlinear dynamics.

Thanks are due to the Army Research Office for supporting this research under Grant No. DAAL03-89-K-0180.

I dedicate this work to the memory of my grandfather Hasan Ahmad Nayfeh for his incredible foresight on the value of an education even under the most adverse conditions, and to my grandmother Khadrah Nayfeh who in spite of her illiteracy insisted that all of her four sons obtain the "highest degrees."

Table of Contents

Introduction 1

Simultaneous Two-to-One Internal Resonances 8

2.1 Introduction 9

2.2 Method of Solution: Multiple Scales 10

2.3 Periodic Motions 14

2.4 Stability of the Fixed Points 17

2.5 Numerical Results for Fixed-Point Solutions 21

2.6 Modulated Motions 46

2.6.1 Floquet Theory 47

2.6.2 Shooting Method 50

2.6.3 Limit Cycles of the Modulation Equations 53

2.6.4 Quasiperiodic solutions 59

2.7 Conclusions 84

Combination Internal Resonance 85

3.1 Introduction 86

3.2 The Time-Averaged-Lagrangian Method of Solution 86

3.3 Fixed-Point Solutions 90
3.3.1 Amplitude-Response Curves 97
3.3.2 Frequency-Response Curves 101
3.3.3 Experiments 106
3.3.3.1 Frequency-response curves 107
3.3.3.2 Amplitude-response curves 116
3.4 Limit-Cycle Solutions 118
3.5 Conclusions 118

Conclusions 125
4.1 Present Work 125
4.2 Recommendations for Future Work 127
4.3 Closing Remarks 127

References 129

Vita 133

CHAPTER 1

Introduction

The responses of nonlinear systems to harmonic excitations often exhibit complicated long-time behaviors (attractors) when their natural frequencies are commensurable [1,2]; that is, when the system has an internal or autoparametric resonance. For example, in 1863 Froude [3] observed that a ship whose pitch frequency is twice its roll frequency has undesirable seakeeping characteristics. The explanation cannot be found in the linearized equations governing the motion of the ship because the yaw, sway, and roll modes are not coupled with the pitch, heave, and surge modes.

Mettler and Weidenhammer [4], Sethna [5], and Haxton and Barr [6] used the method of averaging to analyze primary resonances of systems governed by equations with quadratic nonlinearities when one natural frequency is twice another. Nayfeh, Mook, and Marshall [7] used the method of multiple scales

[8,9] to analyze a simple system of two coupled oscillators with quadratic nonlinearities as a model for the coupling of pitch and roll motions of ships. They investigated the primary resonances of both the first and the second mode. When $\omega_2 \approx 2\omega_1$ and $\Omega \approx \omega_2$, where Ω is the excitation frequency, and the ω_i are the linear natural frequencies, they found a saturation phenomenon. Moreover, when $\omega_2 \approx 2\omega_1$ and $\Omega \approx \omega_1$, they showed that there are conditions for which stable periodic steady-state motions do not exist. Instead, there exist amplitude- and phase-modulated motions in which the energy is continuously exchanged between the two modes.

Later, Yamamoto and co-workers [10,11] used the method of harmonic balance and analog-computer simulations to investigate the forced responses of systems with quadratic and cubic nonlinearities to harmonic excitations when one frequency is twice another. They observed amplitude- and phase-modulated steady-state motions in their analog-computer simulations when $\Omega \approx \omega_2$ and $\Omega \approx \omega_1$. Nayfeh and Mook [12] used the method of multiple scales to analyze the response of a beam to a harmonic excitation. They accounted for the interaction of lateral and longitudinal vibrations. Hatwal, Mallik, and Ghosh [13] reported analytical and numerical results for the response of two internally resonant coupled oscillators to a harmonic excitation when the excitation frequency Ω is near ω_2. Their results for small amplitudes are equivalent to those of Sethna [5] and Nayfeh, Mook, and Marshall [7]. However, their numerical results for sufficiently large amplitudes show that periodic responses are unstable and give way to periodically modulated motions. Miles [14] used the method of averaging to investigate

the responses of two internally resonant, quadratically coupled oscillators to harmonic excitations. He examined the stability of the analytical solutions and investigated the possible bifurcations. He presented numerical results that demonstrate chaotically and periodically modulated motions when the excitation frequency Ω is near the lower frequency ω_1. Nayfeh and Raouf [15,16] used the method of multiple scales to investigate the response of a circular cylindrical shell to a harmonic internal pressure when the natural frequency ω_2 of the breathing mode is twice the natural frequency ω_1 of a flexural mode. They also found the saturation phenomenon when $\Omega \approx \omega_2$ and presented numerical results that demonstrate chaotically and periodically modulated motions. Nayfeh [17] used the method of multiple scales to analyze the pitching and rolling motion of a ship subject to a primary-resonant excitation. He found conditions for the existence of Hopf bifurcations (periodic motions lose their stability when a complex conjugate pair of eigenvalues crosses the imaginary axis with nonzero speed) when $\omega_2 \approx 2\omega_1$ and $\Omega \approx \omega_2$.

Hatwal, Mallik, and Ghosh [18] reported experimental data and numerical results that demonstrate chaotic motions. Haddow, Barr, and Mook [19] conducted an experiment using a two-degree-of-freedom model consisting of two light-weight beams and two concentrated masses and observed the saturation phenomenon when $\Omega \approx \omega_2$ and the nonexistence of periodic steady-state motions when $\Omega \approx \omega_1$. Using a model similar to that of Haddow, Barr, and Mook [19], Nayfeh and Zavodney [20] observed amplitude- and phase-modulated motions when $\Omega \approx \omega_1$. Nayfeh et al. [21], Nayfeh and Balachandran [22], Balachandran and Nayfeh [23,24] performed experimental

studies on metallic and composite structures with quadratic nonlinearities and a two-to-one internal resonance. They observed periodically and chaotically modulated motions when $\Omega \approx \omega_2$.

Mook, Marshall, and Nayfeh [25] analyzed the cases of subharmonic and superharmonic resonances in the pitch and roll motions of ships. Mook and co-workers [26,27] used the method of multiple scales to investigate the influence of a two-to-one internal resonance on the response of a system with quadratic nonlinearities to a combination resonance (i.e., $\Omega \approx \omega_2 + \omega_1$) and a subharmonic resonance of the higher mode (i.e., $\Omega \approx 2\omega_2$). They applied the results to an arch and found that the internal resonance significantly reduces the response. Balachandran and Nayfeh [28] experimentally investigated subharmonic and combination resonant excitations of internally resonant metallic and composite structures.

All of the previously mentioned works dealt with a single internal resonance of the two-to-one type. Nayfeh and Mook [29] investigated the response of a three-degree-of-freedom system with the combination internal resonance $\omega_3 \approx \omega_2 + \omega_1$. They demonstrated the existence of the saturation phenomenon when the higher mode is excited by a primary resonance; that is, $\Omega \approx \omega_3$.

Ibrahim and Barr [30] investigated the response of a fluid-filled circular container resting on a vibrating structure with an autoparametric coupling involving the first antisymmetric liquid sloshing mode and two orthogonal structural modes. Ibrahim, Woodall, and Heo [31] investigated the response of a three-degree-of freedom structure with the internal resonant condition

$\omega_i \approx |\omega_j \pm \omega_k|$. They found that the system achieves a "quasi-steady response" and exhibits an energy exchange between the directly excited mode and the two indirectly excited modes. Nayfeh, Nayfeh, and Mook [32] theoretically and experimentally investigated the primary resonant response of a structure exhibiting an autoparametric combination resonance of the additive type. They demonstrated the saturation phenomenon.

Sridhar, Mook, and Nayfeh [33] and Hadian and Nayfeh [34] studied the response of a circular plate with $\omega_1 + 2\omega_2 \approx \omega_3$ (essentially a three-degree-of-freedom problem). When $\Omega \approx \omega_3$, Hadian and Nayfeh [34] found that the equations describing the amplitudes and phases of the interacting modes posses periodic solutions that undergo a period-doubling sequence leading to chaos.

Bux and Roberts [35], Ashworth and Barr [36], and Cartmell and Roberts [37] investigated the response of a structure that consists of two beams and one mass. The first beam is a cantilever mounted in the horizontal direction and the second beam is vertically mounted at the end of the first but is rotated so that its transverse vibrations occur out of plane with respect to the horizontal beam (essentially a four-degree-of-freedom structure). They studied the effect of simultaneous combination and two-to-one internal resonances; that is, $\omega_2 \approx \omega_B + \omega_T$ and $\omega_1 \approx 2\omega_B$, where ω_1 is the frequency of the first in-plane bending mode of the first beam, ω_2 is the frequency of the second in-plane bending mode of the first beam, ω_B is the frequency of the out-of-plane bending of the second beam, and ω_T is the torsional frequency of the mass and the second beam. They found that the large-amplitude motion

of the directly excited mode can be absorbed by the modes that are excited through the internal resonance. Balachandran and Nayfeh [23,28] experimentally studied the response of a three-degree-of-freedom composite structure with two light-weight composite beams and two concentrated masses. The structure possesses the two internal resonances $\omega_2 \approx 3\omega_1$ and $\omega_2 \approx 2\omega_t$, where ω_1 and ω_2 are the frequencies of the first two bending modes and ω_t is the frequency of the first torsional mode. They found saturation, planar and nonplanar nonlinear periodic motions, and periodically modulated motions when the lower bending mode was excited by a primary resonance. They also found nonplanar, nonlinear periodic, periodically modulated, and chaotically modulated motions when the higher bending mode was excited by a primary resonance.

Ibrahim [38] considered the case when $\omega_3 \approx 2\omega_2$, $\omega_2 \approx 2\omega_1$, and $\Omega \approx \omega_3$ simultaneously. He used the method of multiple scales to determine the equations describing the amplitudes and phases of the interacting modes. He determined the fixed points and their stability.

Tadjbakhsh and Wang [39] investigated the response of wind-driven cables. They modeled the cable as a three-degree-of freedom system with quadratic nonlinearities with the internal resonant conditions $\omega_3 \approx 2\omega_2$ and $\omega_2 \approx 2\omega_1$. They considered the case when the second mode is excited (i.e., $\Omega \approx \omega_2$) and found that the system exhibits both the saturation and jump phenomena.

The objective of this work is to study the long-time behavior of two three-degree-of-freedom systems that possess quadratic nonlinearities in the

restoring and/or inertial force terms. In the case of the internal resonant conditions $\omega_3 \approx 2\omega_2$ and $\omega_2 \approx 2\omega_1$, our goal is to analytically study the behavior of the system. In the case of the internal resonant condition $\omega_3 \approx \omega_1 + \omega_2$, we wish to experimentally verify the fixed point solutions obtained by Nayfeh and Mook [29] and to analytically study long-time behavior of the systems.

To this end, in Chapter 2 the work of Ibrahim [38] is extended. The method of multiple time scales is used to obtain the equations that govern the amplitudes and phases. The fixed points of these equations exhibit Hopf bifurcations. Using various numerical simulations, we show that these equations possess complicated solutions, such as periodic, two-period quasiperiodic, and chaotic solutions. The phase-locking phenomenon is also demonstrated. In Chapter 3, the work of Nayfeh and Mook [29] and Nayfeh, Nayfeh, and Mook [33] is extended. The time-averaged-Lagrangian method is used to obtain the equations that govern the amplitudes and phases. Then we determine the fixed points of these equations and investigate their stability. The fixed points of these equations are shown to undergo Hopf bifurcations which lead to periodically modulated motions. We also perform experiments and find that the experimentally and theoretically obtained fixed points show good qualitative agreement. In Chapter 4 we present our conclusions.

CHAPTER 2

Simultaneous Two-to-One Internal Resonances

In this chapter the response of a three-degree-of-freedom structure with quadratic nonlinearities subject to harmonic forcing of its third mode is investigated. The method of multiple scales is used to obtain the equations that govern its amplitudes and phases. The fixed points of these equations are obtained and their stability is determined. The fixed points are found to undergo Hopf bifurcations and hence the response undergoes amplitude- and phase-modulated motions. Regions where the amplitudes and phases undergo periodic, quasiperiodic, and chaotic motions, regions where the overall system response is periodically, quasiperiodically, and chaotically modulated, are determined.

2.1 Introduction

An investigation into the response of a three-degree-of-freedom structure with quadratic nonlinearities to a primary excitation is conducted. The motion of the structure is governed by the three coupled second-order nonlinear ordinary differential equations

$$\ddot{u}_1 + \omega_1^2 u_1 + 2\varepsilon\mu_1\dot{u}_1 = \varepsilon\frac{\partial V}{\partial u_1} \tag{2.1}$$

$$\ddot{u}_2 + \omega_2^2 u_2 + 2\varepsilon\mu_2\dot{u}_2 = \varepsilon\frac{\partial V}{\partial u_2} \tag{2.2}$$

$$\ddot{u}_3 + \omega_3^2 u_3 + 2\varepsilon\mu_3\dot{u}_3 = \varepsilon\frac{\partial V}{\partial u_3} + \varepsilon f\cos\Omega t \tag{2.3}$$

where

$$\begin{aligned} V = {} & \alpha_1 u_1^3 + \alpha_2 u_1^2 u_2 + \alpha_3 u_1 u_2^2 + \alpha_4 u_1^2 u_3 + \alpha_5 u_1 u_3^2 + \alpha_6 u_2^3 \\ & + \alpha_7 u_2^2 u_3 + \alpha_8 u_2 u_3^2 + \alpha_9 u_3^3 + \alpha_{10} u_1 u_2 u_3 \end{aligned} \tag{2.4}$$

and the ω_n, α_n, f, Ω, and μ_n are constants, ε is a small dimensionless parameter, and the dots represent time derivatives. The case of simultaneous internal (autoparametric) resonances of the type $\omega_3 \approx 2\omega_2$ and $\omega_2 \approx 2\omega_1$ is considered.

2.2 Method of Solution: Multiple Scales

We seek a first-order uniform expansion of equations (2.1)-(2.4) in the form

$$u_n(t;\varepsilon) = u_{no}(T_0, T_1) + \varepsilon u_{n1}(T_0, T_1) + \ldots \tag{2.5a}$$

where $T_0 = t$ is a fast scale associated with changes occurring at the frequencies Ω and ω_n, and $T_1 = \varepsilon t$ is a slow scale associated with the modulations of the amplitudes and the phases due to the nonlinearities, damping, and resonances. The first- and second-order time derivatives transform as

$$\frac{d}{dt} = D_0 + \varepsilon D_1, \text{ and } \frac{d^2}{dt^2} = D_0^2 + 2\varepsilon D_0 D_1 + \ldots \tag{2.5b}$$

where $D_n = \partial/\partial T_n$. Substituting equations (2.5) into equations (2.1)-(2.4) and equating coefficients of like powers of ε, one obtains

Order ε^0 :

$$D_0^2 u_{10} + \omega_1^2 u_{10} = 0 \tag{2.6}$$

$$D_0^2 u_{20} + \omega_2^2 u_{20} = 0 \tag{2.7}$$

$$D_0^2 u_{30} + \omega_3^2 u_{30} = 0 \tag{2.8}$$

Order ε :

$$D_0^2 u_{11} + \omega_1^2 u_{11} = -2D_0 D_1 u_{10} - 2\mu_1 D_0 u_{10} + 3\alpha_1 u_{10}^2 + 2\alpha_2 u_{10} u_{20} + \alpha_3 u_{20}^2 + 2\alpha_4 u_{10} u_{30} + \alpha_5 u_{30}^2 + \alpha_{10} u_{20} u_{30} \tag{2.9}$$

$$D_0^2 u_{21} + \omega_2^2 u_{21} = -2D_0 D_1 u_{20} - 2\mu_2 D_0 u_{20} + \alpha_2 u_{10}^2 + 2\alpha_3 u_{10} u_{20} + 3\alpha_6 u_{20}^2 + 2\alpha_7 u_{20} u_{30} + \alpha_8 u_{30}^2 + \alpha_{10} u_{10} u_{30} \tag{2.10}$$

$$D_0^2 u_{31} + \omega_3^2 u_{31} = -2D_0 D_1 u_{30} - 2\mu_3 D_0 u_{30} + \alpha_4 u_{10}^2 + 2\alpha_5 u_{10} u_{30} + \alpha_7 u_{20}^2 + 2\alpha_8 u_{20} u_{30} + 3\alpha_9 u_{30}^2 + \alpha_{10} u_{10} u_{20} + f \cos \Omega T_0 \tag{2.11}$$

The general solutions of equations (2.6)-(2.8) can be expressed in the form

$$u_{no} = A_n(T_1) \exp(i\omega_n T_0) + cc \tag{2.12}$$

for n = 1, 2, and 3, where cc denotes the complex conjugate of the preceding terms, and the A_n are to be determined through the elimination of secular and small-divisor terms from the next-order equations. In this paper, we analyze the case $\omega_3 \approx 2\omega_2$, $\omega_2 \approx 2\omega_1$, and $\Omega \approx \omega_3$.

Substituting equations (2.12) into equations (2.9)-(2.11) and recalling the resonances being studied, we obtain

$$D_0^2 u_{11} + \omega_1^2 u_{11} = -2i\omega_1 (A_1' + \mu_1 A_1) e^{i\omega_1 T_0} + 2\alpha_2 A_2 \bar{A}_1 e^{i(\omega_2 - \omega_1) T_0} + cc + NST \tag{2.13}$$

$$D_0^2 u_{21} + \omega_2^2 u_{21} = -2i\omega_2 (A_2' + \mu_2 A_2) e^{i\omega_2 T_0} + \alpha_2 A_1^2 e^{2i\omega_1 T_0} + 2\alpha_7 A_3 \bar{A}_2 e^{i(\omega_3 - \omega_2) T_0} + cc + NST \tag{2.14}$$

$$D_0^2 u_{31} + \omega_3^2 u_{31} = -2i\omega_3(A_3' + \mu_3 A_3)e^{i\omega_3 T_0} + \alpha_7 A_2^2 e^{2i\omega_2 T_0} + f\cos\Omega T_0 + cc + NST \tag{2.15}$$

where the overbar indicates the complex conjugate, the prime indicates differentiation with respect to T_1, and NST stands for terms that do not produce secular or small-divisor terms. To describe quantitatively the nearness of the resonances, we introduce the detuning parameters σ, σ_2, and σ_3 according to

$$\omega_2 = 2\omega_1 + \varepsilon\sigma_2,\ \omega_3 = 2\omega_2 + \varepsilon\sigma_3,\ \Omega = \omega_3 + \varepsilon\sigma \tag{2.16}$$

Substituting equations (2.16) into equations (2.13)-(2.15) and eliminating the secular terms from u_{11}, u_{21}, and u_{31}, one obtains

$$-2i\omega_1(A_1' + \mu_1 A_1) + 2\alpha_2 A_2 \overline{A}_1 e^{i\sigma_2 T_1} = 0 \tag{2.17}$$

$$-2i\omega_2(A_2' + \mu_2 A_2) + \alpha_2 A_1^2 e^{-i\sigma_2 T_1} + 2\alpha_7 A_3 \overline{A}_2 e^{i\sigma_3 T_1} = 0 \tag{2.18}$$

$$-2i\omega_3(A_3' + \mu_3 A_3) + \alpha_7 A_2^2 e^{-i\sigma_3 T_1} + \frac{1}{2} f e^{i\sigma T_1} = 0 \tag{2.19}$$

Expressing the A_n in the polar form

$$A_1 = \frac{\sqrt{2\omega_1\omega_2}}{\alpha_2} a_1 e^{i\beta_1},\quad A_2 = \frac{\omega_1}{\alpha_2} a_2 e^{i\beta_2},\quad \text{and}\quad A_3 = \frac{\omega_2}{\alpha_7} a_3 e^{i\beta_3} \tag{2.20}$$

and separating equations (2.17)-(2.19) into real and imaginary parts yields the modulation equations

$$a_1' = -\mu_1 a_1 + a_1 a_2 \sin \gamma_1 \tag{2.21}$$

$$a_2' = -\mu_2 a_2 - a_1^2 \sin \gamma_1 + a_2 a_3 \sin \gamma_2 \tag{2.22}$$

$$a_3' = -\mu_3 a_3 - \Gamma a_2^2 \sin \gamma_2 + F \sin \gamma_3 \tag{2.23}$$

$$a_1 \beta_1' = -a_1 a_2 \cos \gamma_1 \tag{2.24}$$

$$a_2 \beta_2' = -a_1^2 \cos \gamma_1 - a_2 a_3 \cos \gamma_2 \tag{2.25}$$

$$a_3 \beta_3' = -\Gamma a_2^2 \cos \gamma_2 - F \cos \gamma_3 \tag{2.26}$$

where

$$\gamma_1 = \beta_2 - 2\beta_1 + \sigma_2 T_1, \quad \gamma_2 = \beta_3 - 2\beta_2 + \sigma_3 T_1, \quad \gamma_3 = \sigma T_1 - \beta_3 \tag{2.27}$$

$$\Gamma = \omega_1^2 \alpha_7^2 / 2\omega_2 \omega_3 \alpha_2^2, \quad F = f\alpha_7 / 2\omega_2 \omega_3 \tag{2.28}$$

Solving equations (2.27) for the β_n yields

$$\beta_3 = \sigma T_1 - \gamma_3, \quad \beta_2 = \frac{1}{2}(\sigma + \sigma_3) T_1 - \frac{1}{2}\gamma_2 - \frac{1}{2}\gamma_3, \tag{2.29}$$

$$\beta_1 = \frac{1}{4}(\sigma + 2\sigma_2 + \sigma_3) T_1 - \frac{1}{4}(2\gamma_1 + \gamma_2 + \gamma_3)$$

Substituting equations (2.29) into equations (2.20), using equations (2.16), and substituting the result into equations (2.5a) and (2.12), we obtain to the first approximation

$$u_1 \approx \frac{2\sqrt{2\omega_1\omega_2}}{\alpha_2} a_1 \cos\left[\frac{1}{4}(\Omega t - 2\gamma_1 - \gamma_2 - \gamma_3)\right] \tag{2.30}$$

$$u_2 \approx \frac{2\omega_1}{\alpha_2} a_2 \cos\left[\frac{1}{2}(\Omega t - \gamma_2 - \gamma_3)\right] \tag{2.31}$$

$$u_3 \approx \frac{2\omega_2}{\alpha_7} a_3 \cos(\Omega t - \gamma_3) \tag{2.32}$$

where the a_n and γ_n are given by equations (2.21)-(2.27).

2.3 Periodic Motions

It follows from equations (2.30)-(2.32) that periodic responses correspond to constant a_n and γ_n, which in turn correspond to the fixed points or constant solutions of equations (2.21)-(2.27). It follows from equations (2.29) that

$$\beta_1' = \frac{1}{4}(\sigma + 2\sigma_2 + \sigma_3) = \nu_1,\ \beta_2' = \frac{1}{2}(\sigma + \sigma_3) = \nu_2,\ \beta_3' = \sigma = \nu_3 \tag{2.33}$$

Hence, the fixed points or constant solutions of equations (2.21)-(2.27) are given by the equations

$$-\mu_1 a_1 + a_1 a_2 \sin \gamma_1 = 0 \tag{2.34}$$

$$-\mu_2 a_2 - a_1^2 \sin \gamma_1 + a_2 a_3 \sin \gamma_2 = 0 \tag{2.35}$$

$$-\mu_3 a_3 - \Gamma a_2^2 \sin \gamma_2 + F \sin \gamma_3 = 0 \tag{2.36}$$

$$\nu_1 a_1 = -a_1 a_2 \cos \gamma_1 \tag{2.37}$$

$$\nu_2 a_2 = -a_1^2 \cos \gamma_1 - a_2 a_3 \cos \gamma_2 \tag{2.38}$$

$$\sigma a_3 = -\Gamma a_2^2 \cos \gamma_2 - F \cos \gamma_3 \tag{2.39}$$

There are three possibilities:

(*a*) $a_1 = 0, a_2 = 0,$ and $a_3 \neq 0$

(*b*) $a_1 = 0, a_2 \neq 0,$ and $a_3 \neq 0$

(*c*) $a_1 \neq 0, a_2 \neq 0,$ and $a_3 \neq 0$

Case a.

In this case, $a_1 = a_2 = 0$ and

$$a_3 = \frac{F}{\sqrt{\sigma^2 + \mu_3^2}} \tag{2.40}$$

and hence $u_1 = u_2 = 0$ and

$$u_3 \approx \frac{2\omega_2}{\alpha_7} a_3 \cos(\Omega t - \gamma_3) \tag{2.41}$$

which is essentially the linear solution.

Case b.

In this case, $a_1 = 0$,

$$a_3 = (\mu_2^2 + \nu_2^2)^{1/2} \tag{2.42}$$

and

$$\Gamma a_2^2 = -(\mu_2\mu_3 - \sigma\nu_2) \pm \left[F - (\mu_3\nu_2 + \sigma\mu_2)^2\right]^{1/2} \tag{2.43}$$

Hence,

$$u_1 \approx 0, \quad u_2 \approx \frac{2\omega_1}{\alpha_2} a_2 \cos\left[\frac{1}{2}(\Omega t - \gamma_2 - \gamma_3)\right] \tag{2.44}$$

and

$$u_3 \approx \frac{2\omega_2}{\alpha_7} a_3 \cos(\Omega t - \gamma_3) \tag{2.45}$$

Case c.

In this case,

$$a_2 = \left(\mu_1^2 + \nu_1^2\right)^{1/2} \tag{2.46}$$

$$a_1^2 = -\chi_1 \pm \sqrt{\chi_1^2 - \chi_2} \tag{2.47}$$

$$(\mu_3^2 + \sigma^2)a_3^2 = F^2 - 2\Gamma(\mu_3\mu_1 + \sigma\nu_1)a_1^2 - 2\Gamma(\mu_2\mu_3 - \sigma\nu_2)a_2^2 - \Gamma^2 a_2^4 \tag{2.48}$$

where

$$\chi_1 = \left[\mu_1\mu_2 - \nu_1\nu_2 + \frac{a_2^2}{\mu_3^2 + \sigma^2}(\mu_3\mu_1 + \sigma\nu_1)\right] \tag{2.49}$$

$$\chi_2 = (\mu_2^2 + \nu_2^2)a_2^2 - \frac{a_2^2}{\mu_3^2 + \sigma^2}\left[F^2 - 2\Gamma(\mu_2\mu_3 - \sigma\nu_2)a_2^2 + \Gamma^2 a_2^4\right] \tag{2.50}$$

and the response is given by equations (2.30)-(2.32).

2.4 Stability of the Fixed Points

To analyze the stability of the fixed points of equations (2.21)-(2.27), we let

$$A_1 = \frac{\sqrt{2\omega_1\omega_2}}{\alpha_2}(p_1 - iq_1)e^{i\nu_1 T_1},\quad A_2 = \frac{\omega_1}{\alpha_2}(p_2 - iq_2)e^{i\nu_2 T_1},$$
$$\text{and } A_3 = \frac{\omega_2}{\alpha_7}(p_3 - iq_3)e^{i\nu_3 T_1} \tag{2.51}$$

where the p_n and q_n are real and the ν_n are defined in equations (2.33). Substituting equations (2.51) into equations (2.17)-(2.19) and separating real and imaginary parts, one obtains

$$p_1' + \mu_1 p_1 + \nu_1 q_1 + p_1 q_2 - p_2 q_1 = 0 \tag{2.52}$$

$$q_1' + \mu_1 q_1 - \nu_1 p_1 - p_1 p_2 - q_1 q_2 = 0 \tag{2.53}$$

$$p_2' + \mu_2 p_2 + \nu_2 q_2 + 2 p_1 q_1 + p_2 q_3 - p_3 q_2 = 0 \tag{2.54}$$

$$q_2' + \mu_2 q_2 - \nu_2 p_2 - p_1^2 + q_1^2 - p_2 p_3 - q_2 q_3 = 0 \tag{2.55}$$

$$p_3' + \mu_3 p_3 + \nu_3 q_3 + 2\Gamma p_2 q_2 = 0 \tag{2.56}$$

$$q_3' + \mu_3 q_3 - \nu_3 p_3 - \Gamma(p_2^2 - q_2^2) - F = 0 \tag{2.57}$$

We note that these equations are invariant under the transformations

$$p_1 \to -p_1, q_1 \to -q_1, p_2 \to p_2, q_2 \to q_2, p_3 \to p_3, q_3 \to q_3 \tag{2.58}$$

$$p_1 \to q_1, q_1 \to -p_1, p_2 \to -p_2, q_2 \to -q_2, p_3 \to p_3, q_3 \to q_3 \tag{2.59}$$

$$p_1 \to -q_1, q_1 \to p_1, p_2 \to -p_2, q_2 \to -q_2, p_3 \to p_3, q_3 \to q_3 \tag{2.60}$$

Substituting equations (2.51) into equations (2.12) and using equations (2.16) and (2.33), we find that to the first approximation

$$u_1 \approx \frac{2\sqrt{2\omega_1 \omega_2}}{\alpha_2}\left[p_1 \cos(\frac{1}{4}\Omega t) + q_1 \sin(\frac{1}{4}\Omega t)\right] \tag{2.61}$$

$$u_2 \approx \frac{2\omega_1}{\alpha_2}\left[p_2 \cos(\frac{1}{2}\Omega t) + q_2 \sin(\frac{1}{2}\Omega t)\right] \tag{2.62}$$

$$u_3 \approx \frac{2\omega_2}{\alpha_7}\left[p_3 \cos(\Omega t) + q_3 \sin(\Omega t)\right] \tag{2.63}$$

where the p_i and q_i are given by equations (2.52)-(2.57).

The stability of a particular fixed point with respect to perturbations proportional to $\exp(\lambda T_1)$ depends on the real parts of the roots of the characteristic equation

$$\begin{vmatrix}
\lambda+\mu_1+q_2 & \nu_1-p_2 & -q_1 & p_1 & 0 & 0 \\
-\nu_1-p_2 & \lambda+\mu_1-q_2 & -p_1 & -q_1 & 0 & 0 \\
2q_1 & 2p_1 & \lambda+\mu_2+q_3 & \nu_2-p_3 & -q_2 & p_2 \\
-2p_1 & 2q_1 & -\nu_2-p_3 & \lambda+\mu_2-q_3 & -p_2 & -q_2 \\
0 & 0 & 2\Gamma q_2 & 2\Gamma p_2 & \lambda+\mu_3 & \nu_3 \\
0 & 0 & -2\Gamma p_2 & 2\Gamma q_2 & -\nu_3 & \lambda+\mu_3
\end{vmatrix} = 0 \tag{2.64}$$

Thus, a fixed point given by equations (2.46)-(2.48) is asymptotically stable if and only if the real parts of all the roots of equation (2.64) are negative.

To study the stability of the fixed points corresponding to case a, we let $p_1 = p_2 = q_1 = q_2 = 0$ in equation (2.64) and obtain the eigenvalues

$$\lambda = -\mu_1 \pm i\nu_1, -\mu_3 \pm i\nu_3, -\mu_2 \pm \sqrt{a_3^2 - \nu_2^2} \tag{2.65}$$

Hence, the fixed points corresponding to case a are stable if and only if

$$a_3^2 < \mu_2^2 + \nu_2^2 \tag{2.66}$$

where $a_n^2 = p_n^2 + q_n^2$.

To study the stability of the fixed points corresponding to case b, we let $p_1 = q_1 = 0$ in equation (2.64) and obtain the two roots

$$\lambda = -\mu_1 \pm \sqrt{a_2^2 - \nu_1^2} \tag{2.67}$$

and four roots governed by the characteristic equation

$$\begin{vmatrix} \lambda + \mu_2 + q_3 & \nu_2 - p_3 & -q_2 & p_2 \\ -\nu_2 - p_3 & \lambda + \mu_2 - q_3 & -p_2 & -q_2 \\ 2\Gamma q_2 & 2\Gamma p_2 & \lambda + \mu_3 & \nu_3 \\ -2\Gamma p_2 & 2\Gamma q_2 & -\nu_3 & \lambda + \mu_3 \end{vmatrix} = 0 \tag{2.68}$$

Again, the fixed points in this case are asymptotically stable if and only if the real parts of all the eigenvalues in equations (2.67) and (2.68) are negative.

2.5 Numerical Results for Fixed-Point Solutions

To show the effect of varying the detunings and the excitation amplitude on the fixed points for cases a, b, and c, we let $\Gamma = 0.625$, $\mu_1 = \mu_2 = 0.5$, and $\mu_3 = 0.1$. In all of the figures, continuous lines represent stable solutions, dotted lines represent unstable solutions with positive real eigenvalues, and dashed lines represent unstable solutions with a complex conjugate pair of eigenvalues having a positive real part.

In Figures 2.1-2.3 we show the effect of varying the excitation amplitude F on the response amplitudes a_1 (Figure 2.1), a_2 (Figure 2.2), and a_3 (Figure 2.3). Here, we set $\sigma = \sigma_2 = 0.5$ and $\sigma_3 = 0.0$. The solution corresponding to case b exists when $F > F_1 \approx 0.275$ (Figures 2.2 and 2.3). When $F_1 < F < F_2 \approx 0.284$, case b is double-valued, with the small solution being unstable with a positive real eigenvalue and the large solution being stable (Figure 2.2). The solution corresponding to case c exists when $F > F_3 \approx 0.323$ (Figures 2.1-2.3). When $0 < F < F_1$, only the solution corresponding to case a exists and is stable (Figures 2.2 and 2.3). Hence, the response in this case is periodic consisting of the third mode only. When $F_1 < F < F_2$, three solutions exist: a solution corresponding to case a, which is stable; a solution corresponding to case b, which is stable; and a solution corresponding to case b, which is unstable with a positive real eigenvalue (Figures 2.2 and 2.3). Here, the response is periodic consisting of either the third mode only or the second and third modes. When $F_2 < F < F_3$, there are two possible solutions: a solution corresponding to case

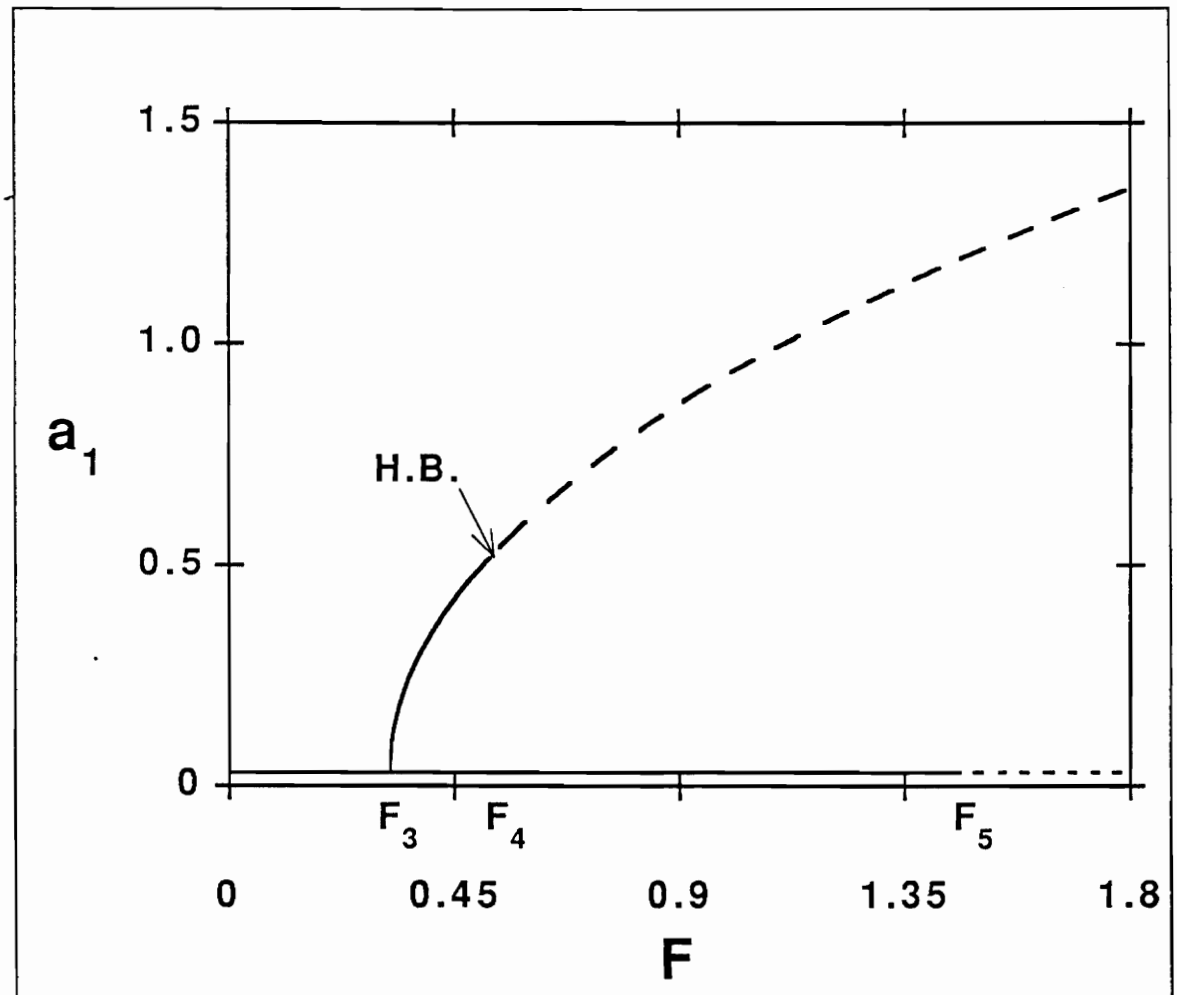

Figure 2.1. Force-response curves for the first mode: (...) unstable with a positive real eigenvalue, (---) unstable with a pair of complex conjugate eigenvalues lying in the right half plane, and (___) stable. Here, $\sigma = 0.5$, $\sigma_2 = 0.5$, $\sigma_3 = 0.0$, $\mu_1 = 0.5$, $\mu_2 = 0.5$, $\mu_3 = 0.1$, and $\Gamma = 0.625$.

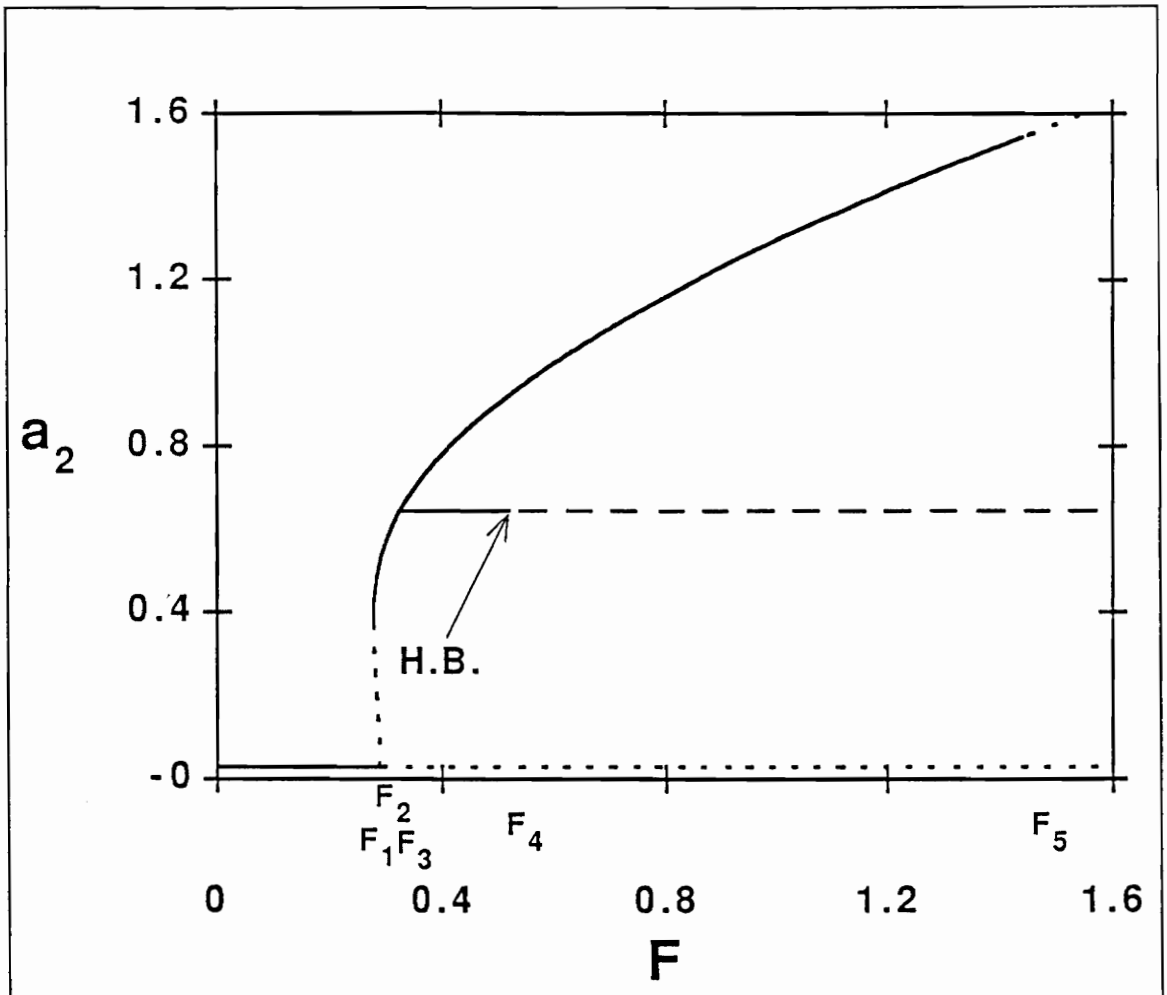

Figure 2.2. **Force-response curves for the second mode:** (...) unstable with a positive real eigenvalue, (---) unstable with a pair of complex conjugate eigenvalues lying in the right half plane, and (___) stable. Here, $\sigma = 0.5$, $\sigma_2 = 0.5$, $\sigma_3 = 0.0$, $\mu_1 = 0.5$, $\mu_2 = 0.5$, $\mu_3 = 0.1$, and $\Gamma = 0.625$.

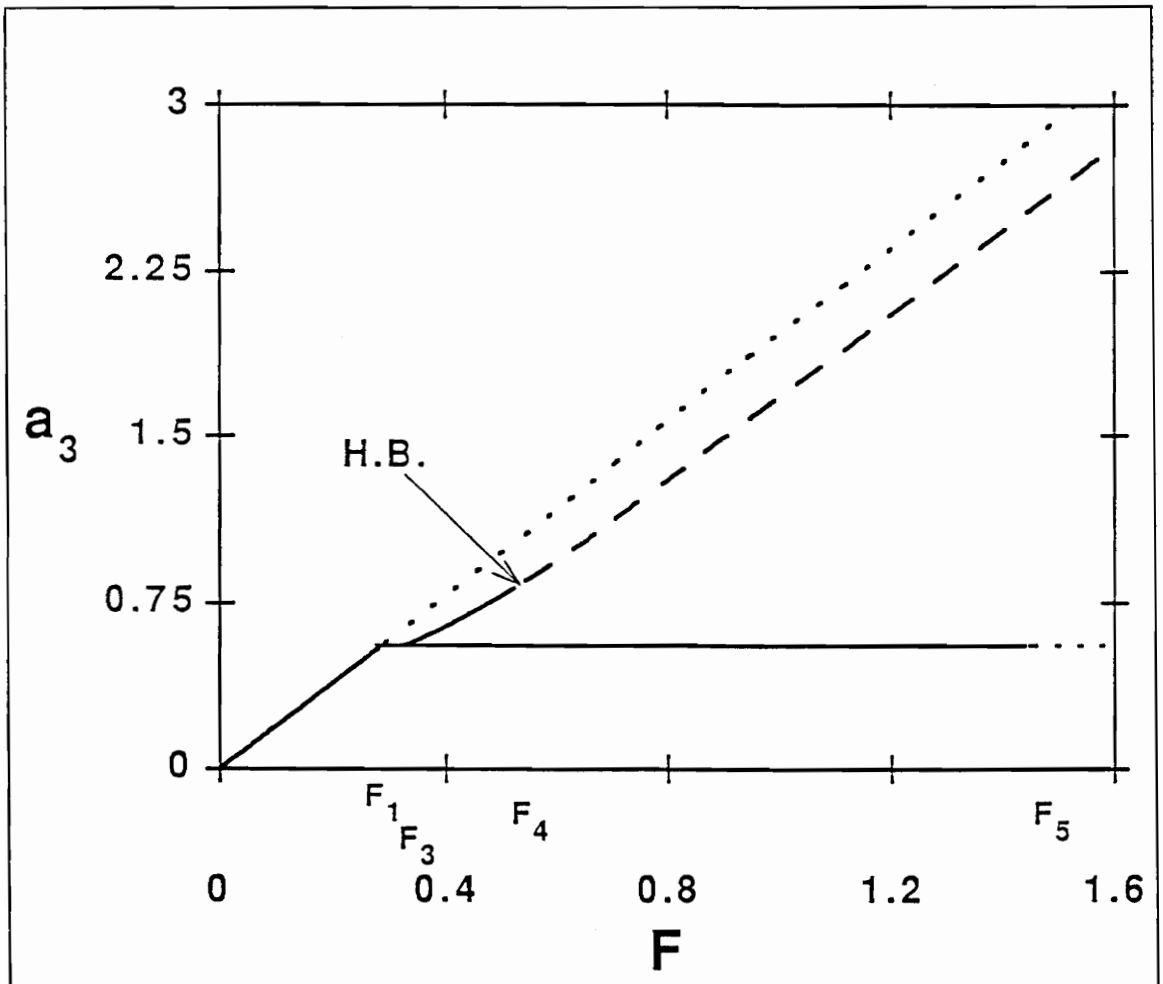

Figure 2.3. **Force-response curves for the third mode:** (...) unstable with a positive real eigenvalue, (---) unstable with a pair of complex conjugate eigenvalues lying in the right half plane, and (___) stable. Here, $\sigma = 0.5$, $\sigma_2 = 0.5$, $\sigma_3 = 0.0$, $\mu_1 = 0.5$, $\mu_2 = 0.5$, $\mu_3 = 0.1$, and $\Gamma = 0.625$.

a, which is unstable with a positive real eigenvalue, and a solution corresponding to case b, which is stable (Figures 2.2 and 2.3). Here, the response is periodic consisting of the second and third modes. When $F_3 < F < F_4 \approx 0.528$, three possible solutions exist: a solution corresponding to case a, which is unstable with a positive real eigenvalue; a solution corresponding to case b, which is stable; and a solution corresponding to case c, which is stable (Figures 2.1-2.3). In this case, the response is periodic consisting of either the second and third modes or all three modes. When $F_4 < F < F_5 \approx 1.444$, three possible solutions exist: a solution corresponding to case a, which is unstable with a positive real eigenvalue; a solution corresponding to case b, which is stable; and a solution corresponding to case c, which is unstable with the real part of a pair of complex conjugate eigenvalues being positive (Figures 2.1-2.3). Here, the response is either a periodic motion consisting of the second and third modes or an amplitude- and phase-modulated motion consisting of all three modes. We note that F_4 is a Hopf-bifurcation point. When $F > F_5$, there are three possible solutions: a solution corresponding to case a, which is unstable with a positive real eigenvalue; a solution corresponding to case b, which is also unstable with a positive real eigenvalue; and a solution corresponding to case c, which is unstable with the real part of a pair of complex conjugate eigenvalues being positive (Figure 2.1-2.3). Here, the response is an amplitude- and phase-modulated motion consisting of all three modes.

In many nonlinear systems the response is dependant on the sweep direction. As we sweep the excitation amplitude up from $F = 0$, we begin with

the solution corresponding to case a, which is stable (Figures 2.1-2.3). Hence, the response is periodic and consists of only the third mode. The amplitude a_3 of the third mode, the directly excited mode, increases linearly with F until F reaches the critical value F_2. When F is increased beyond F_2 (Figure 2.2), the solution corresponding to case a becomes unstable with a positive real eigenvalue. Hence, the response jumps up to the solution corresponding to case b, which is stable. Here the response is periodic with the second and third modes present. As F is increased further, the amplitude a_3 of the excited mode remains constant (saturated), independent of F (Figure 2.3), and is given by equation (2.42). As F is increased beyond F_5, case b becomes unstable with a positive real eigenvalue (Figures 2.1-2.3), and the response jumps to the solution corresponding to case c, which is unstable with the real part of a pair of complex conjugate eigenvalues being positive (Figures 2.1-2.3). Here, the response is an amplitude- and phase-modulated motion consisting of all three modes. As we sweep F down from say $F > 2.5$, at first the solution corresponds to case c, which is unstable with a pair of complex conjugate eigenvalues lying in the right-half of the complex plane, and the response is an amplitude- and phase-modulated motion. As F is decreased, the response remains an amplitude- and phase-modulated motion until F reaches the critical value F_4. As F is decreased below the Hopf-bifurcation point F_4, the solution corresponding to case c becomes stable, and hence the response becomes periodic consisting of all three modes (Figures 2.1-2.3). The response remains periodic consisting of all three modes until F is decreased below F_3 where the solution corresponding to case c ceases to exist and the response latches onto

the solution corresponding to case b (Figures 2.1-2.3). Hence, the response is periodic consisting of the second and third modes. As F is decreased below F_1 the solution corresponding to case b ceases (Figures 2.2 and 2.3), and the response jumps down to the solution corresponding to case a, which is periodic consisting of the third mode only. The overhang region between F_1 and F_2 corresponds to a subcritical instability. In this interval, the response may correspond to either case a or case b, depending on the initial conditions.

In Figures 2.4-2.8 we show variations of the amplitudes a_1 (Figure 2.4), a_2 (Figure 2.5), and a_3 (Figure 2.6-2.8) with σ. Here, we set $F = 0.5$, $\sigma_2 = 0.5$, and $\sigma_3 = 0.0$. When $\sigma < \sigma^{(1)} \approx -0.909$ or $\sigma > \sigma^{(10)} \approx 0.909$, only solution a is possible and it is stable (Figures 2.5 and 2.6). The response in this case is periodic consisting of the third mode only (essentially a linear response). Solution b exists when σ is between $\sigma^{(1)}$ and $\sigma^{(10)}$. When $\sigma^{(1)} < \sigma < \sigma^{(3)} \approx -0.782$ or $0.781 \approx \sigma^{(7)} < \sigma < \sigma^{(10)}$, case b is double-valued: the smaller solution is unstable with a real eigenvalue being positive and the larger solution is stable (Figure 2.5). When $\sigma^{(1)} < \sigma < \sigma^{(2)} \approx -0.858$ or $0.902 \approx \sigma^{(9)} < \sigma < \sigma^{(10)}$, there are two possible solutions: a solution corresponding to case a, which is stable, and a solution corresponding to case b, which is also stable (Figures 2.7 and 2.8). Here the response is periodic consisting of either the third mode only or the second and third modes. When $\sigma^{(2)} < \sigma < \sigma^{(3)}$ or $0.844 \approx \sigma^{(8)} < \sigma < \sigma^{(9)}$, there are three possible solutions: a solution corresponding to case a, which is stable; a solution corresponding to case b, which is stable; and a solution corresponding to case c, which is unstable with the real part of a pair of complex conjugate eigenvalues being positive (Figures 2.7 and 2.8). Here, the

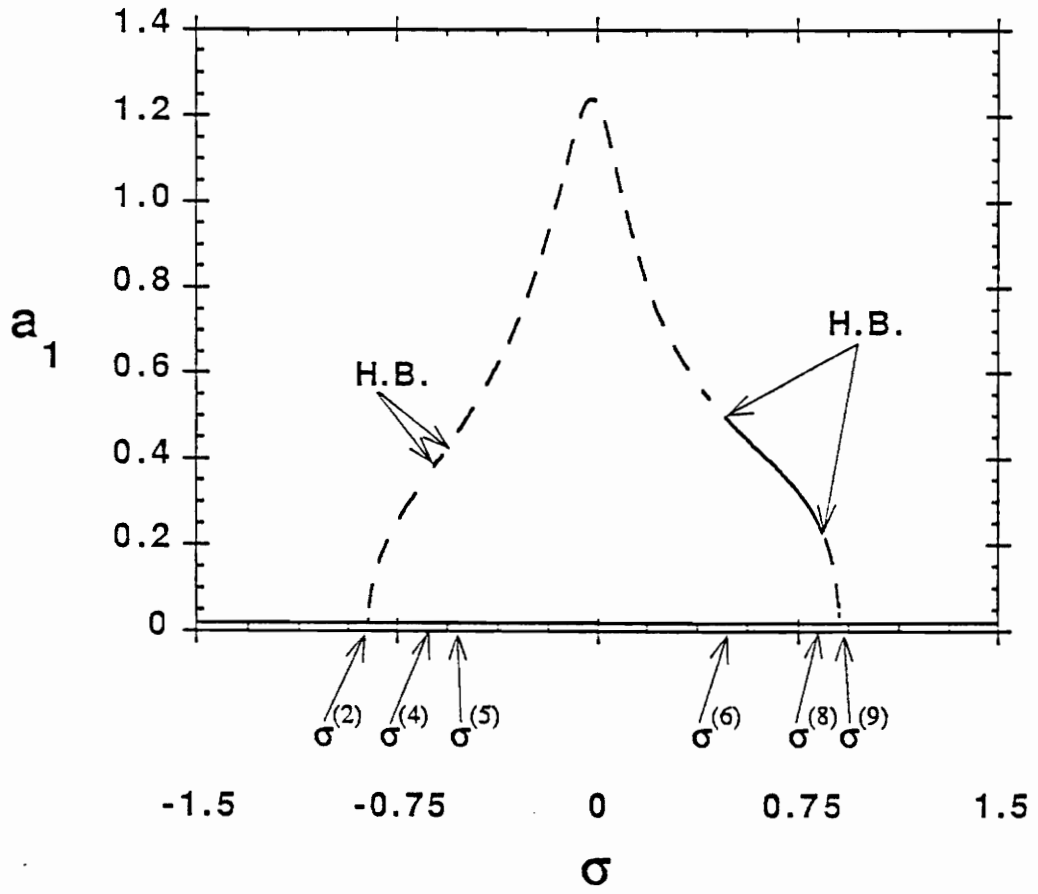

Figure 2.4. **Frequency-response curves for the first mode:** (...) unstable with a positive real eigenvalue, (---) unstable with a pair of complex conjugate eigenvalues lying in the right half plane, and (___) stable. Here, $F = 0.5$, $\sigma_2 = 0.5$, $\sigma_3 = 0.0$, $\mu_1 = 0.5$, $\mu_2 = 0.5$, $\mu_3 = 0.1$, and $\Gamma = 0.625$.

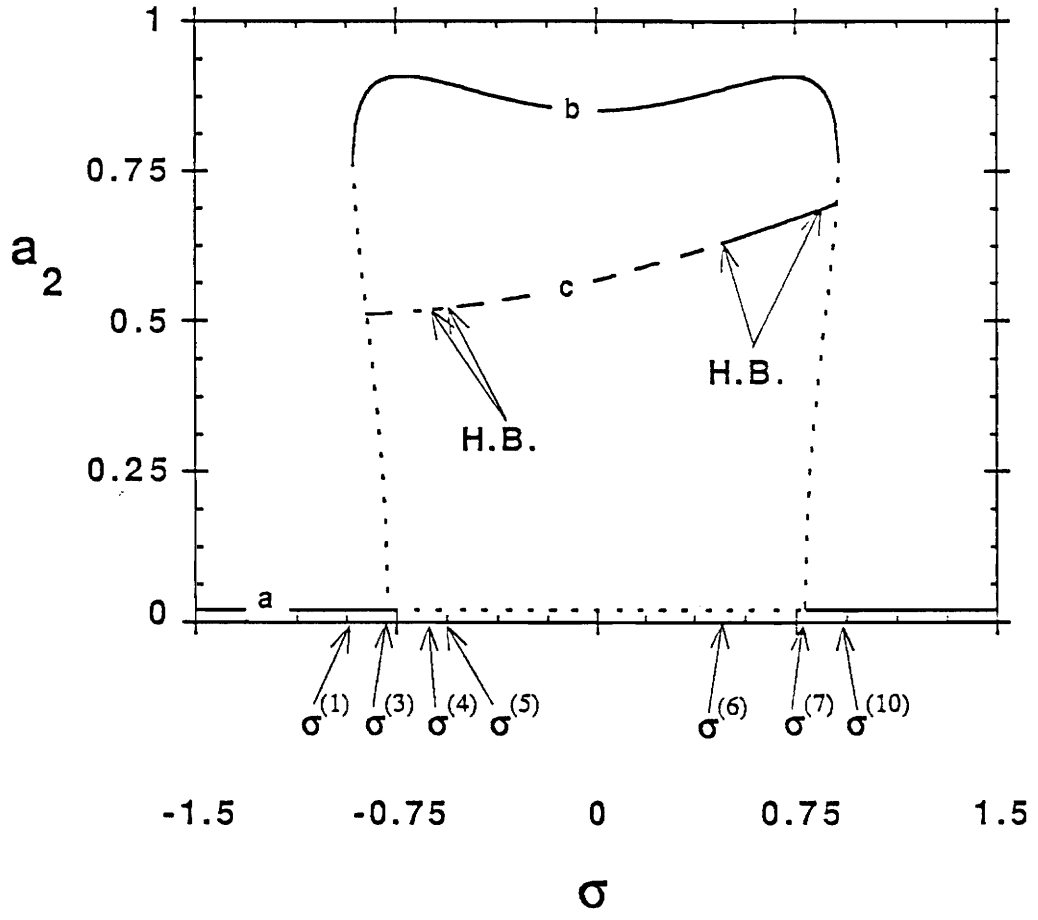

Figure 2.5. **Frequency-response curves for the second mode:** (...) unstable with a positive real eigenvalue, (---) unstable with a pair of complex conjugate eigenvalues lying in the right half plane, and (___) stable. Here, $F = 0.5$, $\sigma_2 = 0.5$, $\sigma_3 = 0.0$, $\mu_1 = 0.5$, $\mu_2 = 0.5$, $\mu_3 = 0.1$, and $\Gamma = 0.625$.

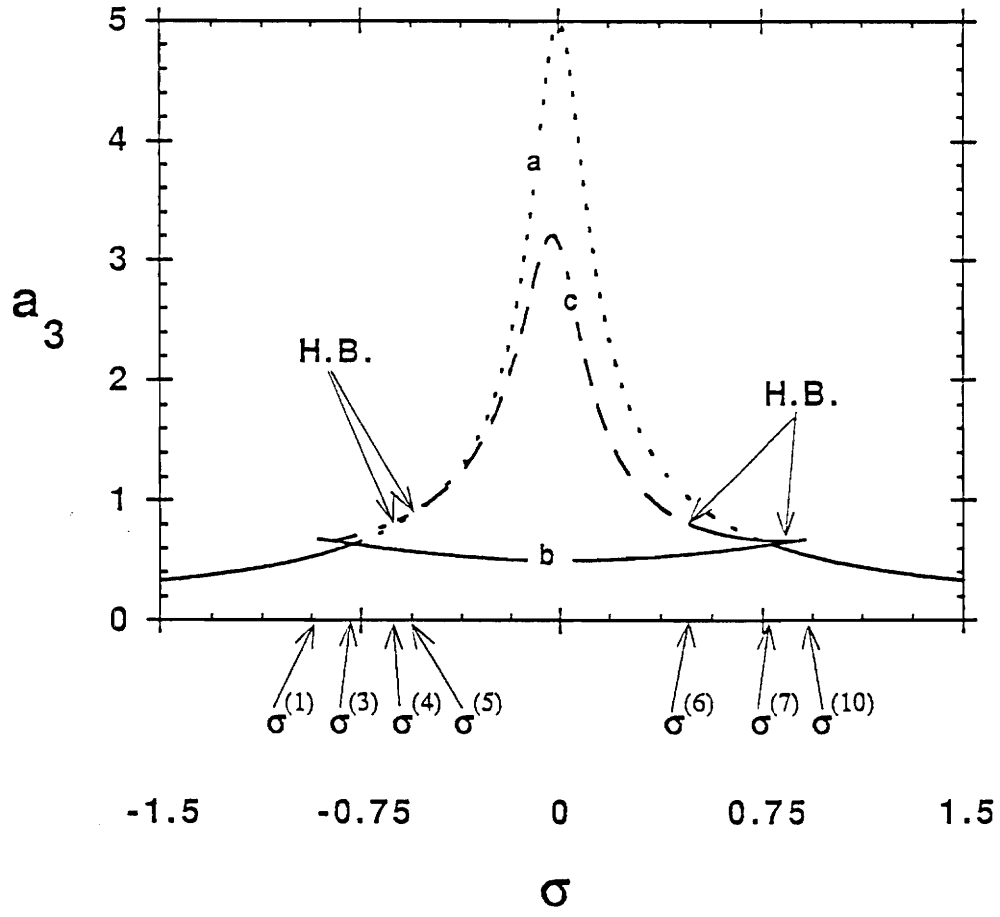

Figure 2.6. Frequency-response curves for the third mode: (...) unstable with a positive real eigenvalue, (---) unstable with a pair of complex conjugate eigenvalues lying in the right half plane, and (___) stable. Here, $F = 0.5$, $\sigma_2 = 0.5$, $\sigma_3 = 0.0$, $\mu_1 = 0.5$, $\mu_2 = 0.5$, $\mu_3 = 0.1$, and $\Gamma = 0.625$.

response can correspond to case a, be periodic, and consist of the third mode only, or periodic corresponding to case b consisting of the second and third modes, or an amplitude- and phase-modulated motion corresponding to case c consisting of all three modes. When $\sigma^{(3)} < \sigma < \sigma^{(4)} \approx -0.571$ or $-0.474 \approx \sigma^{(5)} < \sigma < \sigma^{(6)} \approx 0.473$, there are three possible solutions: a solution corresponding to case a, which is unstable with a real eigenvalue being positive; a solution corresponding to case b, which is stable; and a solution corresponding to case c, which is unstable with the real part of a pair of complex conjugate eigenvalues being positive (Figures 2.6 and 2.7). Hence, the response consists of either a periodic solution consisting of the second and third modes or an amplitude- and phase-modulated motion consisting of all three modes. When $\sigma^{(4)} < \sigma < \sigma^{(5)}$ or $\sigma^{(6)} < \sigma < \sigma^{(7)}$, three solutions exist: a solution corresponding to case a, which is unstable with a real eigenvalue being positive; a solution corresponding to case b, which is stable; and a solution corresponding to case c, which is stable (Figures 2.4-2.8). In this case, the response is periodic consisting of either the second and third modes or all three modes. When $\sigma^{(7)} < \sigma < \sigma^{(8)}$, three stable solutions exist: a solution corresponding to case a; a solution corresponding to case b; and a solution corresponding to case c. Hence in this case, the response is periodic consisting of the third mode only, the second and third modes only, or all three modes. We note that $\sigma^{(4)}$, $\sigma^{(5)}$, $\sigma^{(6)}$, and $\sigma^{(8)}$ correspond to Hopf-bifurcation points.

As we slowly sweep σ upwards from $\sigma = -1.5$, at first the solution corresponds to case a ($a_1 = a_2 = 0$) (Figures 2.4-2.6), and the response is

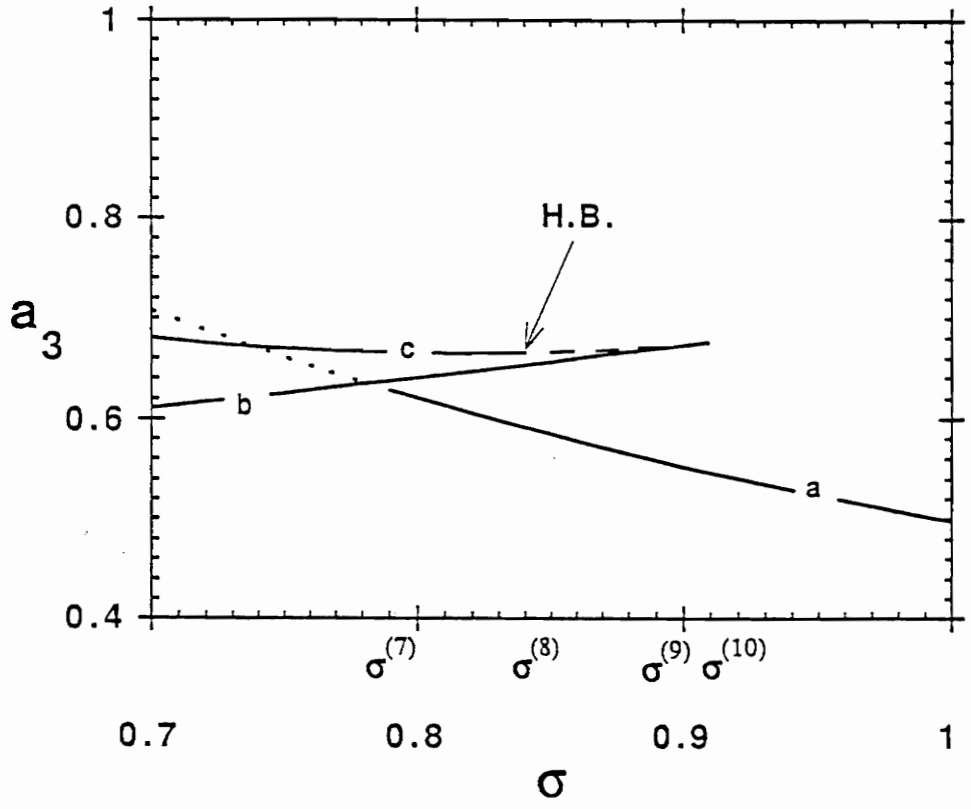

Figure 2.7. Expanded portion of the frequency-response curves for the third mode: (...) unstable with a positive real eigenvalue, (---) unstable with a pair of complex conjugate eigenvalues lying in the right half plane, and (___) stable. Here, $F = 0.5$, $\sigma_2 = 0.5$, $\sigma_3 = 0.0$, $\mu_1 = 0.5$, $\mu_2 = 0.5$, $\mu_3 = 0.1$, and $\Gamma = 0.625$.

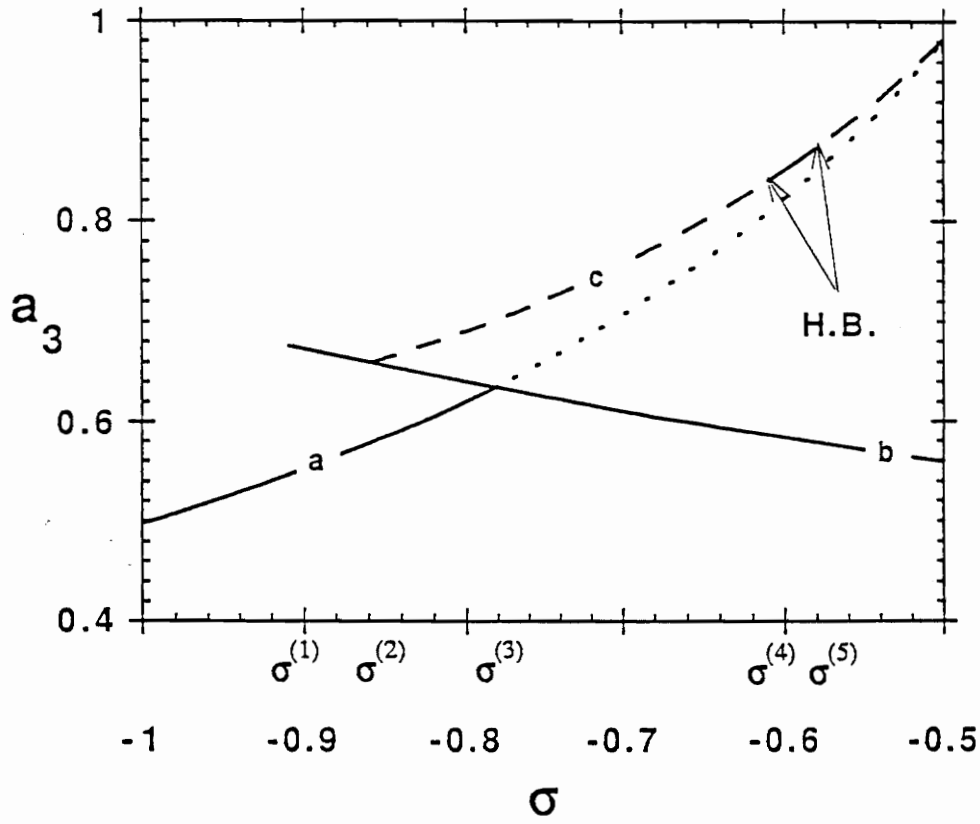

Figure 2.8. Expanded portion of the frequency-response curves for the third mode: (...) unstable with a positive real eigenvalue, (---) unstable with a pair of complex conjugate eigenvalues lying in the right half plane, and (___) stable. Here, $F = 0.5$, $\sigma_2 = 0.5$, $\sigma_3 = 0.0$, $\mu_1 = 0.5$, $\mu_2 = 0.5$, $\mu_3 = 0.1$, and $\Gamma = 0.625$.

periodic consisting of the third mode only. It remains stable until σ reaches the critical value $\sigma^{(3)}$ (Figures 2.5-2.7). As σ is increased beyond $\sigma^{(3)}$, the solution corresponding to case a loses stability with one real eigenvalue becoming positive, and the response jumps to that corresponding to either case b or case c. In the first case, a_1 remains zero, a_3 decreases slightly, and a_2 jumps up from zero to a large value. As σ is increased further, the response stays locked onto the solution corresponding to case b, which is periodic and consists of the second and third modes, until σ reaches the critical value $\sigma^{(10)}$, where the solution for case b ceases to exist (Figures 2.6 and 2.8). As σ is increased beyond $\sigma^{(10)}$, the response jumps down to the solution corresponding to case a. If at $\sigma = \sigma^{(3)}$ the response jumps to that corresponding to case c, it becomes an amplitude- and phase-modulated motion consisting of all three modes. It remains aperiodic (it may even become chaotic) until σ exceeds $\sigma^{(4)}$, where the fixed points of the modulation equations undergo a reverse Hopf bifurcation, and the response becomes periodic consisting of all three modes. As σ is increased beyond $\sigma^{(5)}$, the fixed points undergo a Hopf bifurcation and the response becomes an amplitude- and phase-modulated motion. As σ is increased beyond $\sigma^{(6)}$, the fixed points undergo another reverse Hopf bifurcation and the response becomes periodic again and remains so until σ reaches $\sigma^{(8)}$. When σ exceeds $\sigma^{(8)}$, the fixed points undergo another Hopf bifurcation and again the response becomes an amplitude- and phase-modulated motion. As σ is increased beyond $\sigma^{(9)}$, solution c ceases to exist and the response jumps to the solution corresponding to either case b or case a.

As we slowly sweep σ down from $\sigma = 1.5$, the response is periodic corresponding to case a. It remains stable until σ is decreased below $\sigma^{(7)}$, where it loses stability with a real eigenvalue becoming positive, and the response jumps to either a periodic motion consisting of the second and third modes, corresponding to case b, or a periodic motion consisting of all three modes, corresponding to case c. In the first case, the response remains stable until σ is decreased below $\sigma^{(1)}$, where a_2 jumps down to zero whereas a_3 jumps down to the solution corresponding to case a. If at $\sigma = \sigma^{(7)}$, the response jumps to the solution corresponding to case c, it will be periodic consisting of all three modes. As σ is decreased further the response will remain periodic until σ reaches the value $\sigma^{(6)}$, where the fixed points undergo a Hopf bifurcation and the response becomes an amplitude- and phase-modulated motion consisting of all three modes. As σ is decreased below $\sigma^{(5)}$, the fixed points undergo a reverse Hopf bifurcation and the response becomes periodic again (Figures 2.4-2.7). The response remains periodic until σ is decreased below $\sigma^{(4)}$, where the fixed points undergo a Hopf bifurcation, and the response becomes an amplitude- and phase-modulated motion consisting of all three modes (Figures 2.4-2.6). The response remains modulated until σ is decreased below $\sigma^{(2)}$ where the solution for case c ceases (Figures 2.4-2.6, and 2.7), and the response jumps to that corresponding to either case a or case b.

In Figures 2.9-2.11 we show the effect of varying σ_2 on the response amplitudes a_1 , a_2 , and a_3. Here, we set $F = 0.5$, $\sigma = 0.5$, and $\sigma_3 = 0$.. It follows from equation (2.40) that solution a is independent of σ_2. For the given values of F, σ, and σ_3, solution a is unstable (Figures 2.10 and 2.11) with at least one

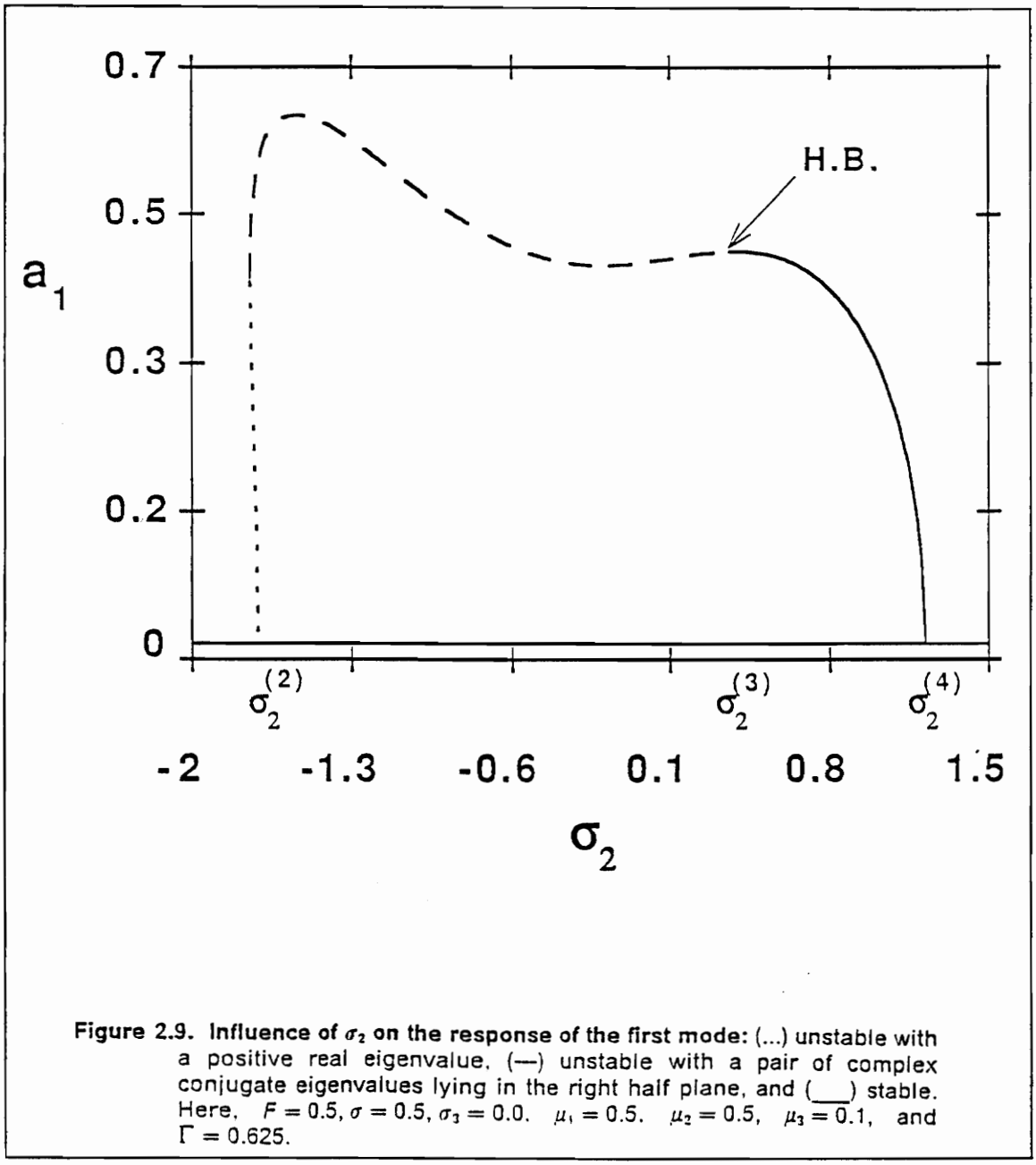

Figure 2.9. Influence of σ_2 on the response of the first mode: (...) unstable with a positive real eigenvalue, (—) unstable with a pair of complex conjugate eigenvalues lying in the right half plane, and (___) stable. Here, $F = 0.5$, $\sigma = 0.5$, $\sigma_3 = 0.0$, $\mu_1 = 0.5$, $\mu_2 = 0.5$, $\mu_3 = 0.1$, and $\Gamma = 0.625$.

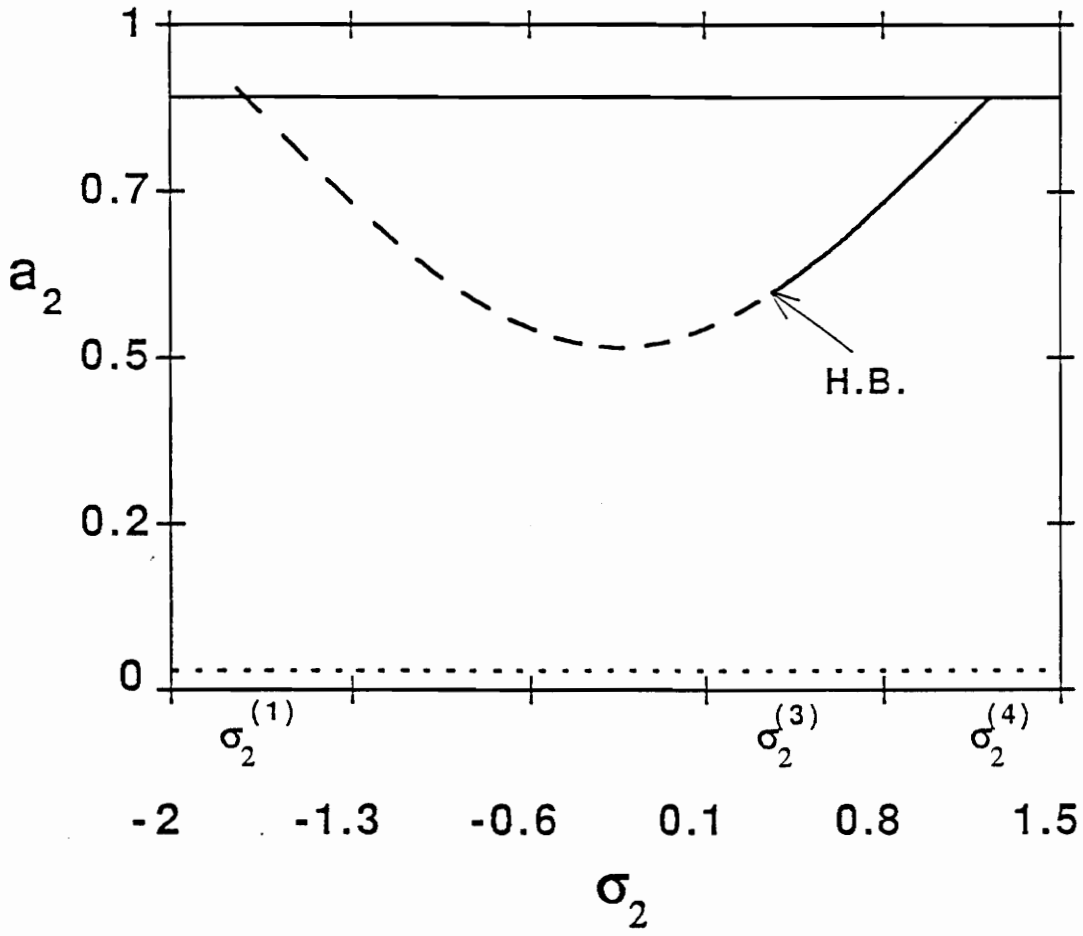

Figure 2.10. Influence of σ_2 on the response of the second mode: (...) unstable with a positive real eigenvalue. (—) unstable with a pair of complex conjugate eigenvalues lying in the right half plane, and (___) stable. Here, $F = 0.5, \sigma = 0.5, \sigma_3 = 0.0, \mu_1 = 0.5, \mu_2 = 0.5, \mu_3 = 0.1$, and $\Gamma = 0.625$.

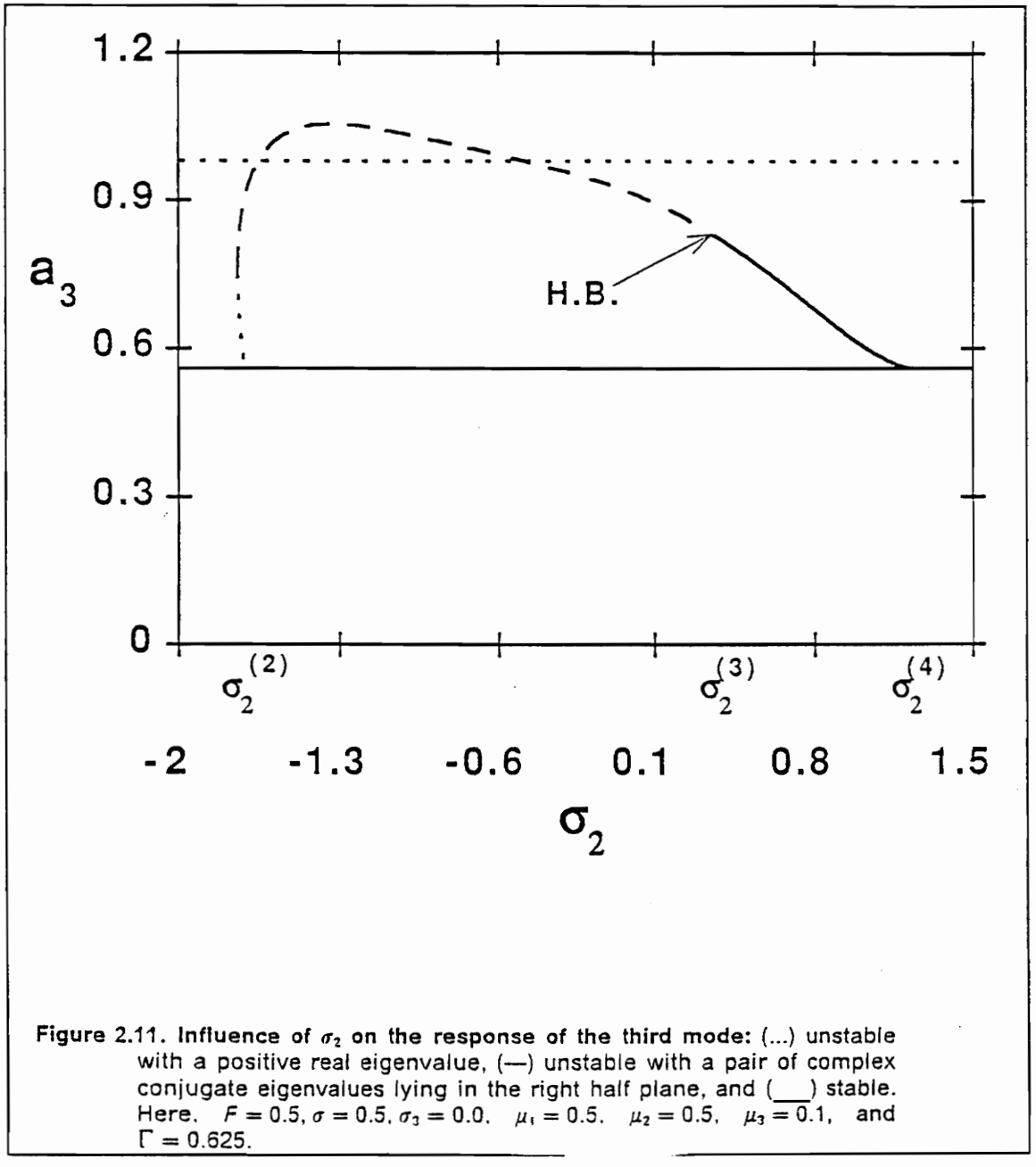

Figure 2.11. Influence of σ_2 on the response of the third mode: (...) unstable with a positive real eigenvalue, (—) unstable with a pair of complex conjugate eigenvalues lying in the right half plane, and (___) stable. Here, $F = 0.5, \sigma = 0.5, \sigma_3 = 0.0$, $\mu_1 = 0.5$, $\mu_2 = 0.5$, $\mu_3 = 0.1$, and $\Gamma = 0.625$.

real eigenvalue being positive. It follows from equations (2.42) and (2.43) that the amplitudes a_2 and a_3 ($a_1 = 0$) in case b are also independent of σ_2. Here, solution b is stable (Figures 2.9-2.11). Solution c exists for values of σ_2 between $\sigma_2^{(1)} = -1.748$ and $\sigma_2^{(4)} = 1.217$. When $\sigma_2^{(1)} < \sigma_2 < \sigma_2^{(2)} = -1.717$, case c is double-valued: the small solution is unstable with a real eigenvalue being positive and the large solution is unstable with the real part of a pair of complex conjugate eigenvalues being positive. When $\sigma_2^{(2)} < \sigma_2 < \sigma_2^{(3)} = 0.353$, case c is single-valued and unstable with the real part of a pair of complex conjugate eigenvalues being positive. When $\sigma_2^{(3)} < \sigma_2 < \sigma_2^{(4)}$, again solution c is single-valued but stable. The point $\sigma_2^{(3)}$ corresponds to a Hopf bifurcation. Combining the three solutions, we conclude that (a) when $\sigma_2 < \sigma_2^{(1)}$ or $\sigma_2 > \sigma_2^{(4)}$, the response corresponds to case b and hence it is periodic consisting of the second and third modes only; (b) when $\sigma_2^{(1)} < \sigma_2 < \sigma_2^{(3)}$, the response corresponds to either case b or case c, and hence it is either a periodic motion consisting of the second and third modes only or an amplitude- and phase-modulated motion consisting of all three modes; and (c) when $\sigma_2^{(3)} < \sigma_2 < \sigma_2^{(4)}$, the response corresponds to either case b or case c, depending on the initial conditions, and hence it is periodic consisting of either the second and third modes only or all three modes.

In Figures 2.12-2.16 we show the effect of varying σ_3 on the response amplitudes a_1 (Figure 2.12), a_2 (Figure 2.13), and a_3 (Figure 2.14). When $\sigma_3 < \sigma_3^{(1)} \approx -2.188$ or $\sigma_3 > \sigma_3^{(11)} \approx 4.500$, only solution a is possible and it is stable. The response in this case is periodic consisting of the third mode only. When $\sigma_3^{(1)} < \sigma_3 < \sigma_3^{(2)} \approx -1.778$ or $-1.632 \approx \sigma_3^{(3)} < \sigma_3 < \sigma_3^{(4)} \approx -1.509$, there are two possible

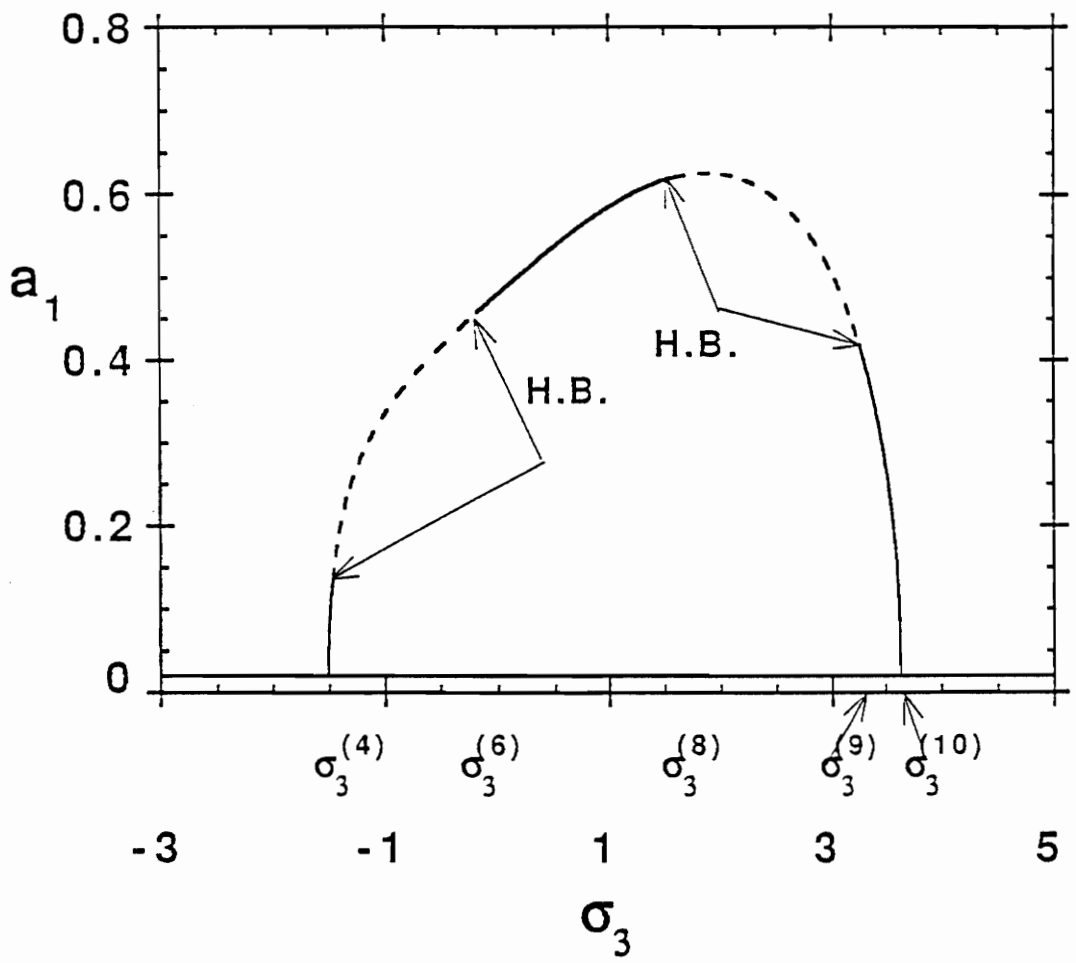

Figure 2.12. Influence of σ_3 on the response of the first mode: (...) unstable with a positive real eigenvalue, (—) unstable with a pair of complex conjugate eigenvalues lying in the right half plane, and (___) stable. Here, $F = 0.5, \sigma = 0.5$. $\sigma_2 = 0.5$. $\mu_1 = 0.5$, $\mu_2 = 0.5, \mu_3 = 0.1$, and $\Gamma = 0.625$.

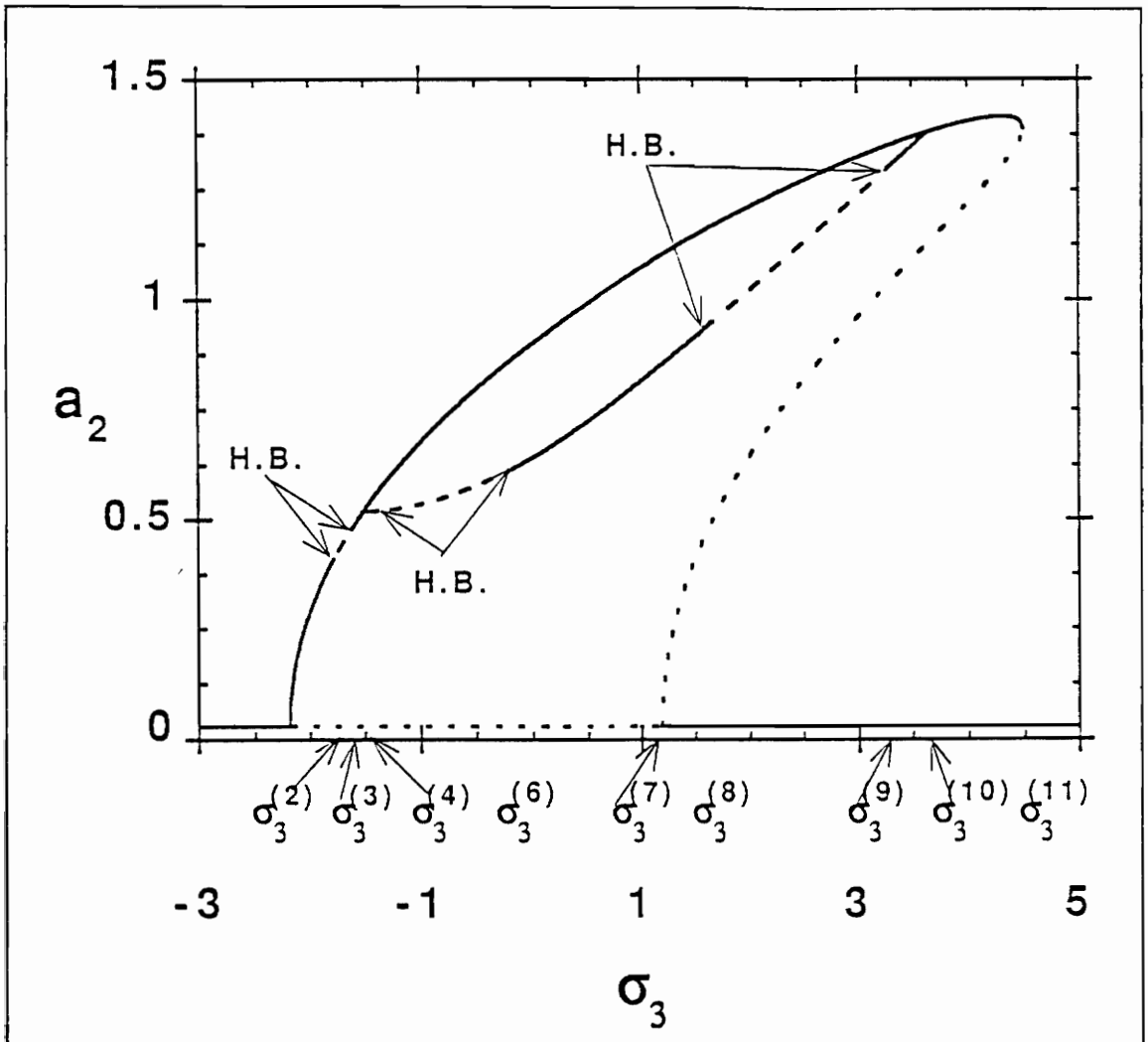

Figure 2.13. Influence of σ_3 on the response of the second mode: (...) unstable with a positive real eigenvalue, (—) unstable with a pair of complex conjugate eigenvalues lying in the right half plane, and (___) stable. Here, $F = 0.5, \sigma = 0.5, \sigma_2 = 0.5, \mu_1 = 0.5, \mu_2 = 0.5, \mu_3 = 0.1$, and $\Gamma = 0.625$.

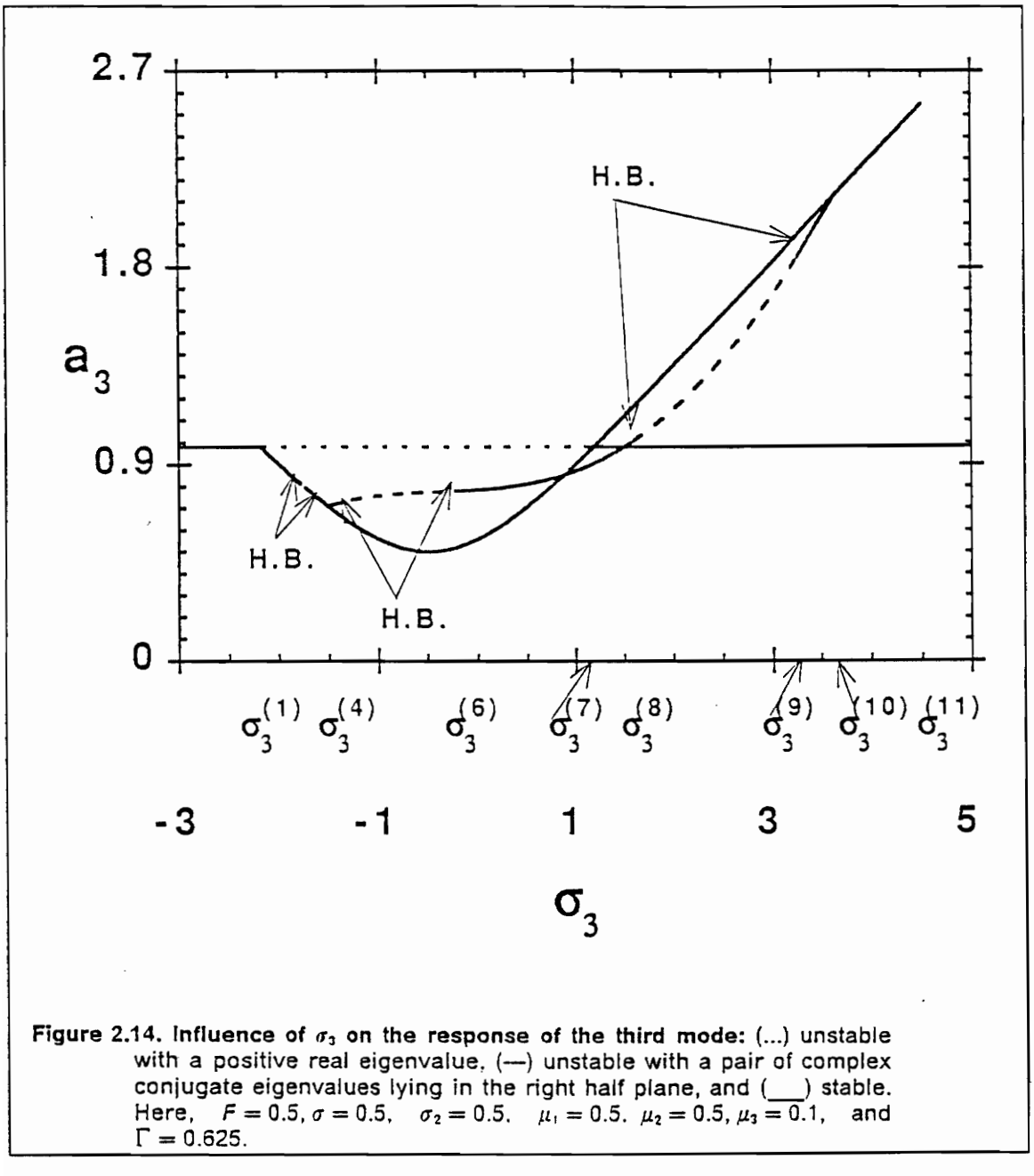

Figure 2.14. Influence of σ_3 on the response of the third mode: (...) unstable with a positive real eigenvalue, (—) unstable with a pair of complex conjugate eigenvalues lying in the right half plane, and (___) stable. Here, $F = 0.5, \sigma = 0.5, \sigma_2 = 0.5, \mu_1 = 0.5, \mu_2 = 0.5, \mu_3 = 0.1$, and $\Gamma = 0.625$.

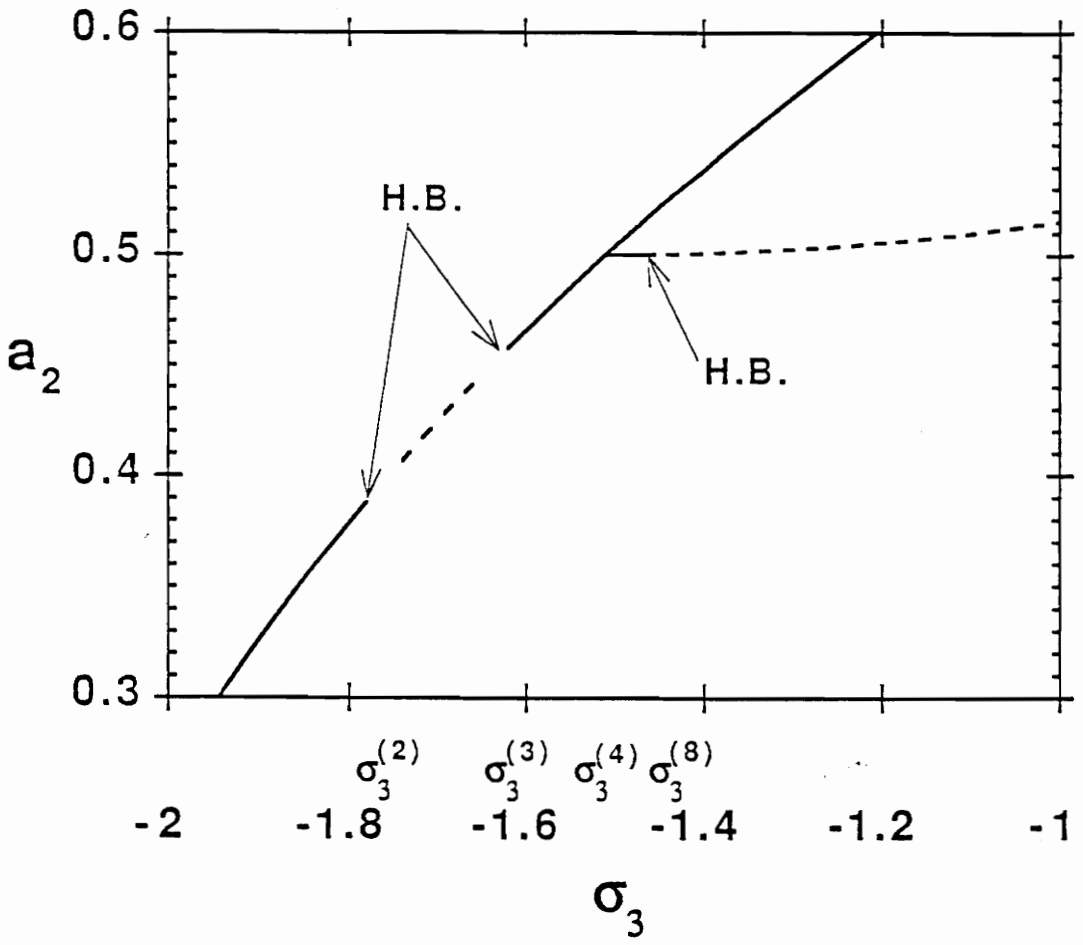

Figure 2.15. Expanded portion of the influence of σ_3 on the response of the second mode: (...) unstable with a positive real eigenvalue, (—) unstable with a pair of complex conjugate eigenvalues lying in the right half plane, and (___) stable. Here, $F = 0.5$, $\sigma = 0.5$, $\sigma_2 = 0.5$, $\mu_1 = 0.5$, $\mu_2 = 0.5$, $\mu_3 = 0.1$, and $\Gamma = 0.625$.

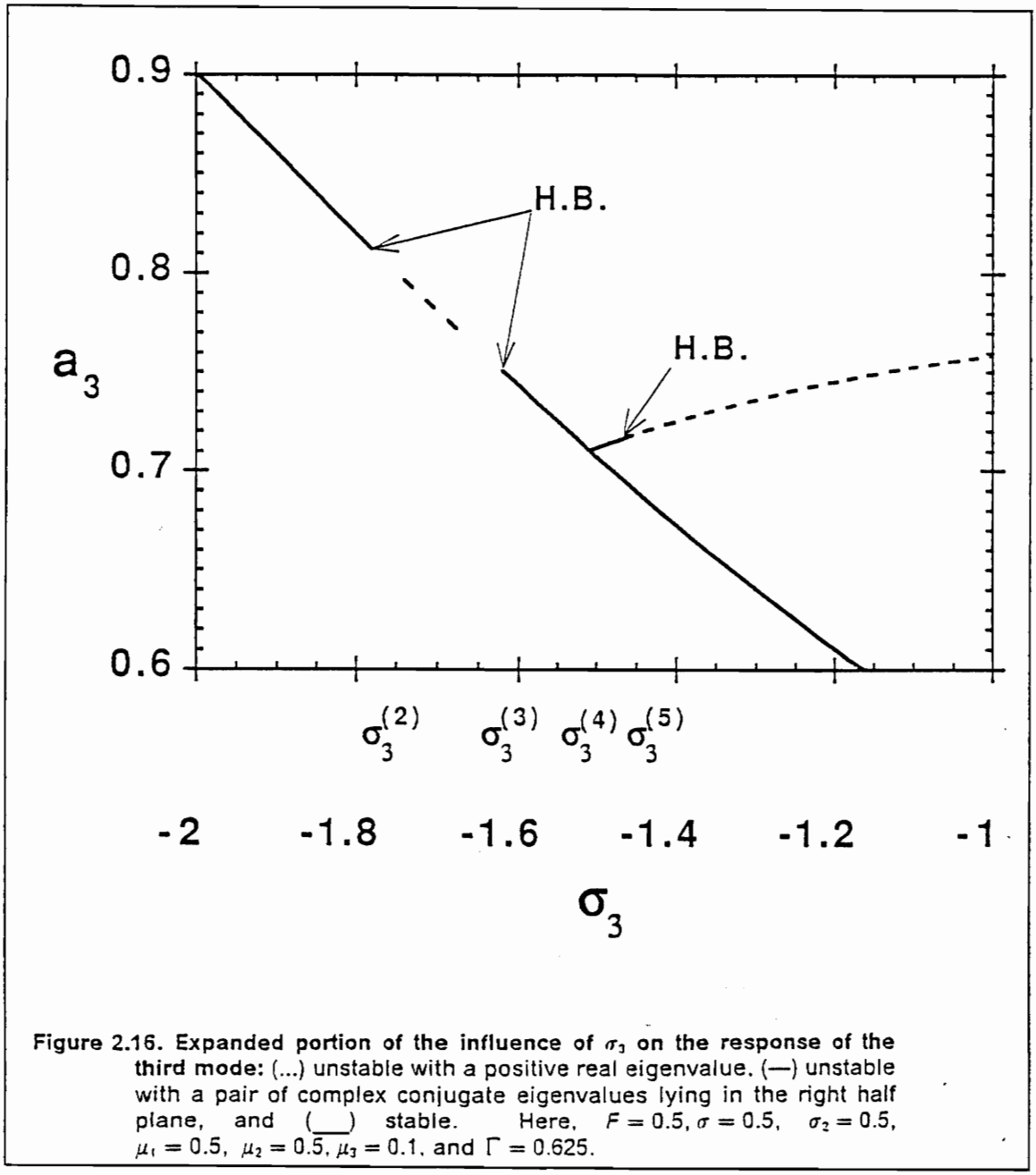

Figure 2.16. Expanded portion of the influence of σ_3 on the response of the third mode: (...) unstable with a positive real eigenvalue, (—) unstable with a pair of complex conjugate eigenvalues lying in the right half plane, and (___) stable. Here, $F = 0.5$, $\sigma = 0.5$, $\sigma_2 = 0.5$, $\mu_1 = 0.5$, $\mu_2 = 0.5$, $\mu_3 = 0.1$, and $\Gamma = 0.625$.

solutions: a solution corresponding to case a, which is unstable with a real eigenvalue being positive, and a solution corresponding to case b, which is stable. Consequently, the response in this case is periodic consisting of the second and third modes. When $\sigma_3^{(2)} < \sigma_3 < \sigma_3^{(3)}$, there are two possible solutions: a solution corresponding to case a, which is unstable with one real eigenvalue being positive, and a solution corresponding to case b, which is unstable with the real part of a pair of complex conjugate eigenvalues being positive (Figures 2.15 and 2.16). The response in this case is an amplitude- and phase-modulated motion consisting of the second and third modes. The values $\sigma_3^{(2)}$ and $\sigma_3^{(3)}$ correspond to Hopf-bifurcation points. When $\sigma_3^{(4)} < \sigma_3 < \sigma_3^{(5)} \approx -1.467$ or $-0.196 \approx \sigma_3^{(6)} < \sigma_3 < \sigma_3^{(7)} \approx 1.187$, there are three possible solutions: a solution corresponding to case a, which is unstable with a real eigenvalue being positive, a solution corresponding to case b, which is stable; and a solution corresponding to case c, which is stable. In this case, the response is periodic consisting of either the second and third modes only or all three modes, depending on the initial conditions. When $1.580 \approx \sigma_3^{(8)} < \sigma_3 < \sigma_3^{(9)} \approx 3.246$, there are three possible solutions: a solution corresponding to case a, which is stable: a solution corresponding to case b, which is also stable; and a solution corresponding to case c, which is unstable with the real part of a pair of complex conjugate eigenvalues being positive. In this case, the response may be either periodic, consisting of either the third mode only or the second and third modes only, or an amplitude- and phase-modulated motion consisting of all three modes, depending on the initial conditions. The values $\sigma_3^{(8)}$ and $\sigma_3^{(9)}$ correspond to Hopf-bifurcation points.

When $\sigma_3^{(7)} < \sigma_3 < \sigma_3^{(8)}$ and $\sigma_3^{(9)} < \sigma_3 < \sigma_3^{(10)} \approx 3.638$, there are three possible solutions corresponding to cases a, b, and c, all of which are stable. In this case, the response is periodic consisting of the third mode only, the second and third modes only, or all three modes, depending on the initial conditions. When $\sigma_3^{(10)} < \sigma_3 < \sigma_3^{(11)} \approx 4.500$, there are two possible solutions: a solution corresponding to case a and a solution corresponding to case b, both of which are stable. Thus, the response is periodic consisting of either the third mode only or the second and third modes only, depending on the initial conditions.

2.6 Modulated Motions

As discussed in Sections 2.4 and 2.5, the fixed points of the modulation equations (2.21)-(2.27) or (2.52)-(2.57) correspond to periodic solutions of (2.1)-(2.3). Moreover, for some excitation and system parameters, the fixed-point solutions of the modulation equations may undergo Hopf bifurcations. Near these Hopf bifurcations, the modulation equations possess limit-cycle solutions, which correspond to either two-period quasiperiodic or phase-locked solutions of (2.1)-(2.3), depending on whether the frequency of the limit cycle is commensurate or incommensurate with Ω. To locate these limit cycles, we use the *shooting* method described by Aprille and Trick [40]. To determine the stability of these limit cycles and the bifurcations that they may undergo, we use Floquet theory [12]. Once these limit-cycle solutions of

equations (2.52)-(2.57) lose stability and are no longer periodic, we resort to the use of Poincaré sections and FFT's to discern the nature of the ensuing bifurcations. In this study, we observed that for some excitation and system parameters the p_i and q_i become two-period quasiperiodic (T^2 torus). The T^2 torus becomes synchronous (frequency locked) in which the ratio of its two base frequencies becomes an integer. Then the torus breaks down and the motion becomes chaotic.

2.6.1 Floquet Theory

The autonomous set of equations (2.52)-(2.57) can be written in the matrix form

$$\dot{x} = F(x) \tag{2.69}$$

where $x(t)$ is a vector of length n (in this case $n = 6$). Then $X(t)$ is a *limit-cycle* or periodic solution of (2.69) if it satisfies (2.69) and

$$X(t) = X(t + T) \tag{2.70}$$

where T is the period.

The stability of the limit-cycle solution can be studied by perturbing the periodic solution $X(t)$ by adding a small disturbance $\xi(t)$; that is, we set

$$x(t) = X(t) + \xi(t) \tag{2.71}$$

Substituting equation (2.71) into equation (2.69), we obtain

$$\dot{X}(t) + \dot{\xi}(t) = F(X + \xi) \tag{2.72}$$

Expanding $F(X + \xi)$ in a Taylor series and keeping only linear terms yields

$$\dot{\xi}(t) = DF(t)\xi(t) \tag{2.73}$$

where

$$DF(t) = \frac{\partial F_i}{\partial x_j}(X) \tag{2.74}$$

is the Jacobian matrix of F(X). Equation (2.73) constitutes a system of n first-order linear ordinary differential equations with periodic coefficients having the period T. The stability of the solutions of equations (2.73) can be found by using Floquet theory.

We define Φ_t to be the fundamental matrix solution; that is, the columns of Φ_t are n linearly independent solutions of equation (2.73). Thus, Φ_t satisfies

$$\dot{\Phi}_t = DF(t)\Phi_t \tag{2.75}$$

It follows from equations (2.75) that

$$\dot{\Phi}_{t+T} = DF(t + T)\Phi_{t+T} \tag{2.76}$$

Because $DF(t)$ is periodic with period T, $DF(t) = DF(t + T)$ and hence Φ_{t+T} also satisfies equations (2.75). However, from the uniqueness theorem a system

of n first-order linear ordinary differential equations can have only n linearly independent solutions. Hence, the columns of Φ_{t+T} are linear combinations of the columns of Φ_t; that is,

$$\Phi_{t+T} = \mathbf{A}\Phi_t \tag{2.77}$$

where **A** is a constant *nxn* matrix. If the initial conditions are $\Phi_0 = \mathbf{I}$, where **I** is the identity matrix, then it follows from equation (2.77) that $\mathbf{A} = \Phi_T$. The matrix **A** is usually called the *Monodromy matrix.*

The long-time behavior of $\xi(t)$ and hence the stability of X(t) depends on the eigenvalues of **A**. To show this, we define the transformation $\Phi_t = \mathbf{P}V(t)$, where **P** is an *nxn* constant nonsingular matrix, substitute it into equations (2.77), and obtain

$$V(t+T) = \mathbf{P}^{-1}\mathbf{A}\mathbf{P}V(t) = \mathbf{B}V(t) \tag{2.78}$$

We choose **P** so that **B** has a Jordan canonical form. Because the transformation $\mathbf{P}^{-1}\mathbf{A}\mathbf{P}$ is a similarity transformation, the eigenvalues of **B** are the same as the eigenvalues of **A**. Furthermore, if the eigenvalues λ_i of **A** (and hence **B**) are distinct, then

$$v_i(t+T) = \lambda_i v_i(t) \text{ for } i = 1,2, ..., n \tag{2.79}$$

where v_i is the ith column of V. These eigenvalues are called Floquet multipliers. It follows from equation (2.79) that

$$v_i(t+kT) = \lambda^k v_i(t) \tag{2.80}$$

where $k = 1,2,3,....$ Thus, the magnitudes of the λ_i determine the long-time behavior of the v_i and hence ξ, which in turn determines the stability of the limit-cycle solution X(t). If $|\lambda_i|$ is less than unity, then v_i decays as time tends to infinity. If $|\lambda_i|$ is greater than unity, then v_i becomes unbounded with time. These results also hold when the eigenvalues of A are not distinct. If λ_i is real and equal to one, v_i is periodic with period T. If λ_i is real and equal to -1, v_i is periodic with period 2T. Because the system of equations (2.69) is autonomous, one of the Floquet multipliers is always unity. Consequently, the limit-cycle solution X(t) is stable if all the other Floquet multipliers lie inside the unit circle in the complex plane and unstable if one or more of the eigenvalues lie outside the unit circle.

2.6.2 Shooting Method

In general, finding a solution to equations (2.69) analytically may not be possible and it may be necessary to solve this system of coupled differential equations numerically. For a linear system, steady-state solutions are unique for a given set of parameters, while for a nonlinear system a number of solutions can coexist for a given set of parameters. Hence, for a linear system, for any set of initial conditions, a single solution can be found. On the other hand, for a nonlinear system, the solution may depend on the initial conditions.

The simplest technique for finding a steady-state response is a long-time integration; that is, the system of equations (2.69) is integrated until all transients decay. If the system is lightly damped this may take a very long time. In addition, for nonlinear systems, reliable methods for determining when these transients will decay generally do not exist. Moreover, long-time integration cannot be used to determine unstable limit cycles. A convenient approach to locate stable and unstable limit cycles is to convert the problem into a two-point boundary-value problem and then use a Newton-Raphson scheme to find a set of initial conditions that will yield a periodic solution without the necessity of long-time integration.

We seek initial conditions η and period T that lead to a periodic solution $x(t;\eta)$ of equations (2.69); that is, if $x(0;\eta)=\eta$ then $x(T;\eta)=\eta$. To find η and T, we use a Newton-Raphson iteration scheme. To this end, we let

$$\eta = \eta_0 + \delta\eta \tag{2.81}$$

where η_0 is the initial guess for η and $\delta\eta$ is the difference between the guess and the actual value; $\delta\eta$ is to be computed for a periodic solution. Moreover, we let

$$T = T_0 + \delta T \tag{2.82}$$

where T_0 is the initial guess for the period and δT is the similar change.

The two-point boundary-value problem can be defined as

$$x(T;\eta) = \eta \tag{2.83}$$

Substituting equations (2.81) and (2.82) into equations (2.83), we obtain

$$x(T_0 + \delta T; \eta_0 + \delta\eta) = \eta_0 + \delta\eta \tag{2.84}$$

Expanding equations (2.84) in a Taylor series and keeping only linear terms, we obtain

$$[\nabla x(T_0; \eta_0) - \mathbf{I}]\delta\eta + \frac{\partial x}{\partial T}(T_0; \eta_0)\delta T = \eta_0 - x(T_0; \eta_0) \tag{2.85}$$

where $\nabla x = \dfrac{\partial x_i}{\partial \eta_j}$ is an nxn matrix. Using equations (2.69) we obtain

$$\frac{\partial x}{\partial T}(T_0; \eta_0) = \dot{x}(T_0; \eta_0) = F(x(T_0; \eta_0)) \tag{2.86}$$

Furthermore,

$$\nabla\dot{x} = \nabla F(x) \tag{2.87}$$

Changing the order of differentiation yields

$$\frac{d}{dt}(\nabla x) = \nabla F(x) \tag{2.88}$$

Hence, integrating equations (2.88), from $t = 0$ to $t = T_0$, using the initial conditions $\nabla x(0) = \mathbf{I}$, we can obtain $\nabla x(T_0)$.

Upon examining equations (2.85), we see that we have n equations for $n + 1$ unknowns. Thus, we need to eliminate one of the unknown $\delta\eta_i$. This is done by setting the η_i that corresponds to the maximum absolute value of F_i equal to zero for every iteration.

If the guessed values of η_0 and T_0 are far away from those corresponding to a periodic solution, the iteration scheme might not converge. Hence, it is desirable, sometimes even necessary, to have a good guess for the limit cycle.

2.6.3 Limit Cycles of the Modulation Equations

As discussed in Section 2.5, the point $F = F_4$ in Figures 2.1-2.3 is a Hopf bifurcation point. Near this point, the modulation equations possess limit-cycle solutions. Using the algorithms described above, we calculated some of these limit cycles and investigated their bifurcations.

As F is increased past F_4, we first obtain a period-one solution. In Figures 2.17-2.21 we show a typical period-one limit-cycle solution obtained when $F = 0.530$. Figures 2.17-2.19 show three projections of the limit cycle. For this system we see that a period-one solution consists basically of a single loop in space, in this case a six dimensional space. The FFT of p_1 is shown in Figure 2.20. The Poincaré section consists of a single point (Figure 2.21).

As F is increased further this limit-cycle solution remains stable until F is nearly equal to 0.531, where one of the Floquet multipliers leaves the unit circle through -1. Hence, the solution is expected to undergo a period-doubling bifurcation. In Figures 2.22-2.26, we show a typical period-doubled limit cycle obtained when $F = 0.533$ In Figures 2.22-2.24 we show three projections of the limit cycle. In Figure 2.25 we show the FFT of the period-two solution. When this FFT is compared to that of the period-one

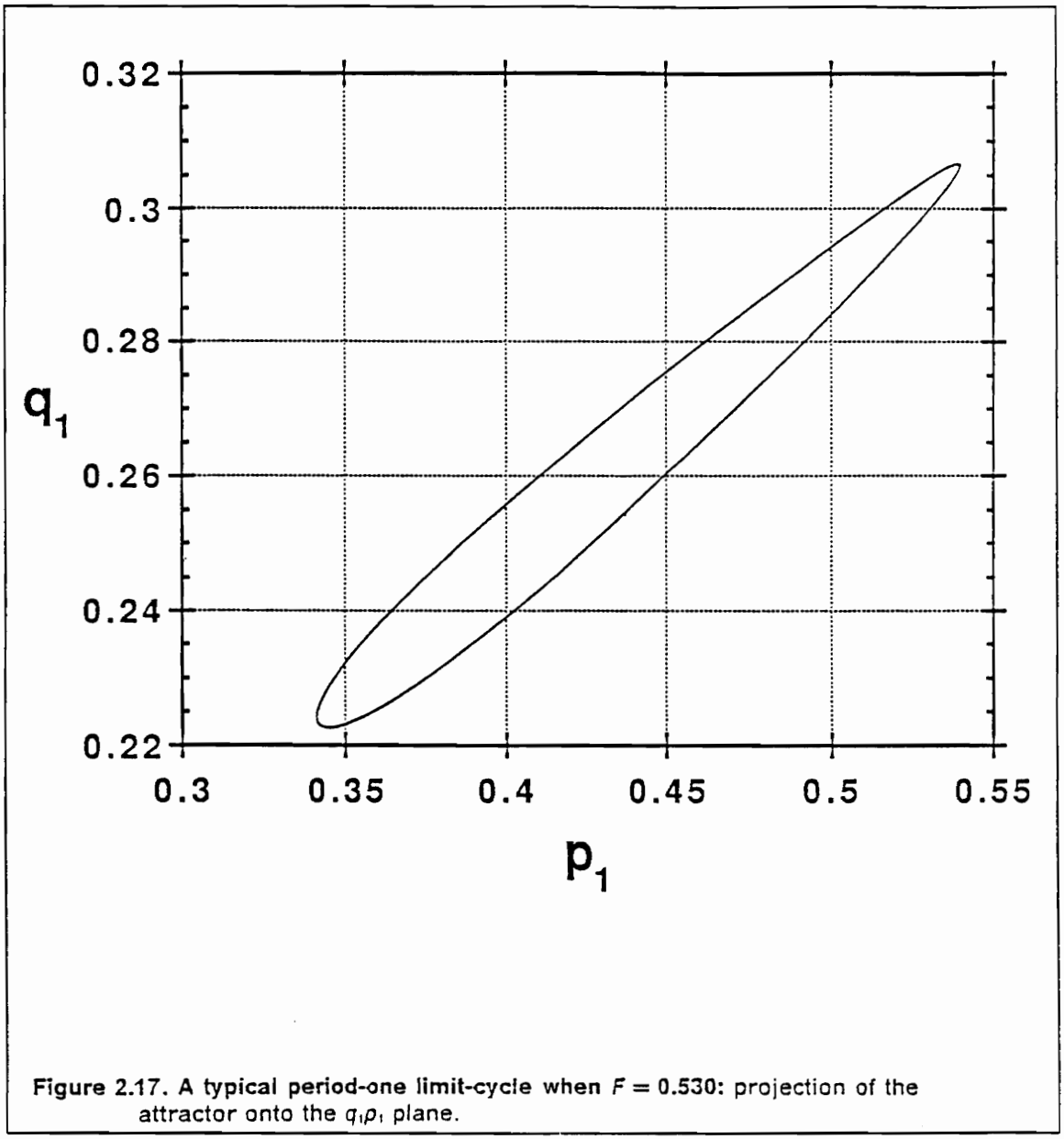

Figure 2.17. A typical period-one limit-cycle when $F = 0.530$: projection of the attractor onto the q_1p_1 plane.

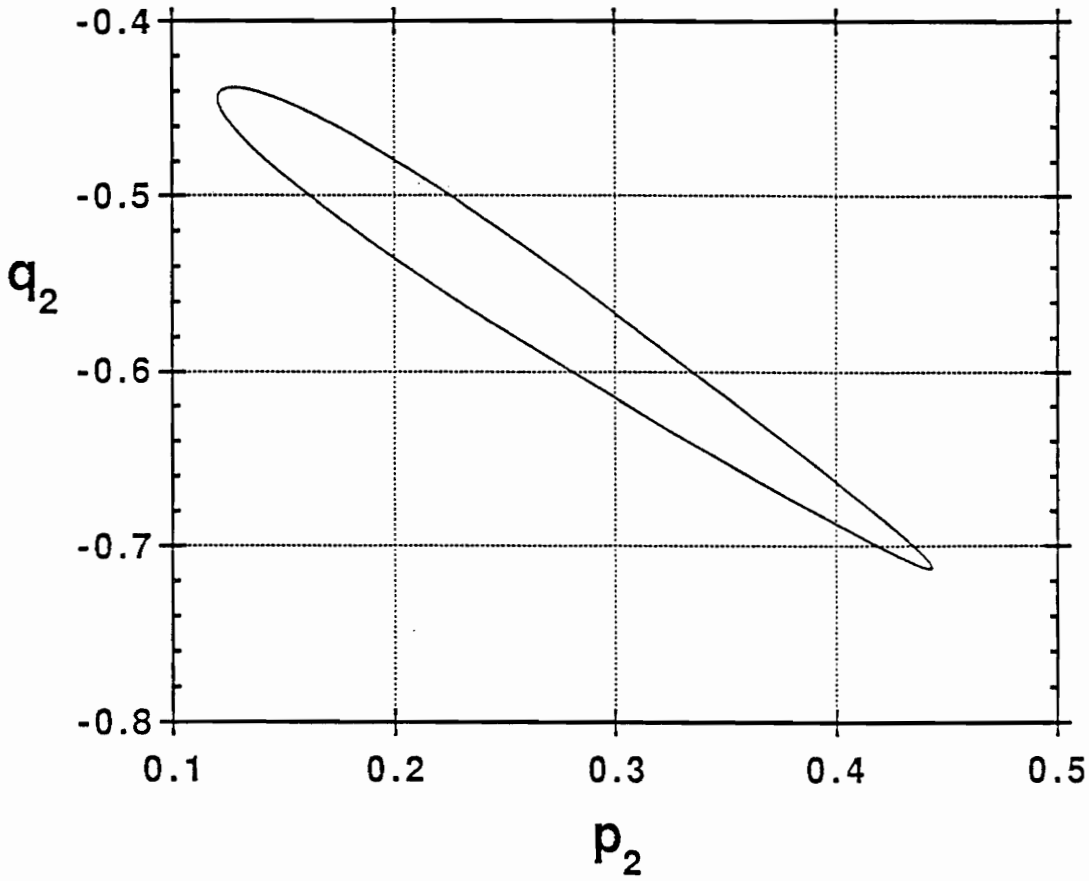

Figure 2.18. A typical period-one limit-cycle when $F = 0.530$: projection of the attractor onto the $q_2 p_2$ plane.

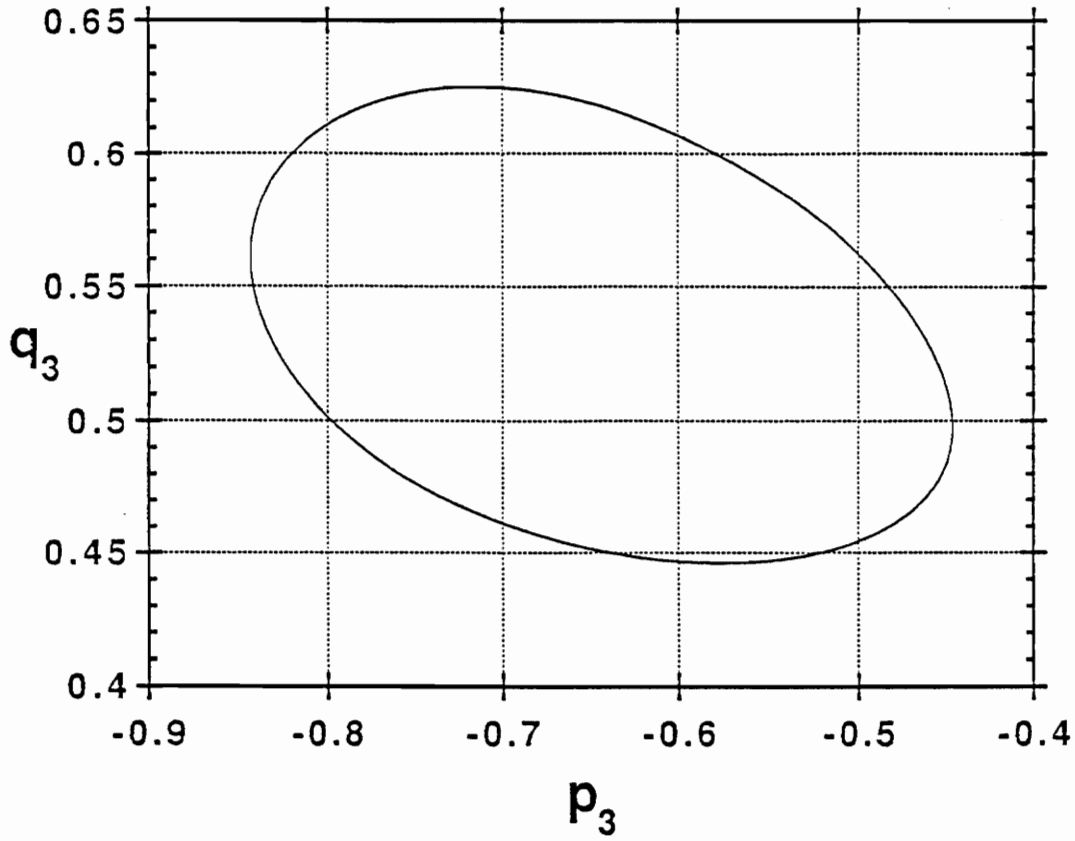

Figure 2.19. A typical period-one limit-cycle when $F = 0.530$: projection of the attractor onto the q_3p_3 plane.

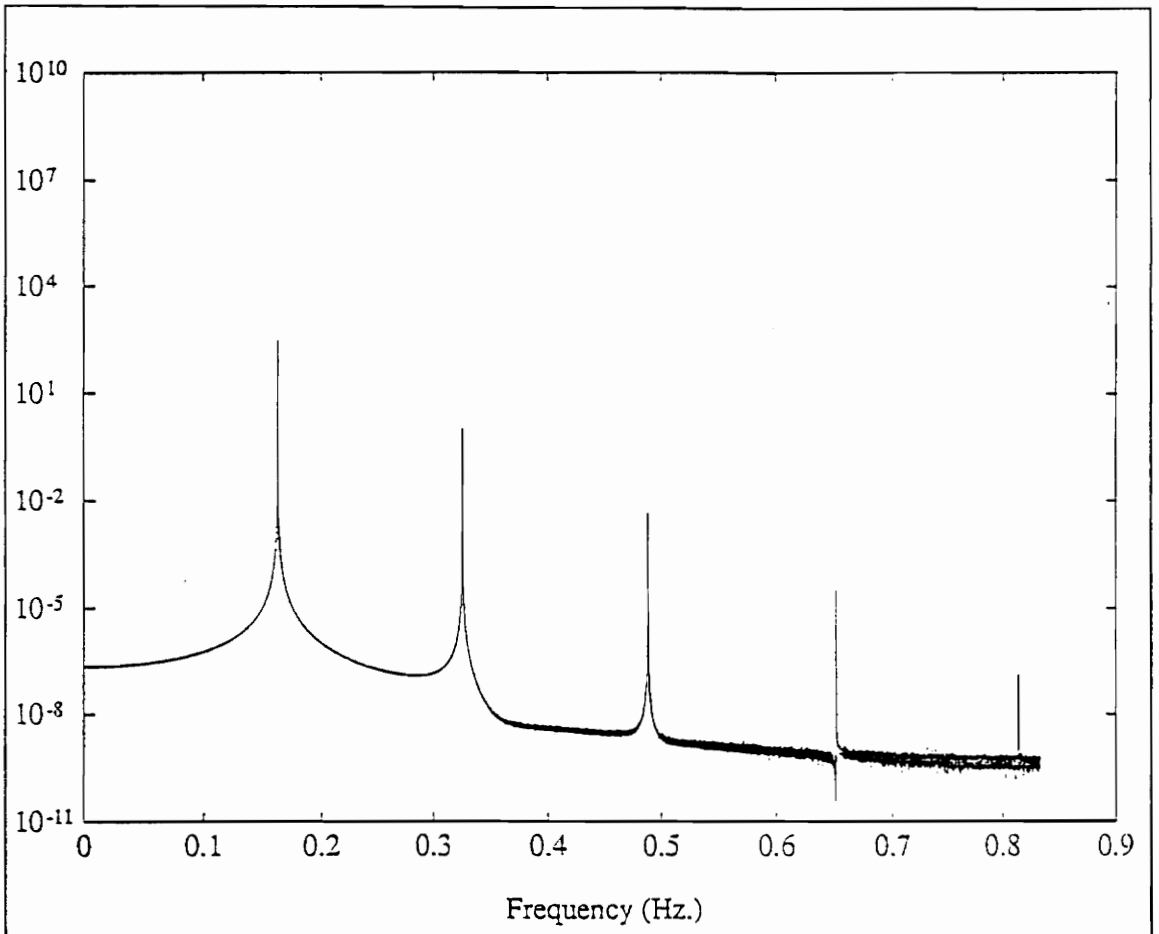

Figure 2.20. The FFT of p_1 for a typical period-one limit-cycle when $F = 0.530$.

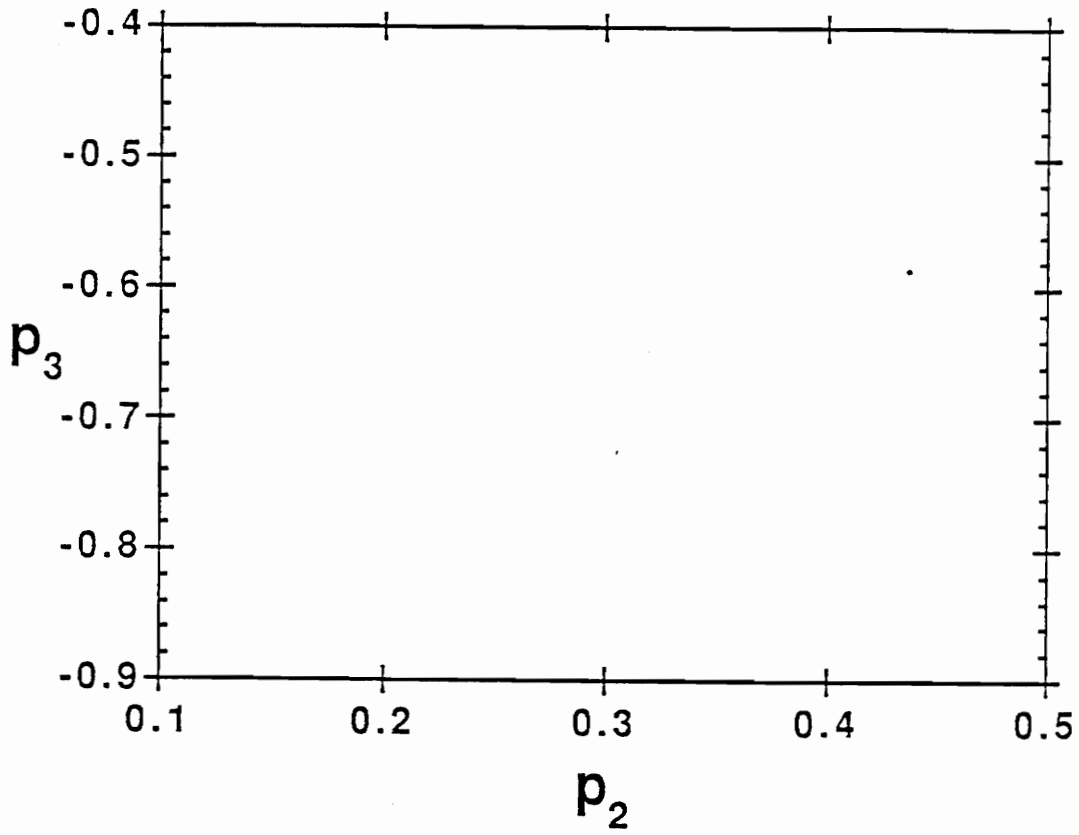

Figure 2.21. A projection of the Poincaré section of a typical period-one limit cycle onto the p_3p_2 plane when $F = 0.530$.

solution in Figure 2.20, we can see that there are distinct peaks midway between the previous peaks. The Poincaré section contains two distinct points as shown in Figure 2.26.

2.6.4 Quasiperiodic solutions

The period-doubled solution remains stable until F reaches approximately 0.5366 where a complex-conjugate pair of Floquet multipliers crosses the unit circle. When this occurs the solution is no longer periodic; instead it becomes quasiperiodic. This type of bifurcation is sometimes referred to as a secondary Hopf or Niemark bifurcation.

In Figures 2.27-2.32 we show a typical two-period quasiperiodic solution (T^2 torus) obtained when $F = 0.537$. In Figures 2.27-2.29, we show three projections of this torus. Unlike the previous limit-cycle solutions, this solution continues to evolve and does not close. When these projections are viewed in real time, they appear as tumbling versions of the limit cycles. In Figure 2.30, we show the FFT of this solution. At a first glance it appears to be chaotic. However, when a portion is expanded (Figure 2.31), we see that it consists of discrete peaks. These peaks are combinations of the two base frequencies of the T^2 torus. In Figure 2.32, we shown a Poincaré section of this solution. Here, the section consists of closed loops. The loops indicate that there are two frequencies present. There are two loops present because the torus itself loops around twice.

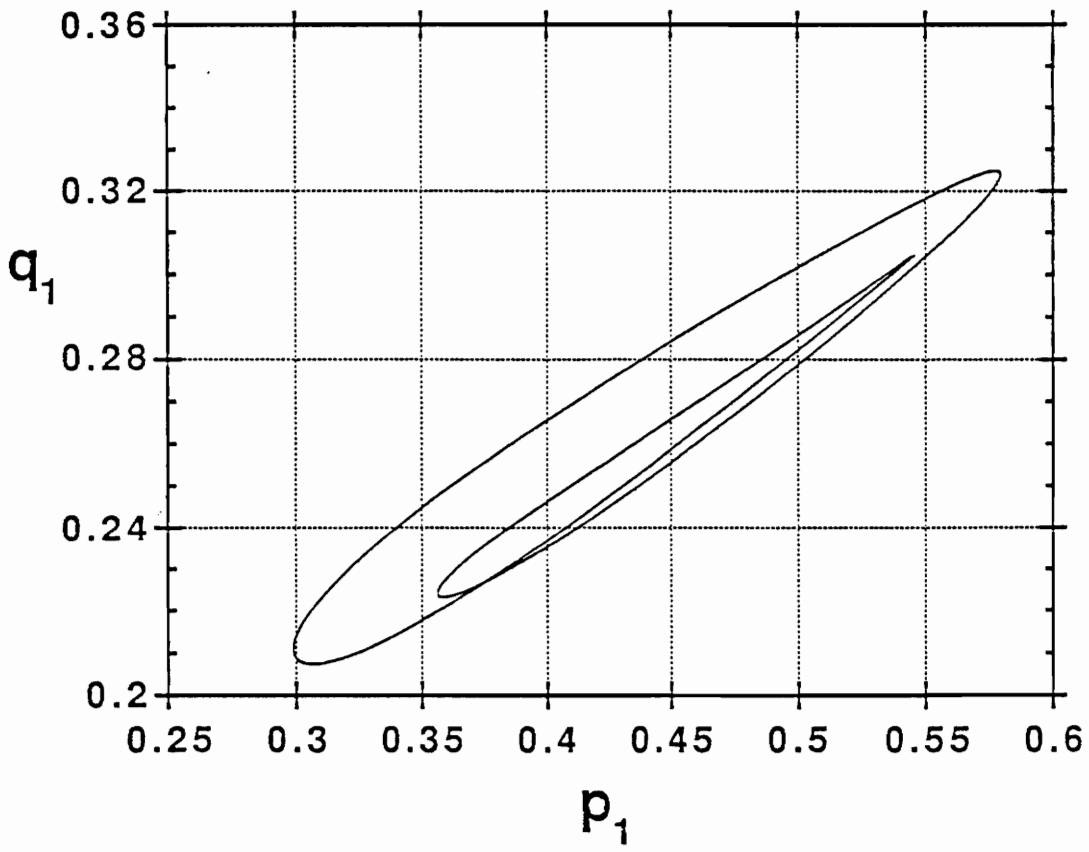

Figure 2.22. A typical period-two limit cycle when $F = 0.533$: projection of the attractor onto the p_1q_1 plane.

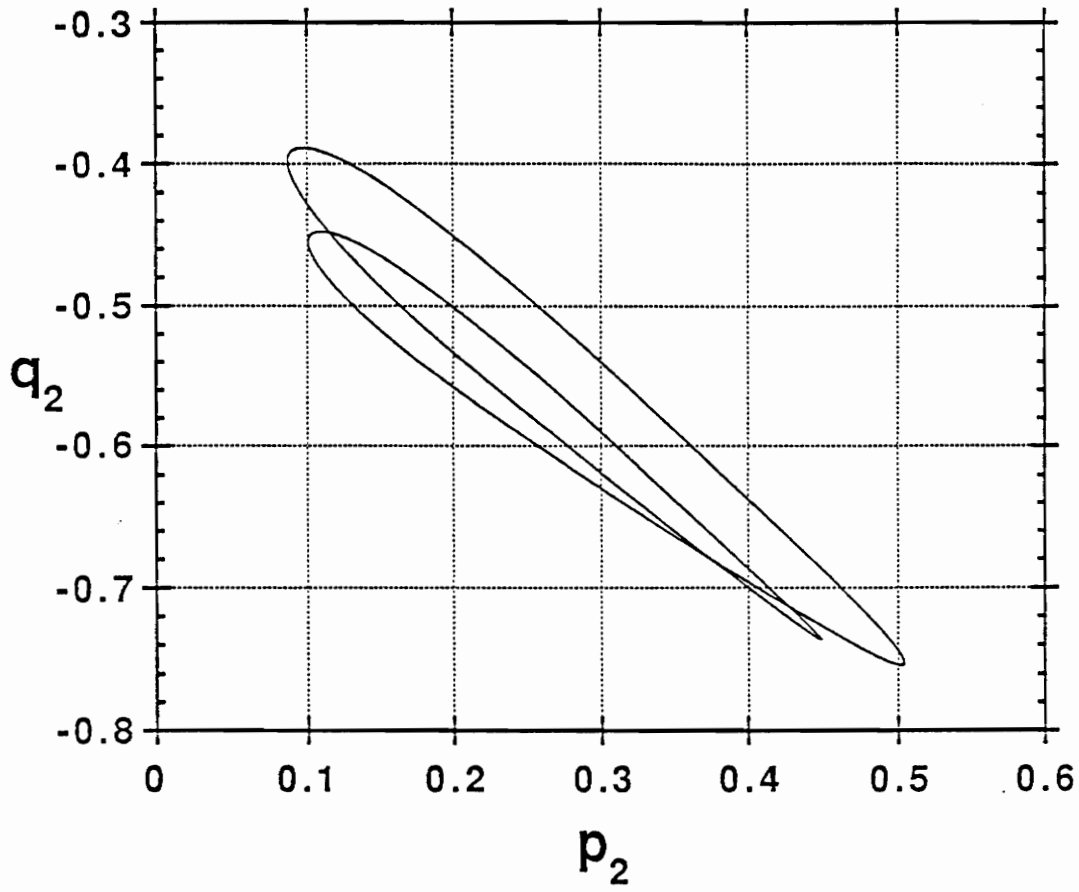

Figure 2.23. .A typical period-two limit cycle when $F = 0.533$: projection of the attractor onto the p_2q_2 plane.

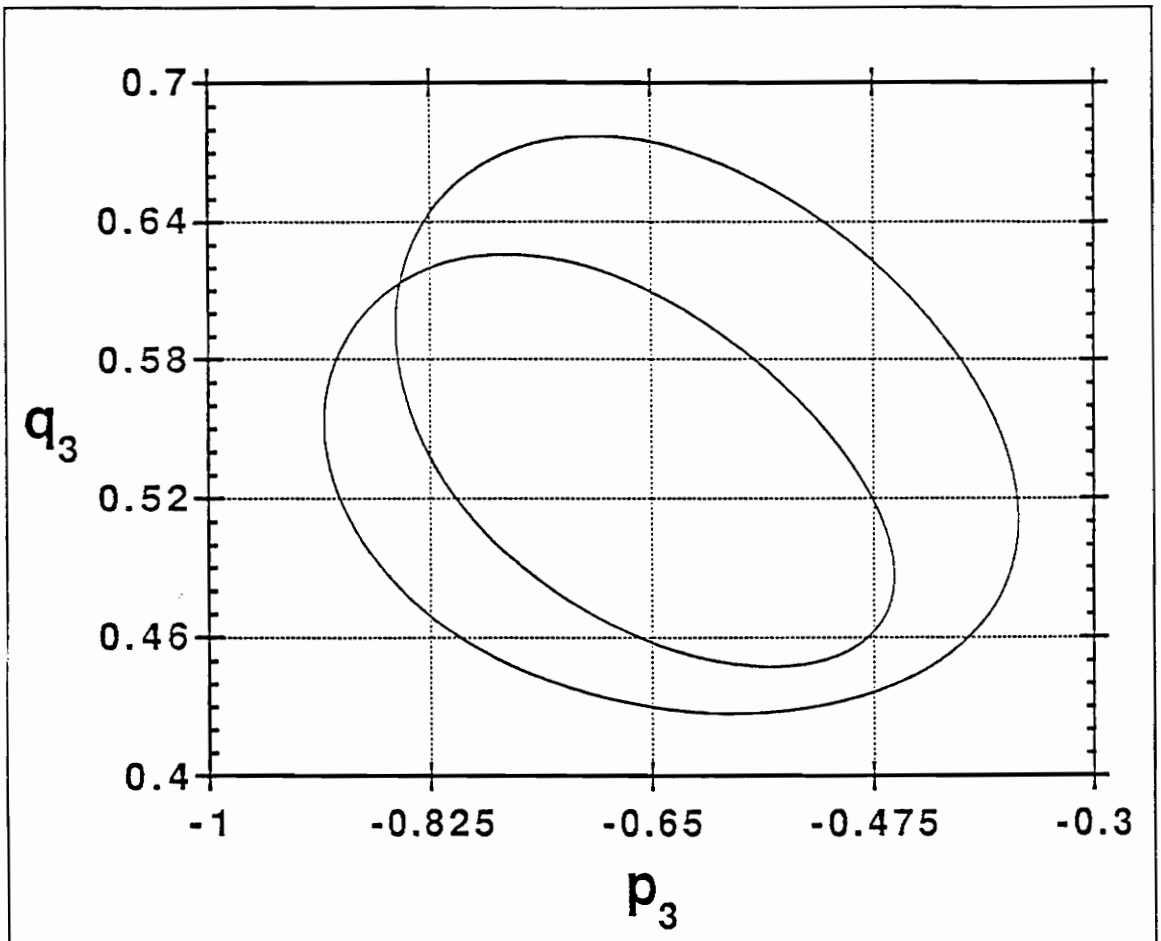

Figure 2.24. A typical period-two limit cycle when $F = 0.533$: projection of the attractor onto the q_3p_3 plane.

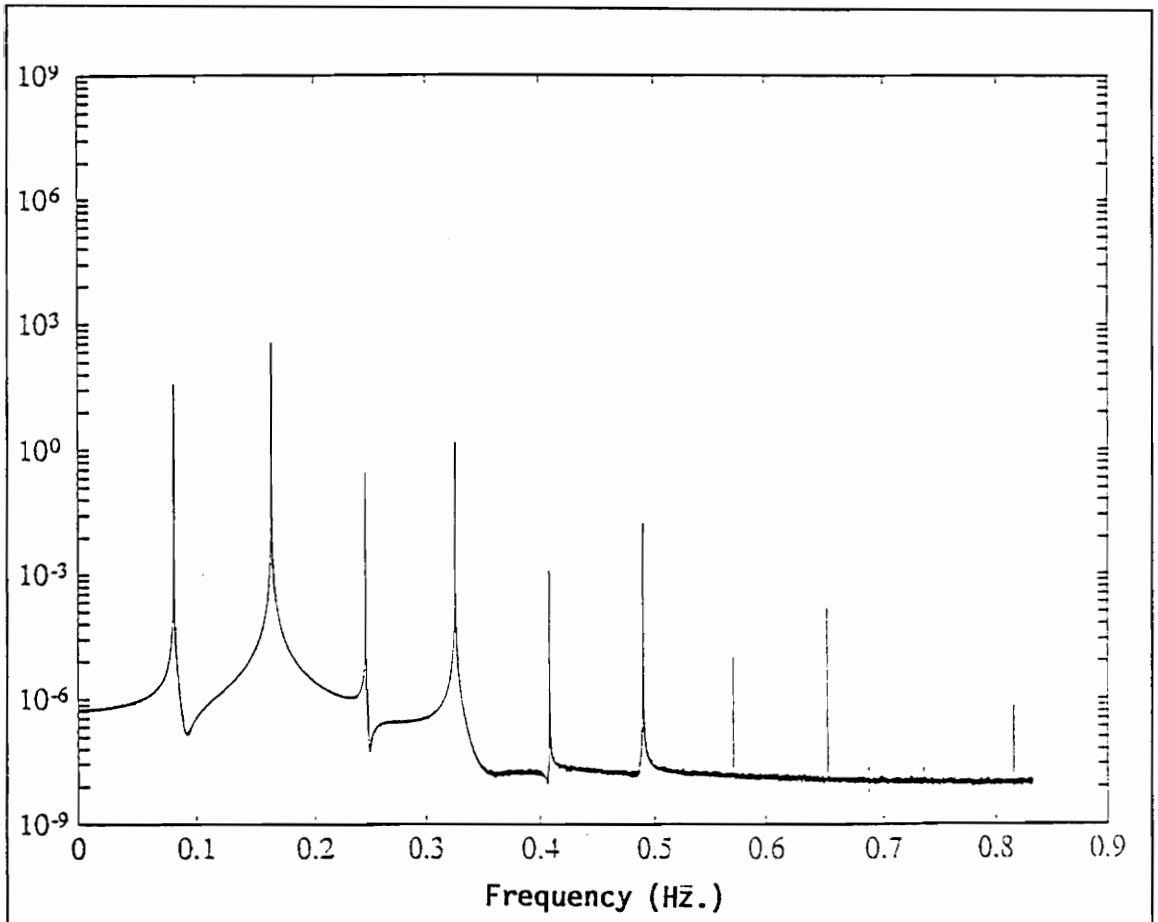

Figure 2.25. The FFT of p_1 for a typical period-two limit-cycle when $F = 0.533$.

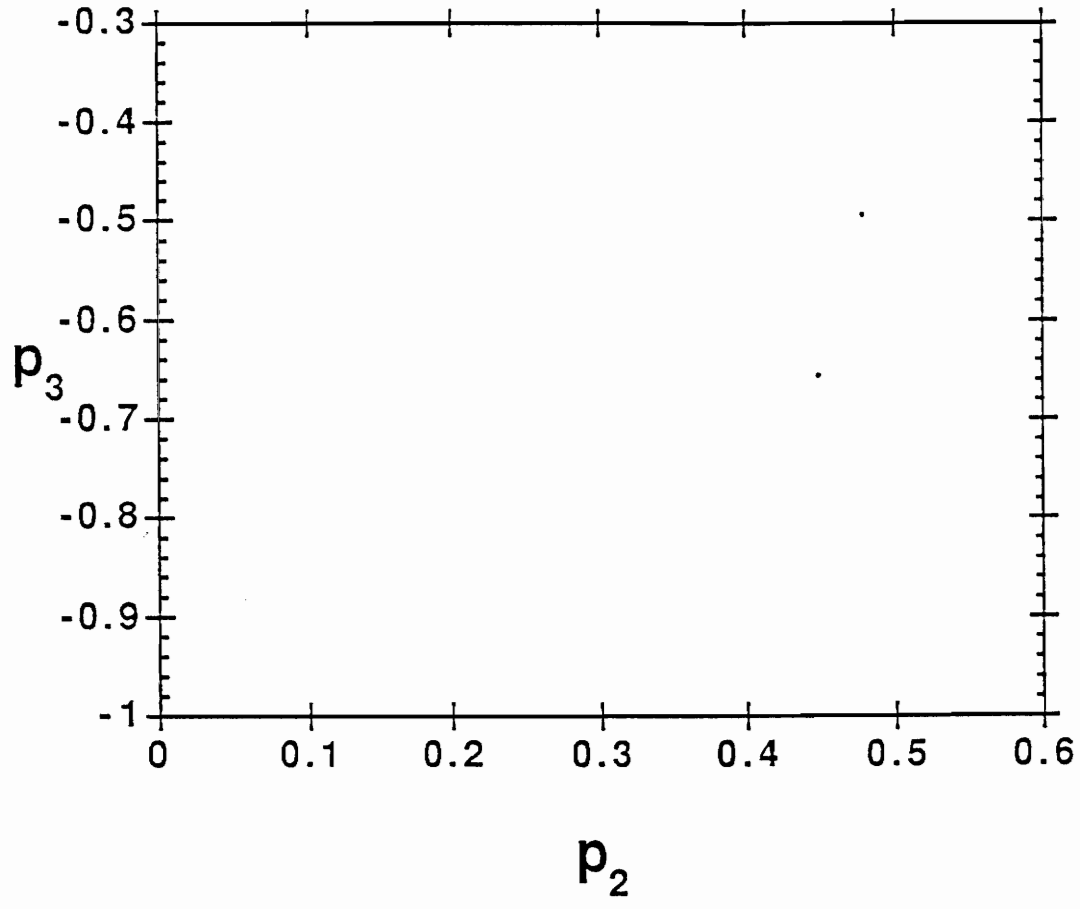

Figure 2.26. A projection of the Poincaré section of a typical period-two limit cycle onto the p_3p_2 plane when $F = 0.533$.

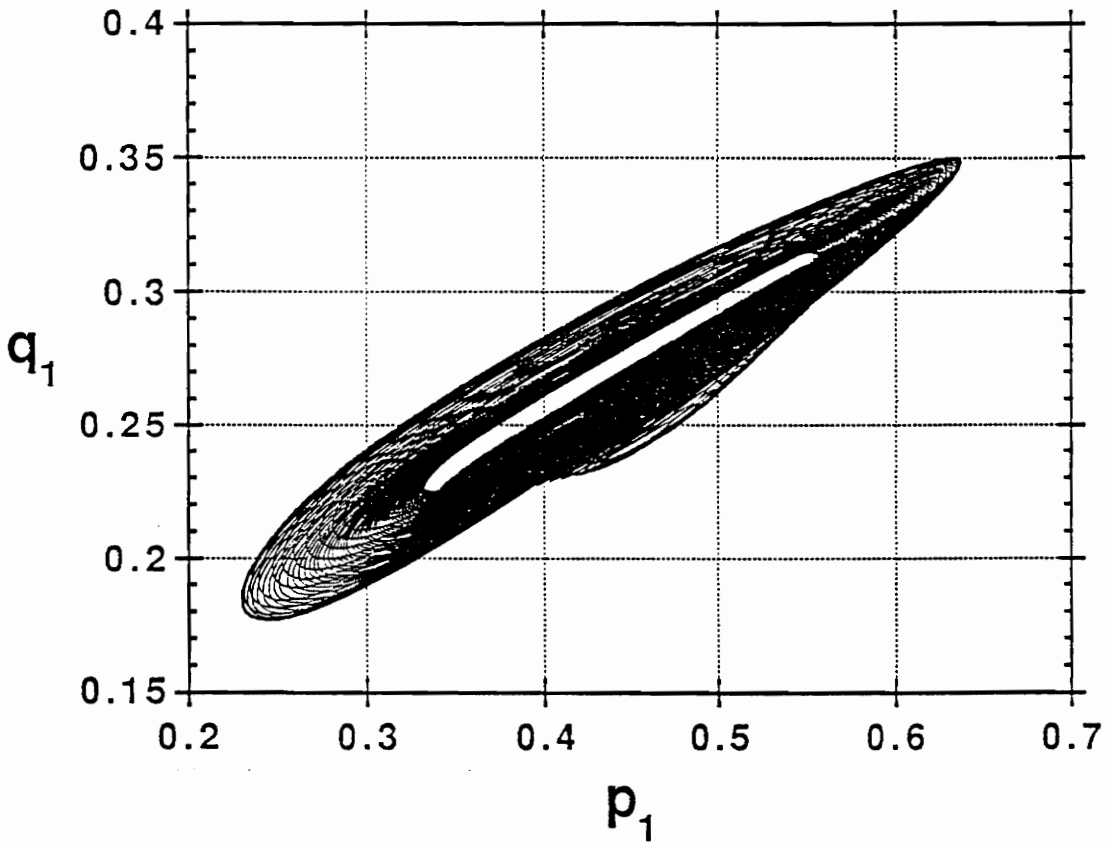

Figure 2.27. A typical quasiperiodic solution when $F = 0.537$: projection of the attractor on the q_1p_1 plane.

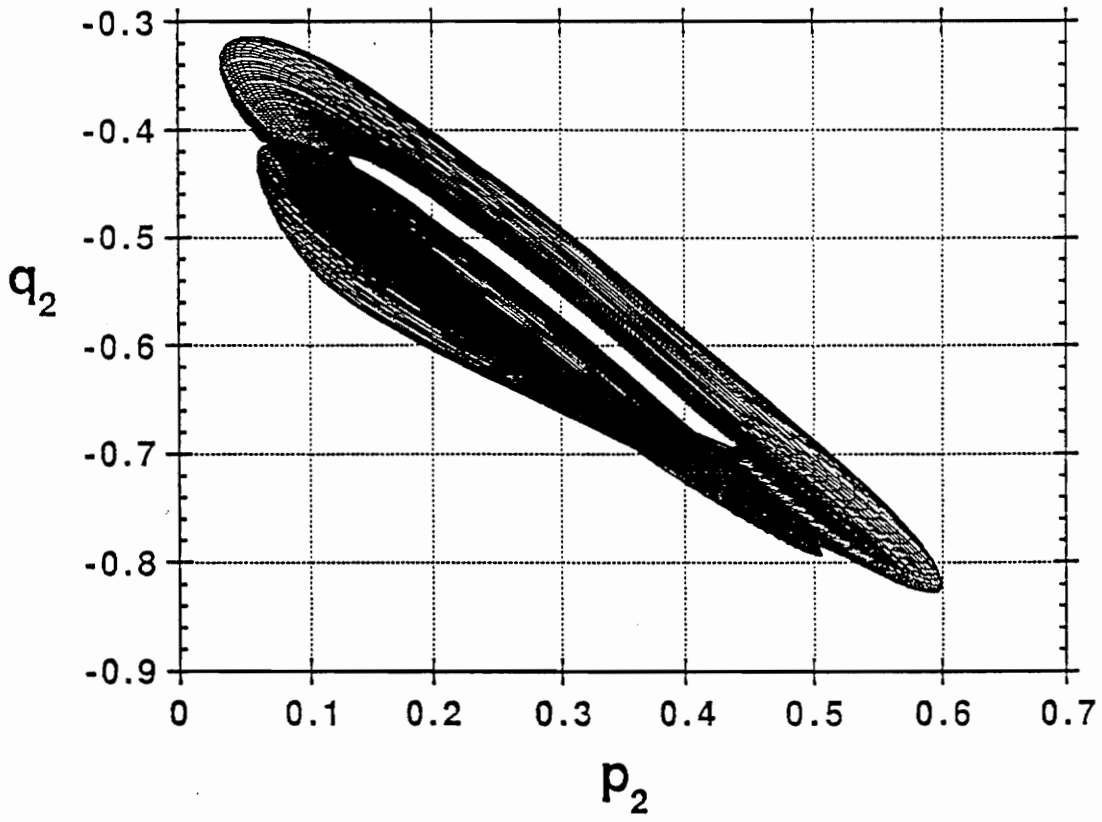

Figure 2.28. A typical quasiperiodic solution when $F = 0.537$: projection of the attractor on the q_2p_2 plane.

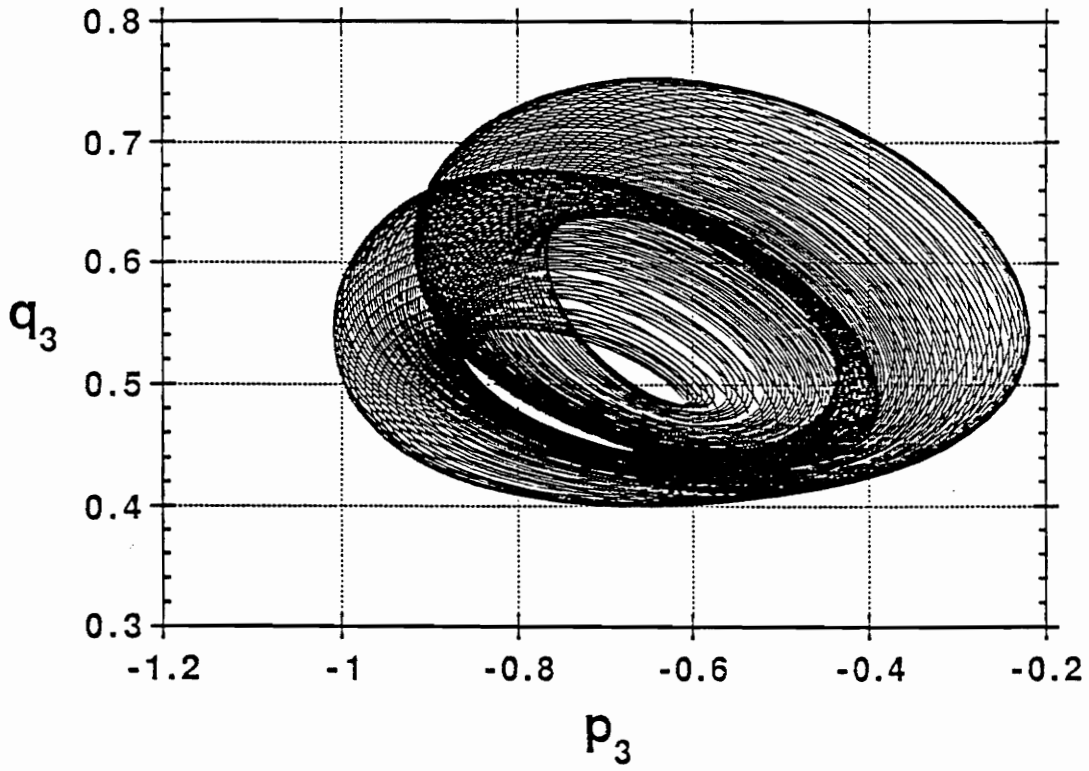

Figure 2.29. A typical quasiperiodic solution when $F = 0.537$: projection of the attractor on the q_3p_3 plane.

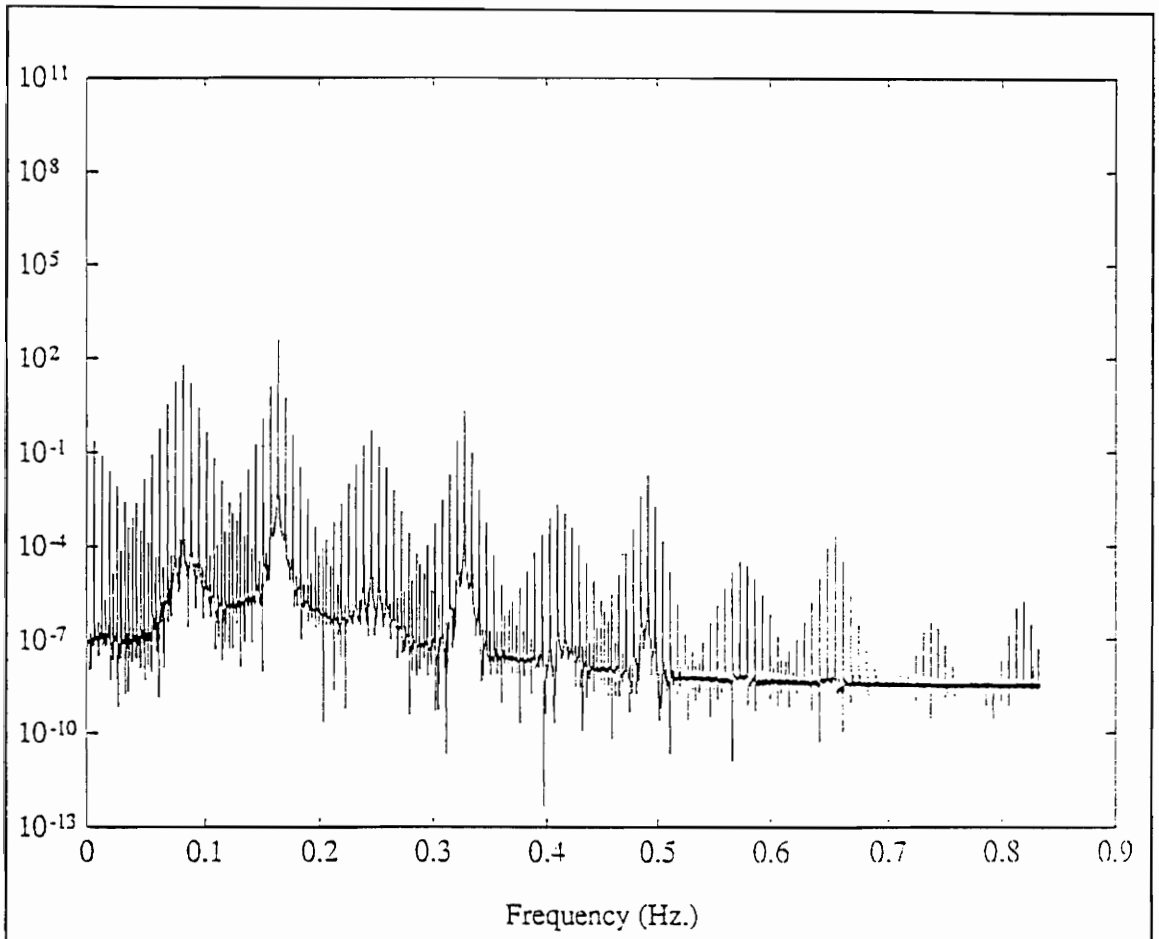

Figure 2.30. The FFT of p_1 for a typical quasiperiodic solution when $F = 0.537$.

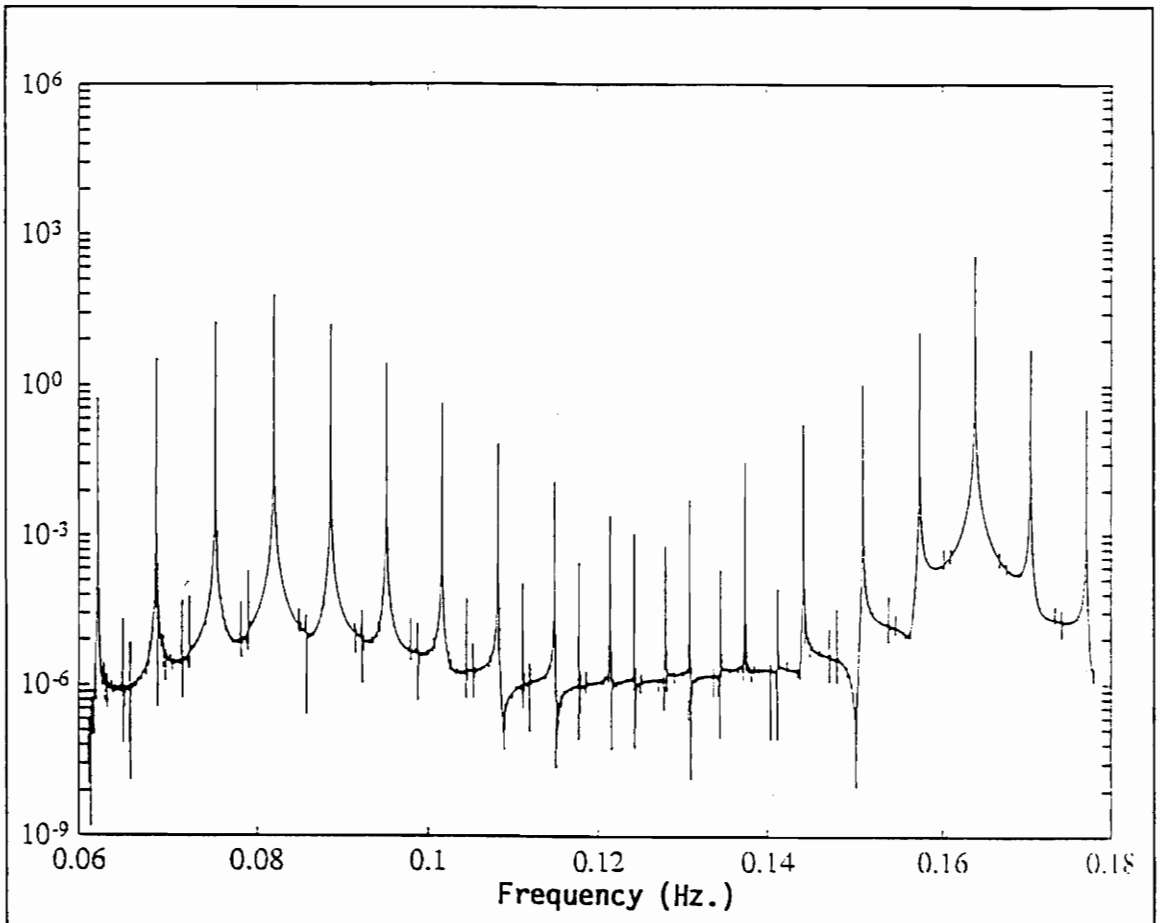

Figure 2.31. Expanded portion of the FFT of p_1 for a typical quasiperiodic solution when $F = 0.537$.

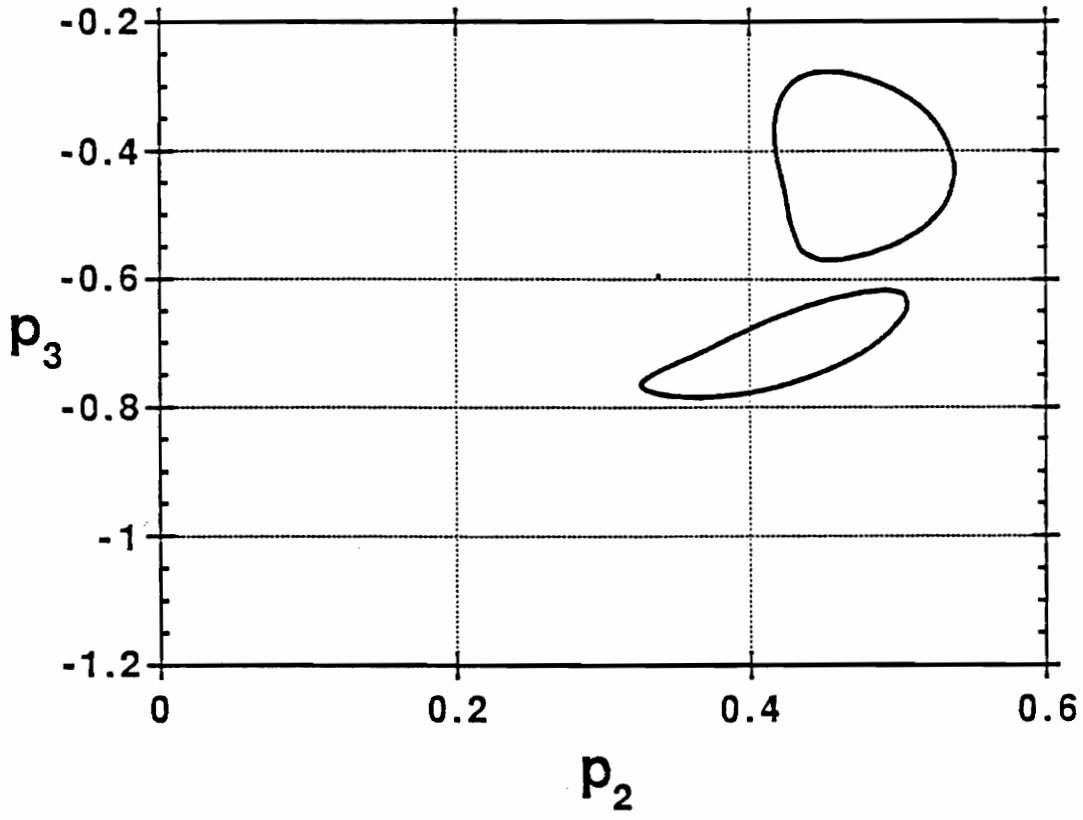

Figure 2.32. A projection of the Poincaré section of a typical quasiperiodic solution onto the p_3p_2 plane when $F = 0.537$.

The T^2 torus breaks down as F is increased past $F = 0.53719$. The motion then becomes synchronous with the ratio of the two base frequencies becoming an integer. In Figures 2.33-2.38, we show a typical frequency-locked solution when $F = 0.5372$. The phase space (Figures 2.33-2.35) closely resembles that of the quasiperiodic solution. However, when it is viewed in real time, the trajectory no longer tumbles. The peaks in the FFT of Figures 2.36 and 2.37 are shifted to the right, indicating a shift in at least one of the base frequencies. The difference between the quasiperiodic and frequency-locked solutions is most apparent in the Poincaré sections. In Figure 2.38, the Poincaré section contains a finite number of points. The total number of points is the ratio between the two base frequencies. The section for the quasiperiodic solution (Figure 2.32) is a set of an infinite number of points.

The frequency-locked solution remains stable until $F \approx 0.539$ where it becomes chaotic and the T^2 torus breaks down. In Figures 2.39-2.44 we show a typical chaotic solution. A portion of the phase space (Figures 2.39-2.41) is almost completely filled up. The FFT (Figures 2.42 and 2.43) of p_1 shows an obvious broadband structure. The Poincaré section (Figure 2.44) consists of scattered points with no definite pattern that do not overlap.

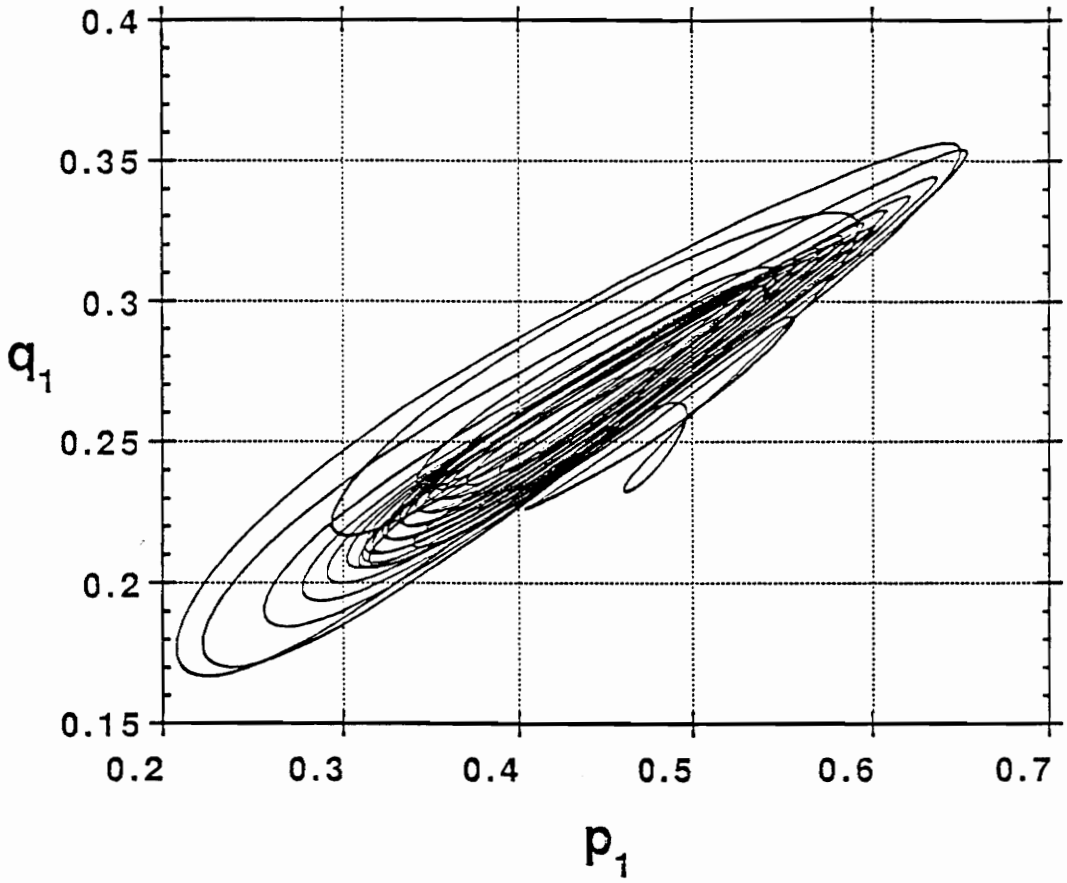

Figure 2.33. A typical synchronous solution when $F = 0.5372$: projection of the attractor onto the q_1p_1 plane.

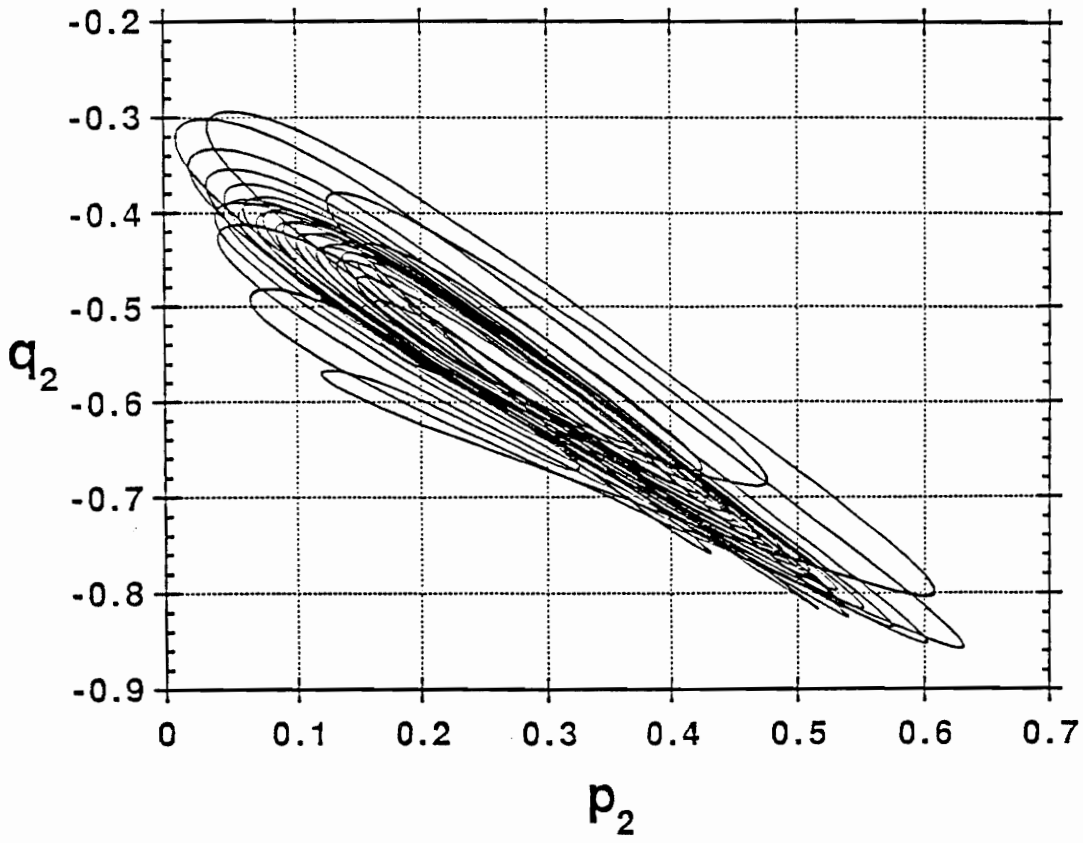

Figure 2.34. A typical synchronous solution when $F = 0.5372$: projection of the attractor onto the q_2p_2 plane.

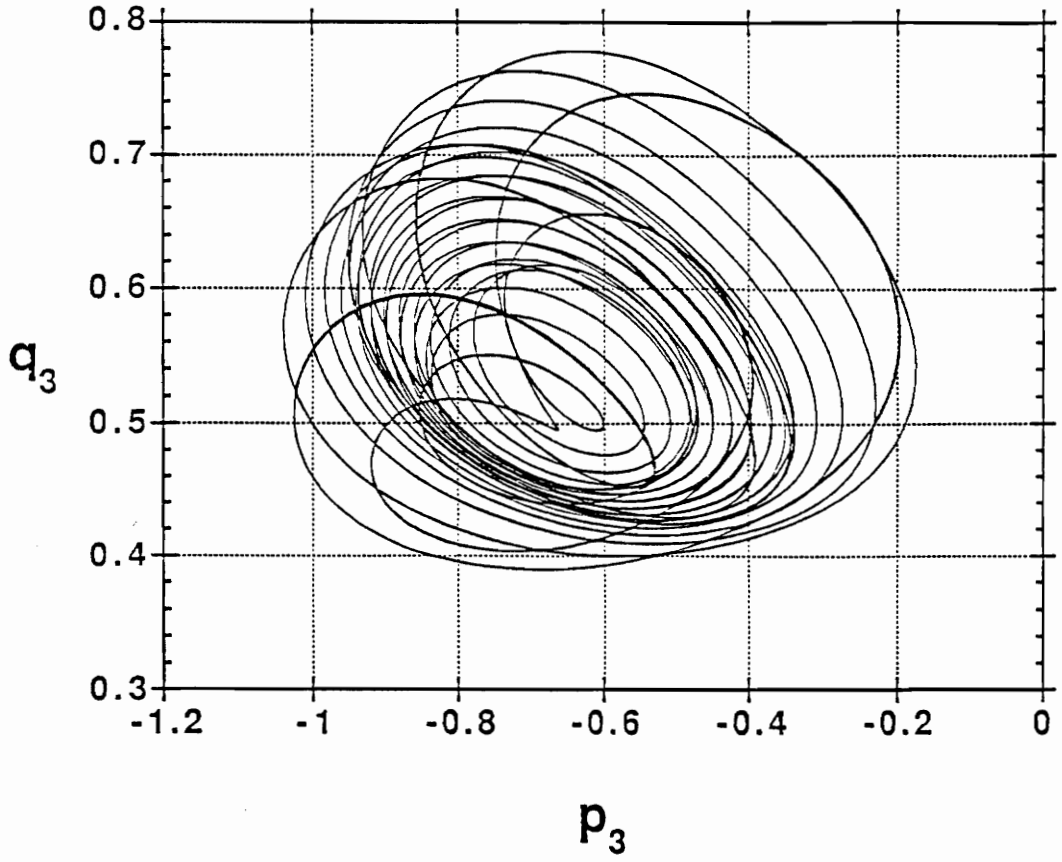

Figure 2.35. A typical synchronous solution when $F = 0.5372$: projection of the attractor onto the q_3p_3 plane.

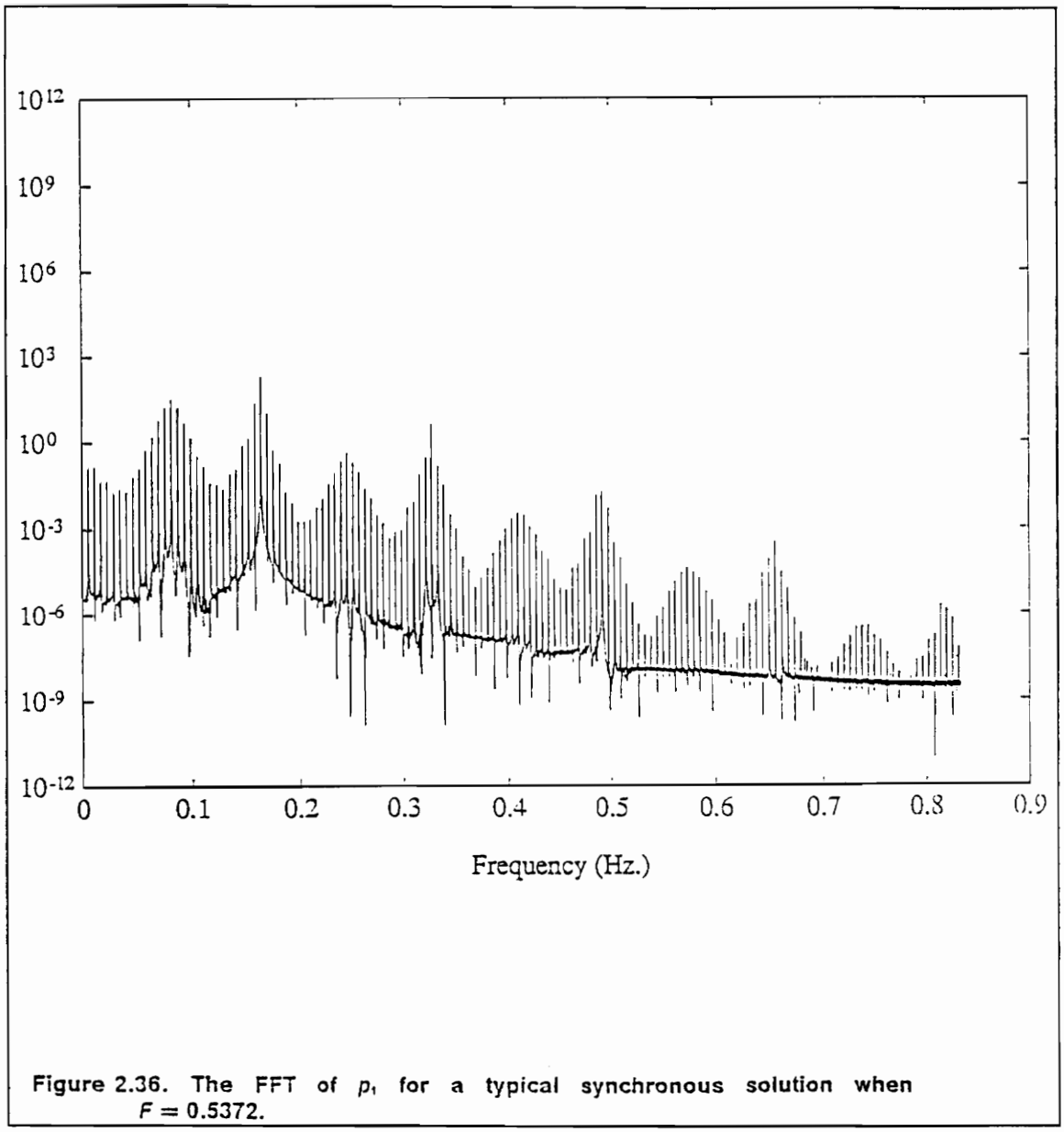

Figure 2.36. The FFT of p_1 for a typical synchronous solution when $F = 0.5372$.

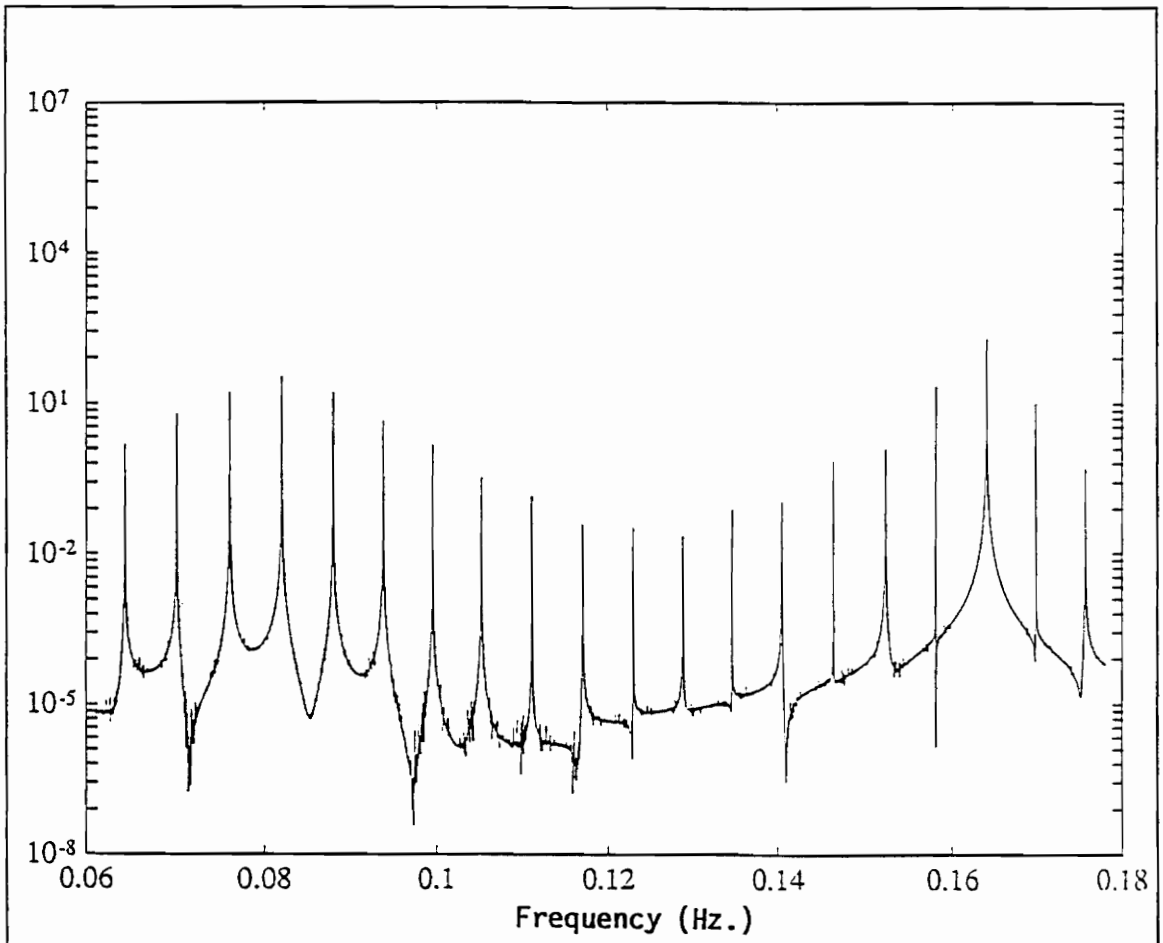

Figure 2.37. Expanded portion of the FFT of p_1 for a typical synchronous solution when $F = 0.5372$.

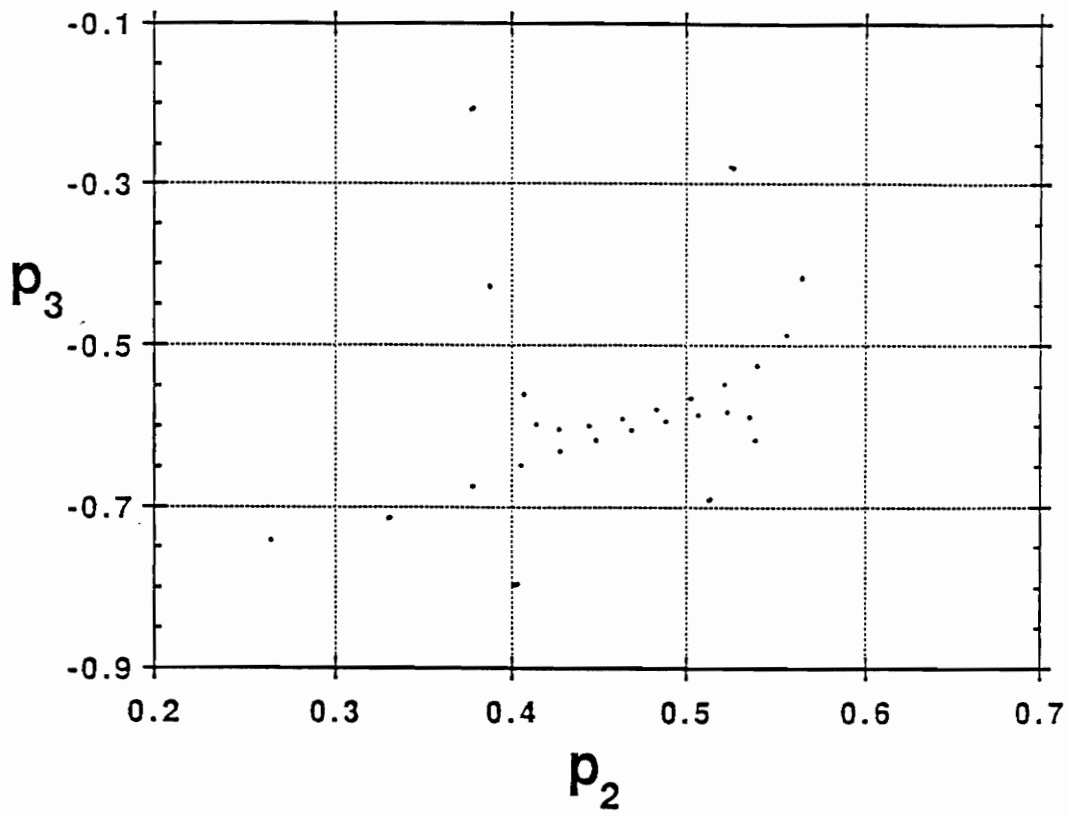

Figure 2.38. A projection of the Poincaré section of a typical synchronous solution onto the p_3p_2 plane when $F = 0.5372$: there are 9000 points in this section.

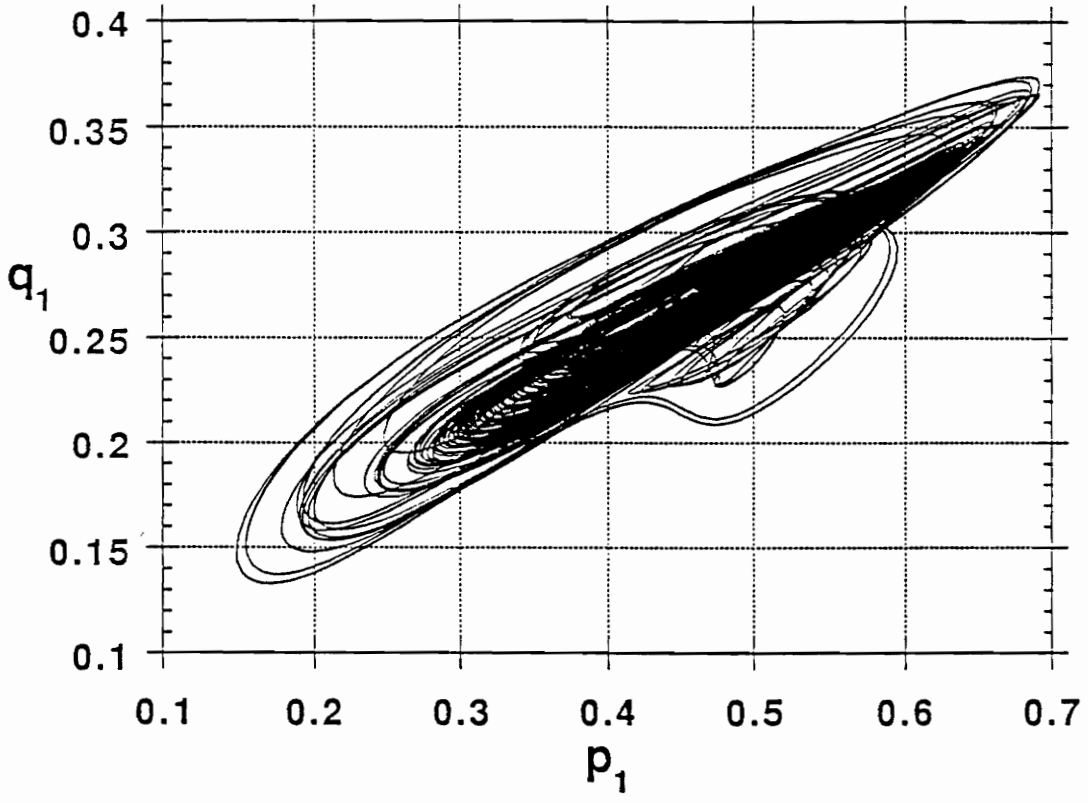

Figure 2.39. A typical chaotic solution when $F = 0.539$: projection of the attractor onto the $q_1 p_1$ plane.

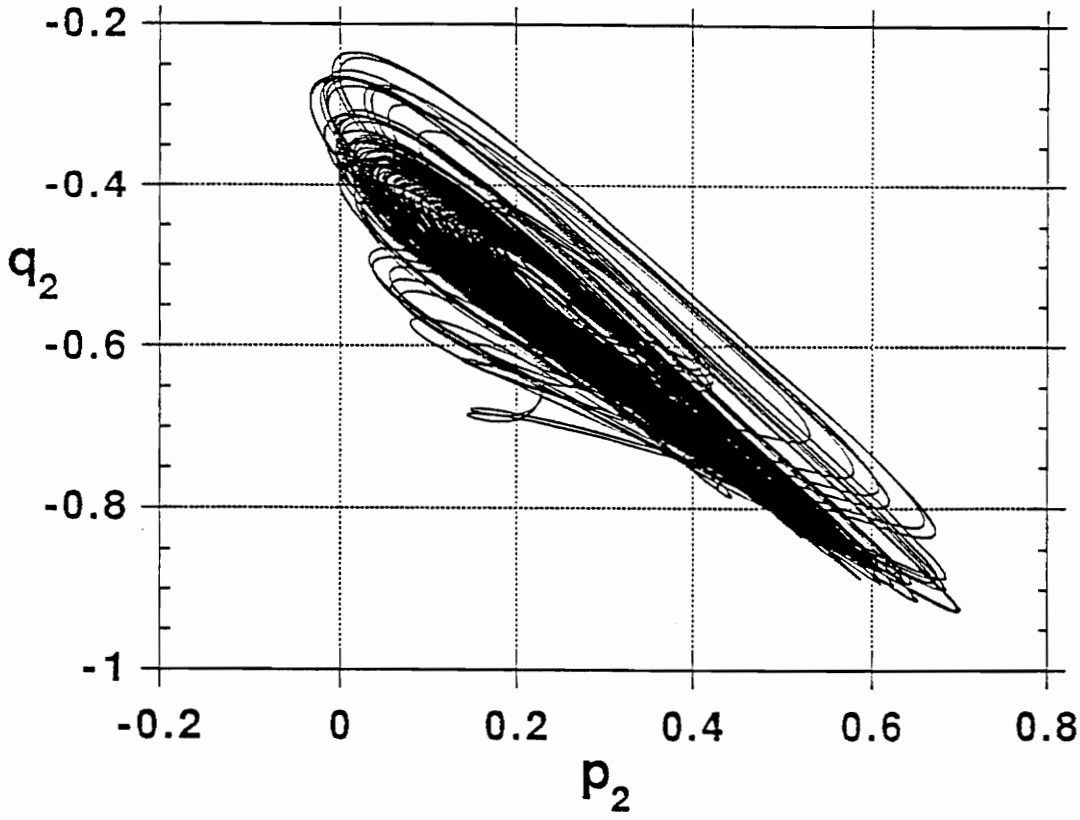

Figure 2.40. A typical chaotic solution when $F = 0.539$: projection of the attractor onto the q_2p_2 plane.

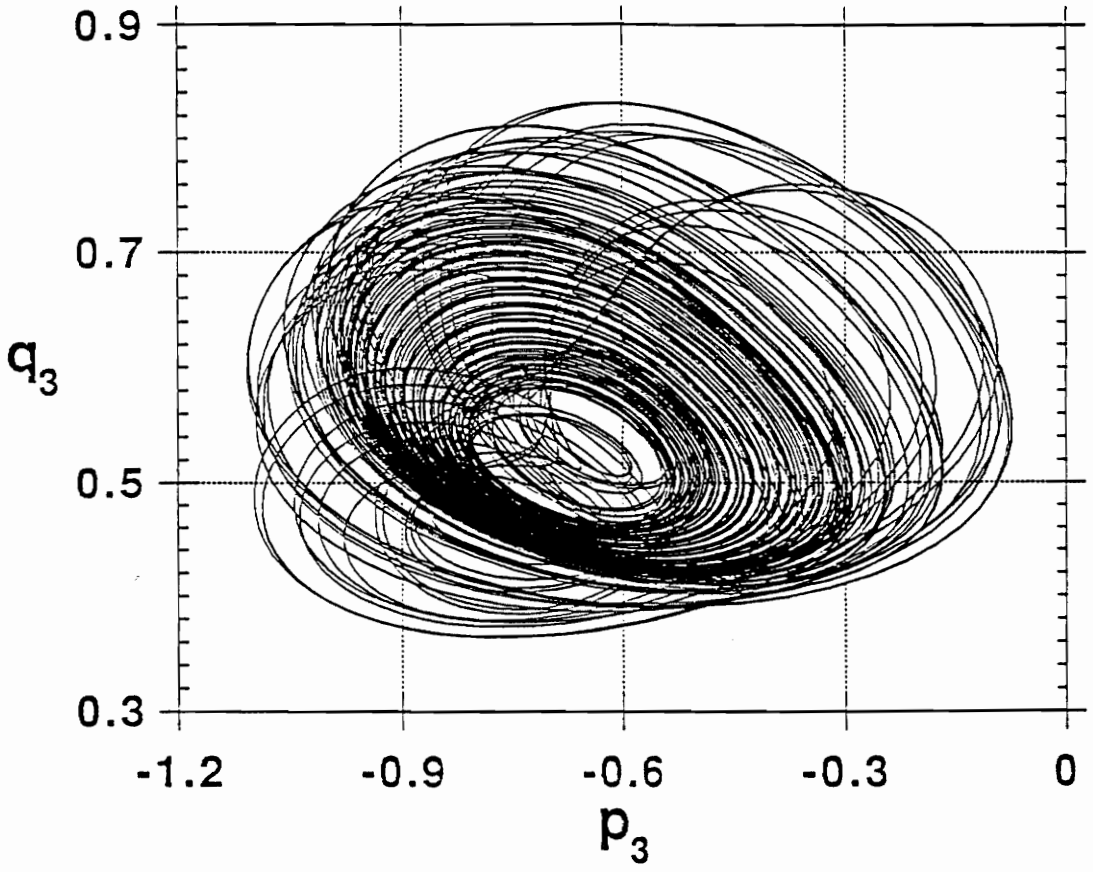

Figure 2.41. A typical chaotic solution when $F = 0.539$: projection of the attractor onto the q_3p_3 plane.

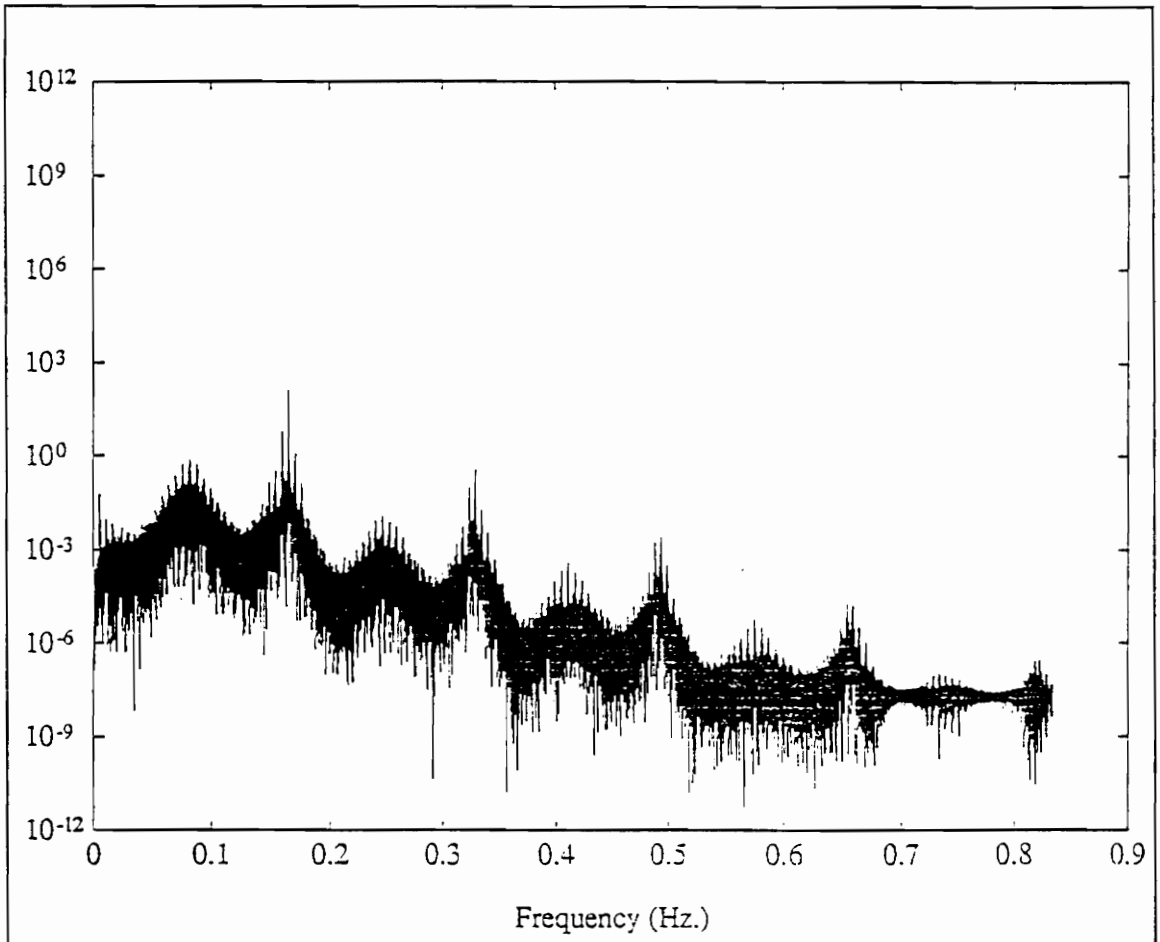

Figure 2.42. The FFT of p_1 for a typical chaotic solution when $F = 0.539$.

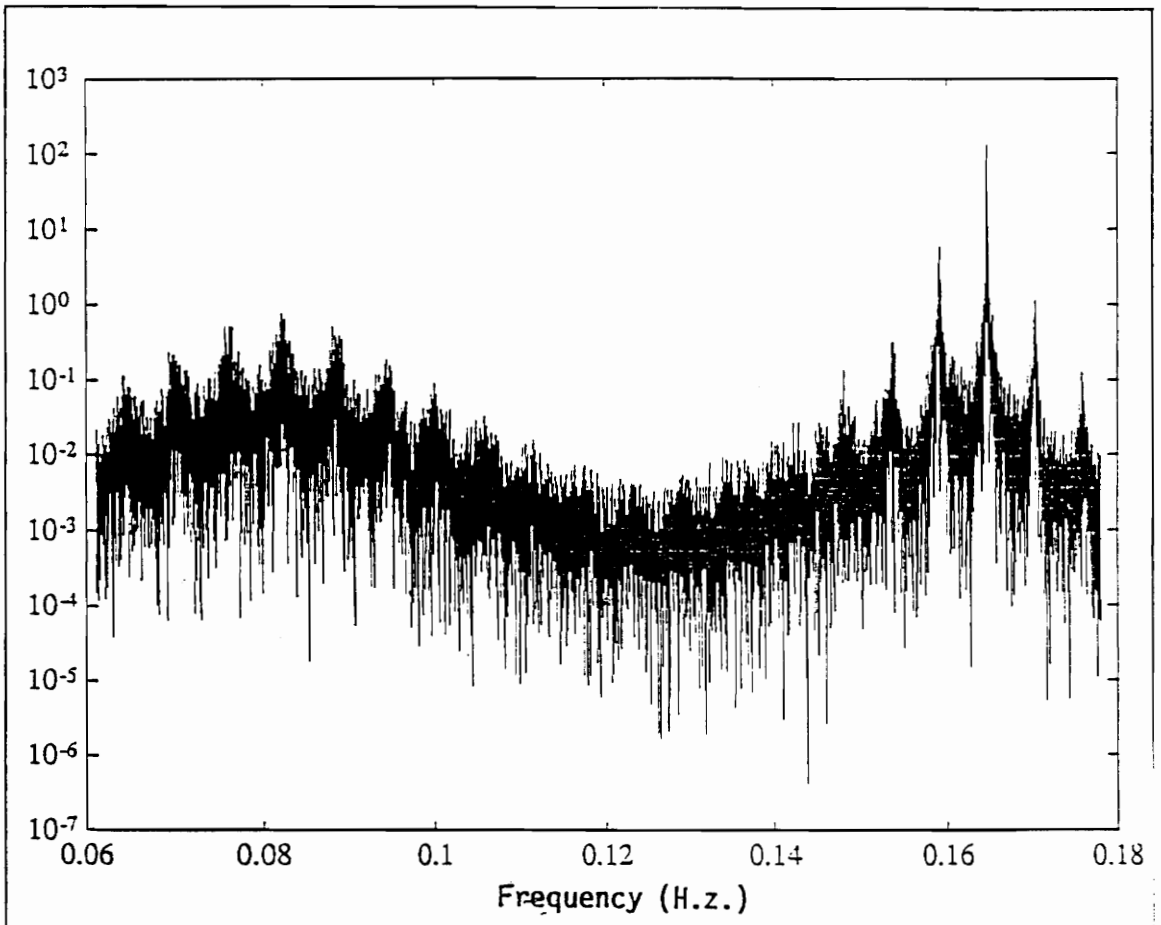

Figure 2.43. Expanded portion of the FFT of p_1 for a typical chaotic solution when $F = 0.539$.

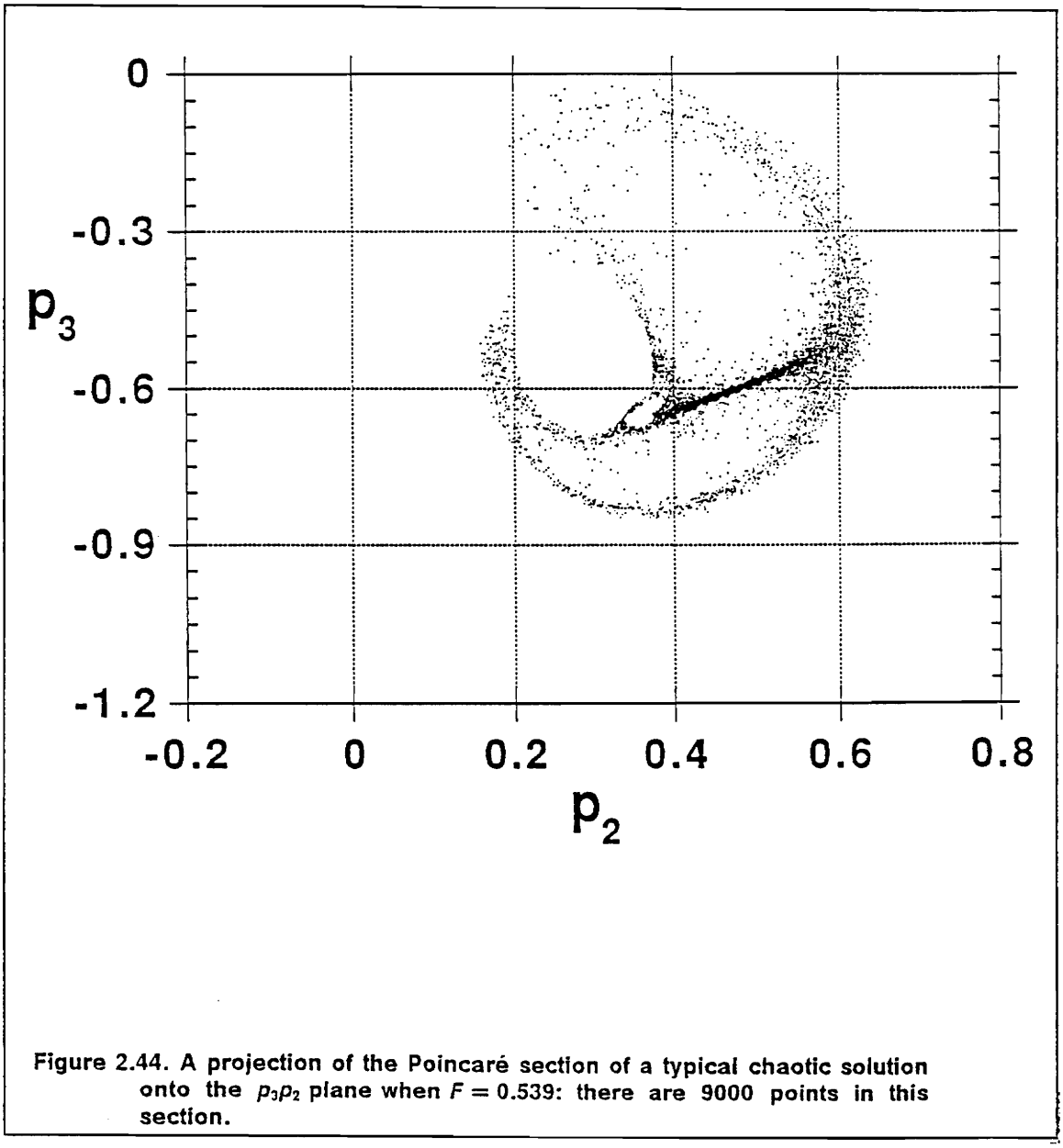

Figure 2.44. A projection of the Poincaré section of a typical chaotic solution onto the p_3p_2 plane when $F = 0.539$: there are 9000 points in this section.

2.7 Conclusions

We study the response of a general three-degree-of-freedom system with the internal resonant conditions $\omega_3 \approx 2\omega_2 \approx 4\omega_1$ to a primary resonant excitation of the third mode. The method of multiple time scales is used to obtain the amplitude- and phase-modulation equations. We determine the fixed-point solutions of these equations and their stability. These fixed points undergo Hopf bifurcations and hence the modulation equations possess limit-cycle solutions near these bifurcations. The limit-cycle solutions undergo a period-doubling bifurcation. Then, the resulting limit cycle undergoes a secondary Hopf bifurcation, resulting in a T^2 torus. The T^2 torus becomes phase-locked and then breaks down into chaos.

CHAPTER 3

Combination Internal Resonance

In this chapter we conduct a theoretical-experimental investigation of the response of a three-degree-of-freedom structure having an autoparametric combination resonance of the additive type to a primary resonant excitation of the highest mode. The structure consists of two light-weight beams and three concentrated masses arranged in a T-shape. The method of multiple scales is used to determine six first-order nonlinear ordinary differential equations describing the modulation of the amplitudes and phases of the three modes with nonlinearity, damping, and resonances. The predicted nonlinear phenomena include the saturation phenomenon, coexistence of stable solutions, jumps, periodic motions, and two- and three-period quasiperiodic motions. The experiment confirms these predictions.

3.1 Introduction

In this chapter, we consider the case of a combination internal resonance of the additive type (i.e., $\omega_3 \approx \omega_2 + \omega_1$) with a primary resonant excitation of the third mode (i.e., $\Omega \approx \omega_3$). The Lagrangian that describes the system considered is

$$\mathscr{L} = \frac{1}{2}\left[\sum_{s}^{3}\left(\dot{u}_s^2 - \omega_s^2 u_s^2 + 2\delta_{s3}\hat{F}_s u_s \cos\Omega_s t\right) - \sum_{i,j,k}^{3}\left(M_{ijk}u_i\dot{u}_j\dot{u}_k + K_{ijk}u_i u_j u_k\right)\right] \quad (3.1)$$

We use the time-averaged-Lagrangian method to obtain the modulation equations which describe the amplitudes and phases of the response.

3.2 The Time-Averaged-Lagrangian Method of Solution

To quantitatively describe the nearness of the internal and primary resonances, we introduce the detuning parameters σ_1 and σ_2 defined as

$$\omega_3 = \omega_2 + \omega_1 + \varepsilon\sigma_1 \text{ and } \Omega = \omega_3 + \varepsilon\sigma_2 \quad (3.2)$$

where ε is a dimensionless parameter that is used as a bookkeeping device and will be set equal to unity in the final solution.

We seek a solution of the form

$$u_s = \varepsilon A_s(T_1)e^{i\omega_s T_0} + \varepsilon \overline{A}_s(T_1)e^{-i\omega_s T_0},\ s = 1,2,\ \text{and}\ 3 \tag{3.3}$$

where $T_0 = t$ is a fast scale that characterizes motions at the frequencies ω_s and Ω, and $T_1 = \varepsilon t$ is a slow scale that characterizes the modulation of the amplitudes and phases. The amplitude of the excitation is scaled so that it appears in the same perturbation equations with the damping and nonlinearities. Hence, we put

$$\hat{F}_s = \varepsilon^2 F_s \tag{3.4}$$

In terms of the T_m, the time derivative of u_s becomes

$$\dot{u}_s = \varepsilon i\omega_s A_s e^{i\omega_s T_0} + \varepsilon^2 A'_s e^{i\omega_s T_0} + cc \tag{3.5}$$

where the prime indicates the derivative with respect to T_1 and cc stands for the complex conjugate of the preceding terms.

Substituting equations (3.3)-(3.5) into equation (3.1) and using the detuning parameters defined in equation (3.2), we obtain

$$\begin{aligned}\mathscr{L} = \frac{1}{2}\varepsilon^3\{&2i[\omega_1(A_1\overline{A}'_1 - A'_1\overline{A}_1) + \omega_2(A_2\overline{A}'_2 - A'_2\overline{A}_2) + \omega_3(A_3\overline{A}'_3 - A'_3\overline{A}_3)] \\ &- 2\Lambda(A_1A_2\overline{A}_3e^{-i\sigma_1 T_1} + \overline{A}_1\overline{A}_2A_3e^{i\sigma_1 T_1}) + F_3(\overline{A}_3e^{i\sigma_2 T_1} + A_3e^{-i\sigma_2 T_1})\} + FVT\end{aligned} \tag{3.6}$$

where

$$2\Lambda = -\omega_1\omega_2(M_{312}+M_{321})+\omega_1\omega_3(M_{213}+M_{231})+\omega_2\omega_3(M_{123}+M_{132}) + K_{123}+K_{132}+K_{213}+K_{231}+K_{312}+K_{321} \tag{3.7}$$

and FVT stands for fast varying terms; that is, terms that vary with the time scale T_0. By averaging the Lagrangian over the fast time scale T_0, we obtain

$$<\mathscr{L}> = \frac{1}{2}\varepsilon^3\Big[2i\omega_1(A_1\overline{A}'_1 - A'_1\overline{A}_1)+2i\omega_2(A_2\overline{A}'_2 - A'_2\overline{A}_2)+2i\omega_3(A_3\overline{A}'_3 - A'_3\overline{A}_3) - 2\Lambda(A_1A_2\overline{A}_3e^{-i\sigma_1T_1}+\overline{A}_1\overline{A}_2A_3e^{i\sigma_1T_1})+F_3(\overline{A}_3e^{i\sigma_2T_1}+A_3e^{-i\sigma_2T_1})\Big] \tag{3.8}$$

Applying Lagrange's equations

$$\frac{d}{dt}\left(\frac{\partial<\mathscr{L}>}{\partial\overline{A}'_s}\right)-\frac{\partial<\mathscr{L}>}{\partial\overline{A}_s}=0 \tag{3.9}$$

and adding modal damping, we obtain the following modulation equations:

$$2i\omega_1(A_1'+\mu_1A_1)+\Lambda A_3\overline{A}_2e^{i\sigma_1T_1}=0 \tag{3.10}$$

$$2i\omega_2(A_2'+\mu_2A_2)+\Lambda A_3\overline{A}_1e^{i\sigma_1T_1}=0 \tag{3.11}$$

$$2i\omega_3(A_3'+\mu_3A_3)+\Lambda A_1A_2e^{-i\sigma_1T_1}-\frac{1}{2}F_3e^{i\sigma_2T_1}=0 \tag{3.12}$$

Next, we express the A_s in the polar form

$$A_s=\frac{1}{2}c_sa_se^{i\beta_s} \tag{3.13}$$

where a_m and β_m are real and

$$c_1 = \frac{4\sqrt{\omega_2\omega_3}}{\Lambda} \quad , \quad c_2 = \frac{4\sqrt{\omega_1\omega_3}}{\Lambda} \quad , \text{ and } \quad c_3 = \frac{4\sqrt{\omega_1\omega_2}}{\Lambda} \tag{3.14}$$

The coefficients c_i are chosen so that the resulting equations are universal. Substituting equation (3.13) into equations (3.10)-(3.11) and separating real and imaginary parts, we obtain the modulation equations

$$a_1' = -\mu_1 a_1 - a_2 a_3 \sin\gamma_1 \tag{3.15}$$

$$a_1\beta_1' = a_2 a_3 \cos\gamma_1 \tag{3.16}$$

$$a_2' = -\mu_2 a_2 - a_1 a_3 \sin\gamma_1 \tag{3.17}$$

$$a_2\beta_2' = a_1 a_3 \cos\gamma_1 \tag{3.18}$$

$$a_3' = -\mu_3 a_3 + a_1 a_2 \sin\gamma_1 + F\sin\gamma_2 \tag{3.19}$$

$$a_3\beta_3' = a_1 a_2 \cos\gamma_1 - F\cos\gamma_2 \tag{3.20}$$

where

$$\gamma_1 = \sigma_1 T_1 + \beta_3 - \beta_2 - \beta_1 \quad , \quad \gamma_2 = \sigma_2 T_1 - \beta_3 \tag{3.21}$$

and

$$F = \frac{F_3\Lambda}{8\omega_3\sqrt{\omega_1\omega_2}} \tag{3.22}$$

We note that equations (3.15)-(3.21) are general and applicable to all dynamic systems having a combination resonance of the additive type with a primary resonant excitation of the highest mode.

3.3 Fixed-Point Solutions

Next, we determine the constant solutions or fixed points of equations (3.15)-(3.21). As we show later, these fixed points correspond to periodic, quasiperiodic, or phase-locked motions of the system. To determine these fixed points, we put $a_m' = 0$ and $\gamma_m' = 0$. Then, it follows from equation (3.21) that

$$\beta_3' = \sigma_2 \text{ and } \beta_1' + \beta_2' = \sigma_1 + \sigma_2 \tag{3.23}$$

Hence, the constant solutions or fixed points are given by

$$\mu_1 a_1 = -a_2 a_3 \sin \gamma_1 \tag{3.24}$$

$$\mu_2 a_2 = -a_1 a_3 \sin \gamma_1 \tag{3.25}$$

$$\mu_3 a_3 = a_1 a_2 \sin \gamma_1 + F \sin \gamma_2 \tag{3.26}$$

$$a_1 a_2 (\sigma_1 + \sigma_2) = (a_1^2 + a_2^2) a_3 \cos \gamma_1 \tag{3.27}$$

$$\sigma_2 a_3 = a_1 a_2 \cos \gamma_1 - F \cos \gamma_2 \tag{3.28}$$

We note that there are two possibilities: either a_1 and a_2 are zero and a_3 is nonzero, or none is zero. When $a_1 = a_2 = 0$, then

$$a_3 = F/(\sigma_2^2 + \mu_3^2)^{1/2} \tag{3.29}$$

which is essentially the solution of the linearized problem. This constant solution corresponds to a periodic motion having the same period as the excitation and to the first approximation consists of the third mode only. We refer to this solution as the single-mode solution.

When a_1 and $a_2 \neq 0$, it follows from equations (3.24) and (3.25) that

$$\mu_1 a_1^2 = \mu_2 a_2^2 \tag{3.30}$$

Using equation (3.30) in equation (3.27), we have

$$a_3 \cos \gamma_1 = \frac{\sigma_1 + \sigma_2}{\mu_1 + \mu_2} \sqrt{\mu_1 \mu_2} \tag{3.31}$$

Moreover, using equation (3.30) in equation (3.24), we have

$$a_3 \sin \gamma_1 = -\sqrt{\mu_1 \mu_2} \tag{3.32}$$

Eliminating γ_1 from equations (3.31) and (3.32) yields

$$a_3 = a_3^* = \sqrt{\mu_1 \mu_2} \left[1 + \left(\frac{\sigma_1 + \sigma_2}{\mu_1 + \mu_2} \right)^2 \right]^{1/2} \tag{3.33}$$

which is independent of both μ_3 and the excitation amplitude F in spite of the fact that the system is being excited by a harmonic load at a frequency near that of the third mode. Using equations (3.30)-(3.32) in equations (3.26) and (3.28), we obtain

$$a_1^2 = \sqrt{\frac{\mu_2}{\mu_1}}\left[\chi_1 \pm \sqrt{F^2 - \chi_2^2}\right] \tag{3.34}$$

where

$$\chi_1 = \frac{\sqrt{\mu_1\mu_2}}{\mu_1 + \mu_2}\left[\sigma_2(\sigma_1 + \sigma_2) - \mu_3(\mu_1 + \mu_2)\right] \tag{3.35}$$

$$\chi_2 = \frac{\sqrt{\mu_1\mu_2}}{\mu_1 + \mu_2}\left[\sigma_2(\mu_1 + \mu_2) + \mu_3(\sigma_1 + \sigma_2)\right] \tag{3.36}$$

Then, a_2 can be obtained from equations (3.30) and (3.34). These constant solutions correspond to a response having the form

$$u_3 = c_3 a_3 \cos(\Omega t - \gamma_3) + \ldots \tag{3.37}$$

$$u_2 = c_2 a_2 \cos(\tilde{\omega}_2 t + \nu_2) + \ldots \tag{3.38}$$

$$u_1 = c_1 a_1 \cos\left[(\Omega - \tilde{\omega}_2)t + \nu_1\right] + \ldots \tag{3.39}$$

where ν_1 and ν_2 are constants,

$$\Omega = \tilde{\omega}_1 + \tilde{\omega}_2 \tag{3.40}$$

$$\tilde{\omega}_1 = \omega_1 + \varepsilon\beta_1' \quad \text{and} \quad \tilde{\omega}_2 = \omega_2 + \varepsilon\beta_2' \tag{3.41}$$

Therefore, if $\tilde{\omega}_1$ and hence $\tilde{\omega}_2$ are not commensurate with Ω, the solution consists of two incommensurate periods and it is usually called a two-period quasiperiodic solution. If $\tilde{\omega}_1$ and hence $\tilde{\omega}_2$ are commensurate with Ω, the solution of the system consists of one period, which is the least common multiple of $2\pi/\Omega$ and $2\pi/\tilde{\omega}_1$, and one speaks of a phase-locked solution.

Next, we determine when the roots of equation (3.34) are real. To this end, we define two critical values of F, namely

$$F_1 = |\chi_2| \quad \text{and} \quad F_2 = \sqrt{\chi_1^2 + \chi_2^2} \tag{3.42}$$

Clearly, F_2 must be greater than F_1. There are two possibilities, depending on the sign of χ_1. When $\chi_1 < 0$, one real solution exists if $F > F_2$. When $\chi_1 > 0$, two real solutions exist if $F_1 < F < F_2$ and one real solution exists if $F > F_2$. Consequently, when $F < F_1$, only the solution given in equation (3.29) exists.

To determine which, if any, of the above solutions corresponds to a possible response, we need to determine the stability of the different fixed points. To determine the stability of the one-mode solution $a_1 = a_2 = 0$ and $A_3 = \frac{1}{2} c_3 a_3 \exp(i\beta_3)$, where $\beta_3 = \sigma_2 T_1 - \gamma_2$, we substitute this solution into equations (3.10) and (3.11) and obtain

$$i\omega_1(A_1' + \mu_1 A_1) + \sqrt{\omega_1\omega_2}\, a_3 \bar{A}_2 e^{i(\sigma_1 + \sigma_2)T_1 - i\gamma_2} = 0 \tag{3.43}$$

$$i\omega_2(A_2' + \mu_2 A_2) + \sqrt{\omega_1\omega_2}\, a_3 \bar{A}_1 e^{i(\sigma_1 + \sigma_2)T_1 - i\gamma_2} = 0 \tag{3.44}$$

Equations (3.43) and (3.44) admit solutions of the form

$$A_1 = b_1 e^{\lambda T_1 + i(\sigma_1 + \sigma_2)T_1 - i\gamma_2} \text{ and } A_2 = b_2 e^{\bar{\lambda} T_1} \tag{3.45}$$

where b_1, b_2, and λ are constants provided that

$$i\omega_1[\lambda + \mu_1 + i(\sigma_1 + \sigma_2)]b_1 + \sqrt{\omega_1\omega_2}\, a_3\bar{b}_2 = 0 \tag{3.46}$$

$$\sqrt{\omega_1\omega_2}\, a_3\bar{b}_1 + i\omega_2(\bar{\lambda} + \mu_2)b_2 = 0 \tag{3.47}$$

or

$$\sqrt{\omega_1\omega_2}\, a_3 b_1 - i\omega_2(\lambda + \mu_2)\bar{b}_2 = 0 \tag{3.48}$$

For a nontrivial solution, the determinant of the coefficient matrix in equations (3.46) and (3.48) must vanish; that is,

$$\lambda^2 + [\mu_1 + \mu_2 + i(\sigma_1 + \sigma_2)]\lambda + \mu_1\mu_2 + i\mu_2(\sigma_1 + \sigma_2) - a_3^2 = 0 \tag{3.49}$$

The roots of equation (3.49) are

$$\begin{aligned}\lambda = & -\frac{1}{2}[\mu_1 + \mu_2 + i(\sigma_1 + \sigma_2)] \pm \frac{1}{2}\{[\mu_1 + \mu_2 + i(\sigma_1 + \sigma_2)]^2 \\ & + 4a_3^2 - 4\mu_1\mu_2 - 4i\mu_2(\sigma_1 + \sigma_2)\}^{1/2}\end{aligned} \tag{3.50}$$

Expressing the radical in equation (3.50) as $x + iy$, where x and y are real, we note that the single-mode solution is stable if $x < \mu_1 + \mu_2$ and unstable if $x > \mu_1 + \mu_2$. The transition from stability to instability corresponds to $x = \mu_1 + \mu_2$. Hence, it corresponds to

$$(\mu_1 + \mu_2 + iy)^2 = [\mu_1 + \mu_2 + i(\sigma_1 + \sigma_2)]^2 + 4a_3^2 - 4\mu_1\mu_2 - 4i\mu_2(\sigma_1 + \sigma_2) \tag{3.51}$$

which, upon equating real and imaginary parts, yields

$$-y^2 = -(\sigma_1 + \sigma_2)^2 - 4\mu_1\mu_2 + 4a_3^2 \tag{3.52}$$

$$(\mu_1 + \mu_2)y = (\sigma_1 + \sigma_2)(\mu_1 - \mu_2) \tag{3.53}$$

It follows from equation (3.53) that

$$y = \frac{(\sigma_1 + \sigma_2)(\mu_1 - \mu_2)}{\mu_1 + u_2} \tag{3.54}$$

Substituting for y in equation (3.52) yields

$$a_3^2 = \mu_1\mu_2\left[1 + \frac{(\sigma_1 + \sigma_2)^2}{(\mu_1 + \mu_2)^2}\right] \tag{3.55}$$

which yields $a_3 = a_3^*$ defined in equation (3.33). Therefore, the single-mode solution is stable if $a_3 < a_3^*$ and unstable if $a_3 > a_3^*$.

To determine the stability of a fixed point corresponding to a three-mode motion, we eliminate β_1 and β_2 from equations (3.15)-(3.20), thereby transforming these equations into the autonomous set

$$a'_1 = -\mu_1 a_1 - a_2 a_3 \sin\gamma_1 \tag{3.56}$$

$$a'_2 = -\mu_2 a_2 - a_1 a_3 \sin\gamma_1 \tag{3.57}$$

$$a'_3 = -\mu_3 a_3 + a_1 a_2 \sin\gamma_1 + F \sin\gamma_2 \tag{3.58}$$

$$\gamma'_1 = \sigma_1 + \left(-\frac{a_2 a_3}{a_1} - \frac{a_1 a_3}{a_2} + \frac{a_1 a_2}{a_3} \right) \cos\gamma_1 - \frac{F}{a_3} \cos\gamma_2 \tag{3.59}$$

$$\gamma'_2 = \sigma_2 - \frac{a_1 a_2}{a_3} \cos\gamma_1 + \frac{F}{a_3} \cos\gamma_2 \tag{3.60}$$

The eigenvalues of the Jacobi matrix of the fifth-order autonomous set are given by

$$\begin{vmatrix} \lambda+\mu_1 & a_3\sin\gamma_1 & a_2\sin\gamma_1 & a_2a_3\cos\gamma_1 & 0 \\ a_3\sin\gamma_1 & \lambda+\mu_2 & a_1\sin\gamma_1 & a_1a_3\cos\gamma_1 & 0 \\ -a_2\sin\gamma_1 & -a_1\sin\gamma_1 & \lambda+\mu_3 & -a_1a_2\cos\gamma_1 & -F\cos\gamma_2 \\ \Gamma_1\cos\gamma_1 & \Gamma_2\cos\gamma_1 & \Gamma_3\cos\gamma_1 - \frac{F}{a_3^2}\cos\gamma_2 & \lambda+\Gamma_4\sin\gamma_1 & -\frac{F}{a_3}\sin\gamma_2 \\ \frac{a_2}{a_3}\cos\gamma_1 & \frac{a_1}{a_3}\cos\gamma_1 & -\frac{a_1a_2}{a_3^2}\cos\gamma_1 + \frac{F}{a_3^2}\cos\gamma_2 & -\frac{a_1a_2}{a_3}\sin\gamma_1 & \lambda+\frac{F}{a_3}\sin\gamma_2 \end{vmatrix} = 0 \tag{3.61}$$

where

$$\Gamma_1 = -\frac{a_2 a_3}{a_1^2} + \frac{a_3}{a_2} - \frac{a_2}{a_3} \tag{3.62}$$

$$\Gamma_2 = \frac{a_3}{a_1} - \frac{a_1 a_3}{a_2^2} - \frac{a_1}{a_3} \tag{3.63}$$

$$\Gamma_3 = \frac{a_2}{a_1} + \frac{a_1}{a_2} + \frac{a_1 a_2}{a_3^2} \tag{3.64}$$

$$\Gamma_4 = -\frac{a_2 a_3}{a_1} - \frac{a_1 a_3}{a_2} + \frac{a_1 a_2}{a_3} \tag{3.65}$$

A given fixed point is asymptotically stable if all the eigenvalues of the Jacobi matrix lie in the left half of the complex plane and unstable if at least one eigenvalue lies in the right half. In all figures showing the fixed points, the dotted portions of the curves are unstable fixed-point solutions with real positive eigenvalues, the solid portions are stable, and the dashed portions are unstable with a pair of complex conjugate eigenvalues lying in the right-half plane.

3.3.1 Amplitude-Response Curves

In Figure 3.1, we show a representative variation of the response amplitudes with the scaled excitation amplitude F when $\chi_1 > 0$. Here we set $\sigma_1 = 0.464$, $\sigma_2 = 0.195$, $\mu_1 = 0.1$, $\mu_2 = 0.2$ and $\mu_3 = 0.1$. As F is increased from zero, a_3 increases linearly with F while a_1 and a_2 remain zero. As F exceeds the threshold value $F_2 \approx 0.059$, a_3 remains constant (saturates) and equal to a_3^* while a_1 and a_2 jump up to points B_1 and B_2 and then slowly increase along the curves B_1C_1 and B_2C_2. If F is set at a value corresponding to points C_1 and C_2 and then slowly decreased, a_3 remains constant and equal to a_3^* while a_1 and

a_2 slowly decrease along the curves $C_1B_1A_1$ and $C_2B_2A_2$. As F is decreased below the second threshold value $F_1 \approx 0.059$, a_1 and a_2 jump down to zero, while a_3 jumps down to point C_3. As F is decreased further, a_1 and a_2 remain zero while a_3 decreases linearly with F until it reaches zero at $F = 0$. If F is set at a value between F_1 and F_2, then the response may consist of the third mode only or the three modes, depending on the initial conditions. The threshold values F_1 and F_2 are called saddle-node (turning-point) and reversed pitchfork bifurcations, respectively.

In Figure 3.2, we show a representative variation of the response amplitudes a_m with the scaled excitation amplitude F when $\chi_1 < 0$. Here we set $\sigma_1 = -0.510$, $\sigma_2 = 0.200$, $\mu_1 = 0.05$, $\mu_2 = 0.1$, and $\mu_3 = 0.05$. As F is increased from zero, the amplitude of the third mode a_3 increases linearly with F while the amplitudes a_1 and a_2 of the first and second modes remain zero. This is essentially the linear solution. However, when the excitation amplitude exceeds the critical amplitude $F_2 \approx 0.033$, a_3 remains constant and equal to a_3^* (i.e., saturates) and the extra input energy spills over into the lower modes, which grow very rapidly and eventually their amplitudes a_1 and a_2 become larger than a_3. The threshold value F_2 is called a pitchfork bifurcation for the lower two modes. As F exceeds the value $F_3 \approx 0.105$, the saturated solution loses stability with a pair of complex conjugate eigenvalues of equation (3.61) transversely crossing into the right half of the complex plane (i.e., a Hopf bifurcation). Hence, beyond $\tilde{F}_3$ the response is an amplitude- and phase-modulated motion consisting of all three modes.

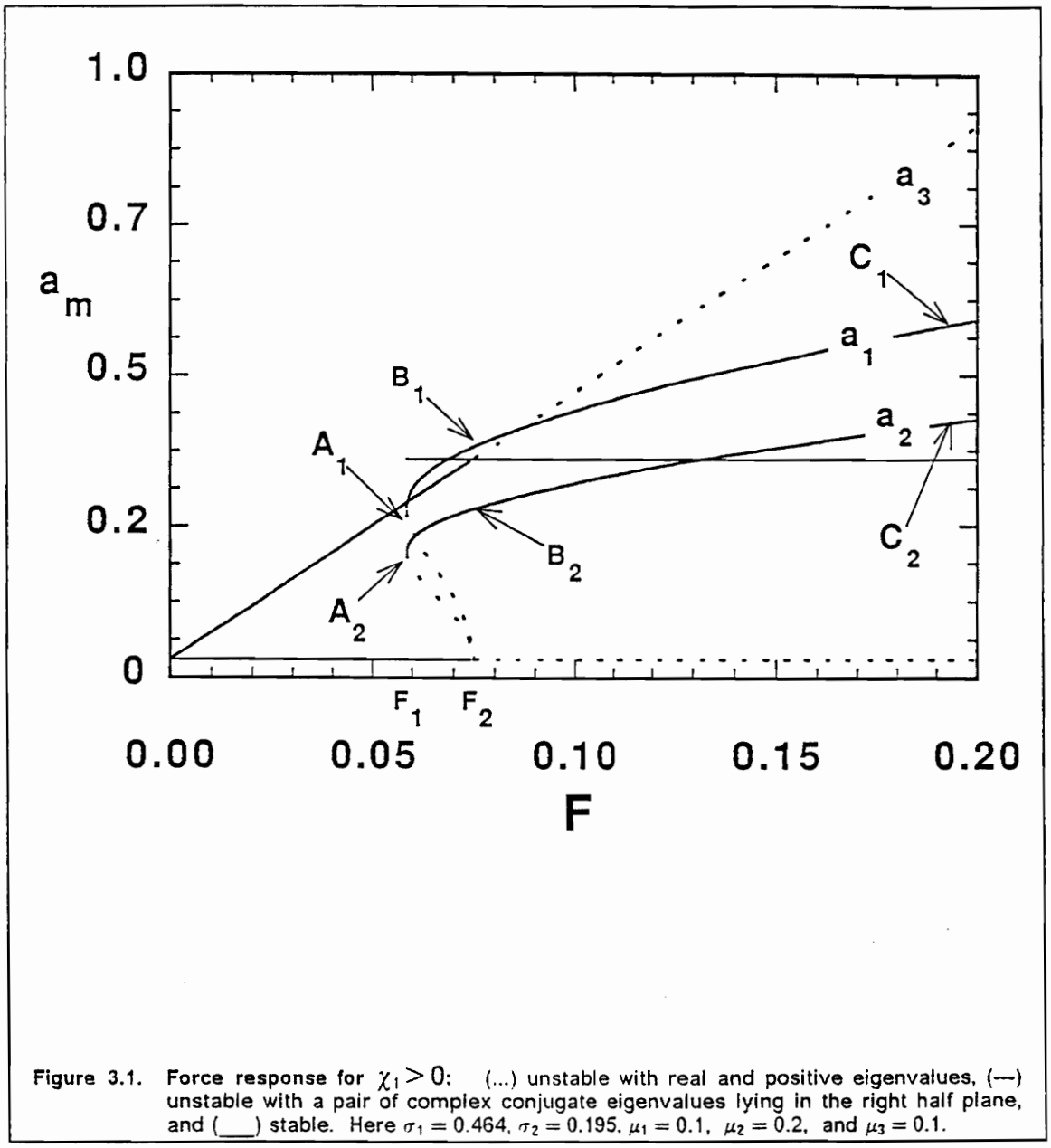

Figure 3.1. **Force response for $\chi_1 > 0$:** (...) unstable with real and positive eigenvalues, (---) unstable with a pair of complex conjugate eigenvalues lying in the right half plane, and (___) stable. Here $\sigma_1 = 0.464$, $\sigma_2 = 0.195$. $\mu_1 = 0.1$, $\mu_2 = 0.2$, and $\mu_3 = 0.1$.

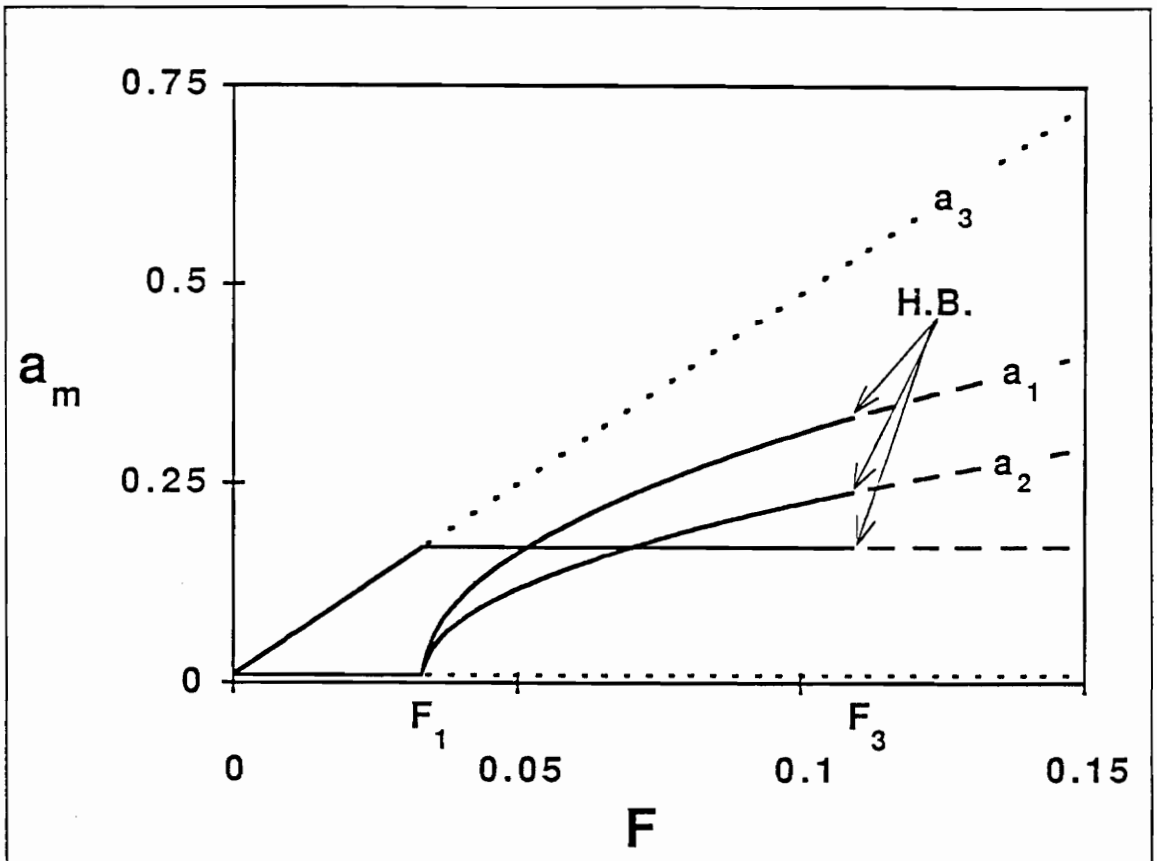

Figure 3.2. **Force response for $\chi_1 < 0$:** (...) unstable with real and positive eigenvalues, (---) unstable with a pair of complex conjugate eigenvalues lying in the right half plane, and (___) stable. Here $\sigma_1 = -0.510$, $\sigma_2 = 0.200$, $\mu_1 = 0.05$, $\mu_2 = 0.1$, and $\mu_3 = 0.05$.

3.3.2 Frequency-Response Curves

In Figures 3.3-3.5, we show representative frequency-response curves when F is fixed at 0.05 and σ_2 is slowly varied from -1.0 to 1.0. Here, we set $\sigma_1 = 0.510$, $\mu_1 = 0.05$, $\mu_2 = 0.1$, and $\mu_3 = 0.05$. When σ_2 is less than $\sigma^{(1)} \approx -0.659$ or greater than $\sigma^{(6)} \approx 0.403$, only the single-mode solution exists, which is stable, and the response consists of only the third mode. When $\sigma^{(1)} < \sigma_2 < \sigma^{(2)} \approx -0.601$ or $0.149 \sigma^{(5)} \approx < \sigma_2 < \sigma^{(6)}$, three solutions exist: a single-mode solution, which is stable; a three-mode solution corresponding to the lower branches in Figures 3.3 and 3.4, which is unstable with positive real eigenvalues; and a three-mode solution corresponding to the upper branches in Figures 3.3 and 3.4, which is stable. Here the response is either periodic consisting of the third mode only or quasiperiodic consisting of all three modes. When $\sigma^{(2)} < \sigma_2 < \sigma^{(3)} \approx -0.155$ or $-0.091 \sigma^{(4)} \approx < \sigma_2 < \sigma^{(5)}$, two solutions are possible: a single-mode solution, which is unstable with positive real eigenvalues, and a three-mode solution, which is stable. Here the response is quasiperiodic consisting of all three modes. When $\sigma^{(3)} < \sigma_2 < \sigma^{(4)}$, there are two possible solutions: a single-mode solution, which is unstable, and a three-mode solution, which is unstable with a pair of complex conjugate eigenvalues lying in the right half of the complex plane. Here the response is an amplitude- and phase-modulated motion consisting of all three modes. The points $\sigma^{(3)}$ and $\sigma^{(4)}$ are Hopf-bifurcation points.

We can see the dependance of the response on sweep direction rather vividly. As we sweep σ_2 upwards from -1.0, the response initially consists of

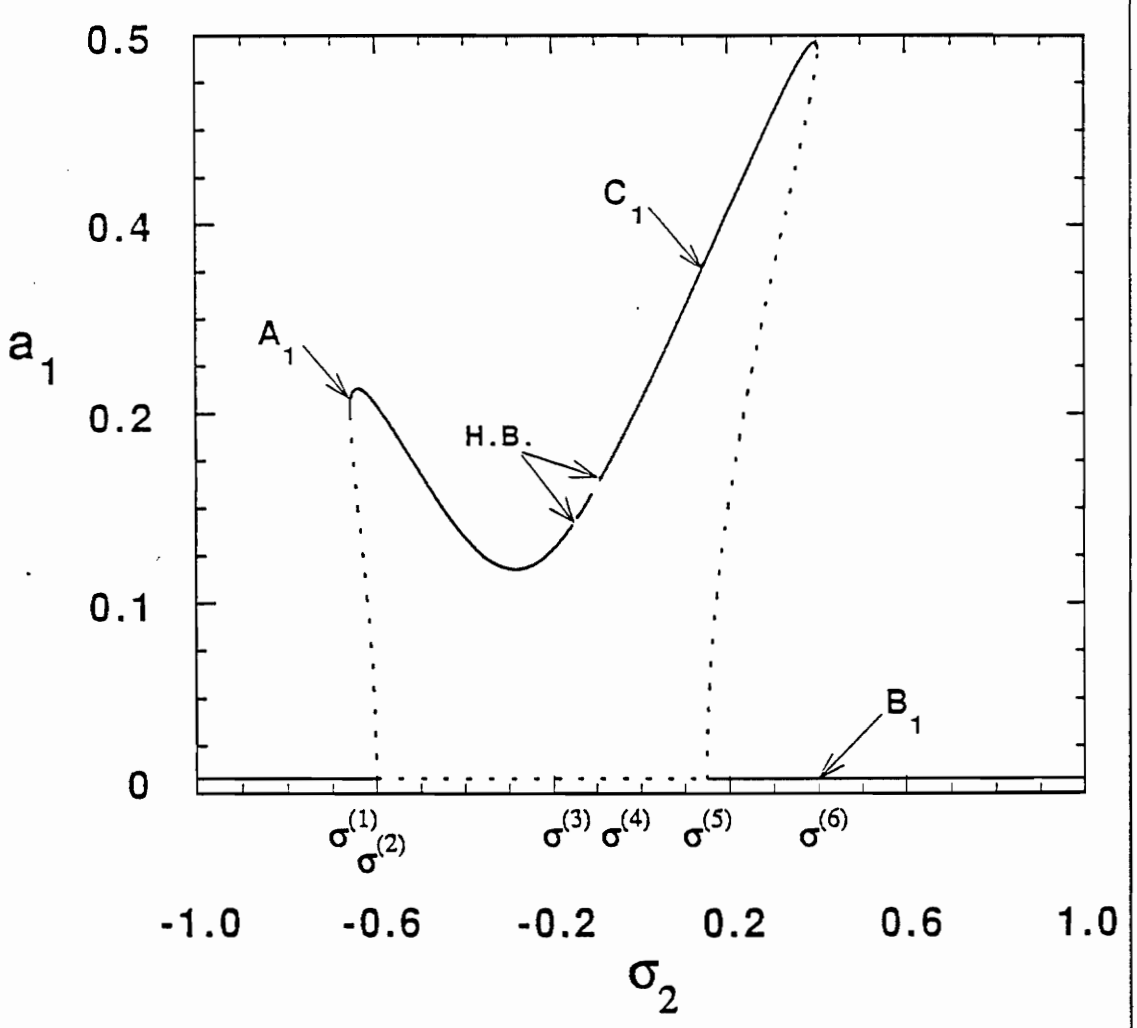

Figure 3.3. **Frequency response of the first mode when $\sigma_1 > 0$:** (...) unstable with real and positive eigenvalues, (---) unstable with a pair of complex conjugate eigenvalues lying in the right half plane, and (___) stable. Here $F = 0.05$, $\sigma_1 = 0.510$, $\mu_1 = 0.05$, $\mu_2 = 0.1$, and $\mu_3 = 0.05$.

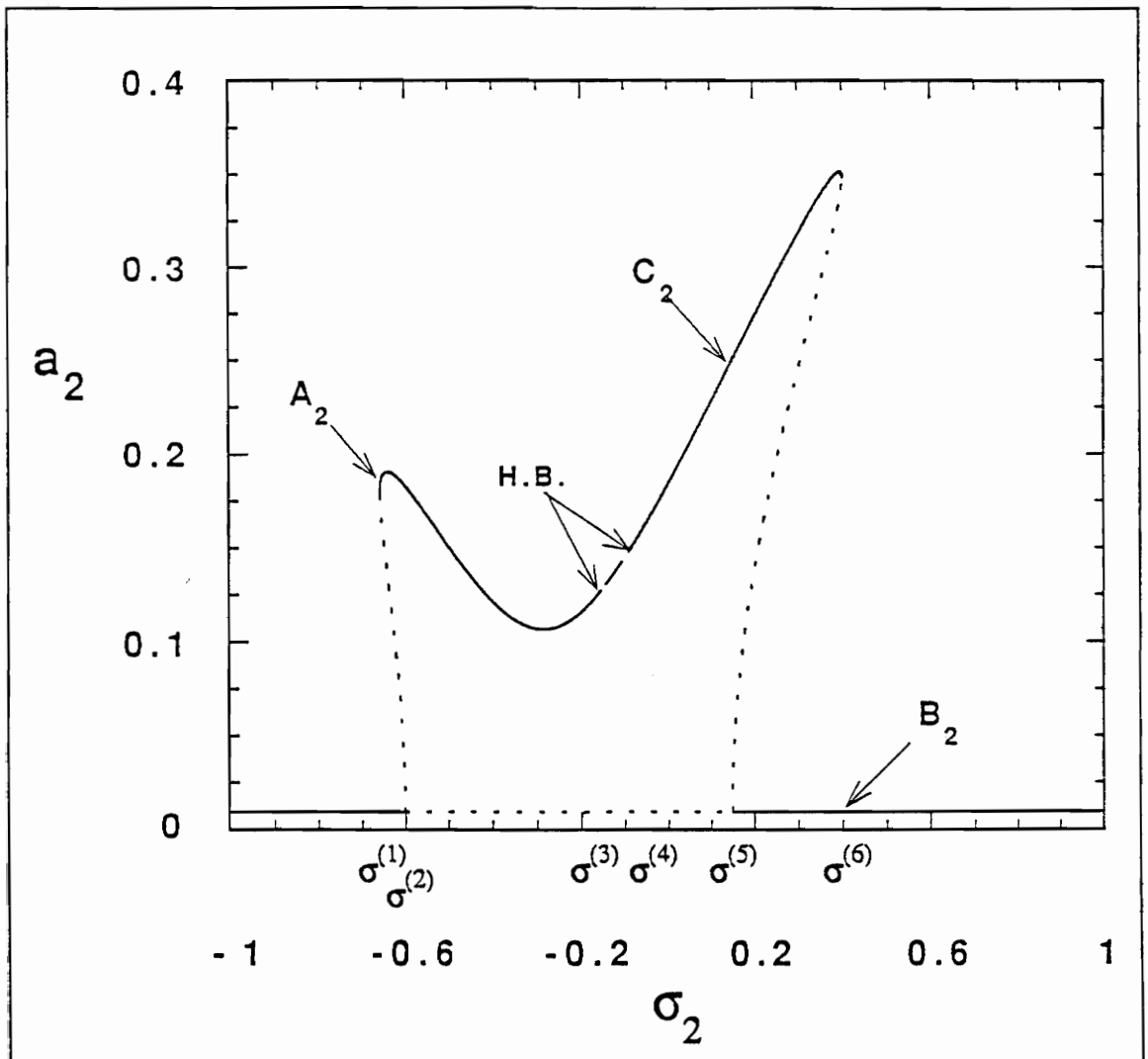

Figure 3.4. **Frequency response of the second mode when $\sigma_1 > 0$:** (...) unstable with real and positive eigenvalues, (---) unstable with a pair of complex conjugate eigenvalues lying in the right half plane, and (___) stable. Here $F = 0.05$, $\sigma_1 = 0.510$, $\mu_1 = 0.05$, $\mu_2 = 0.1$, and $\mu_3 = 0.05$.

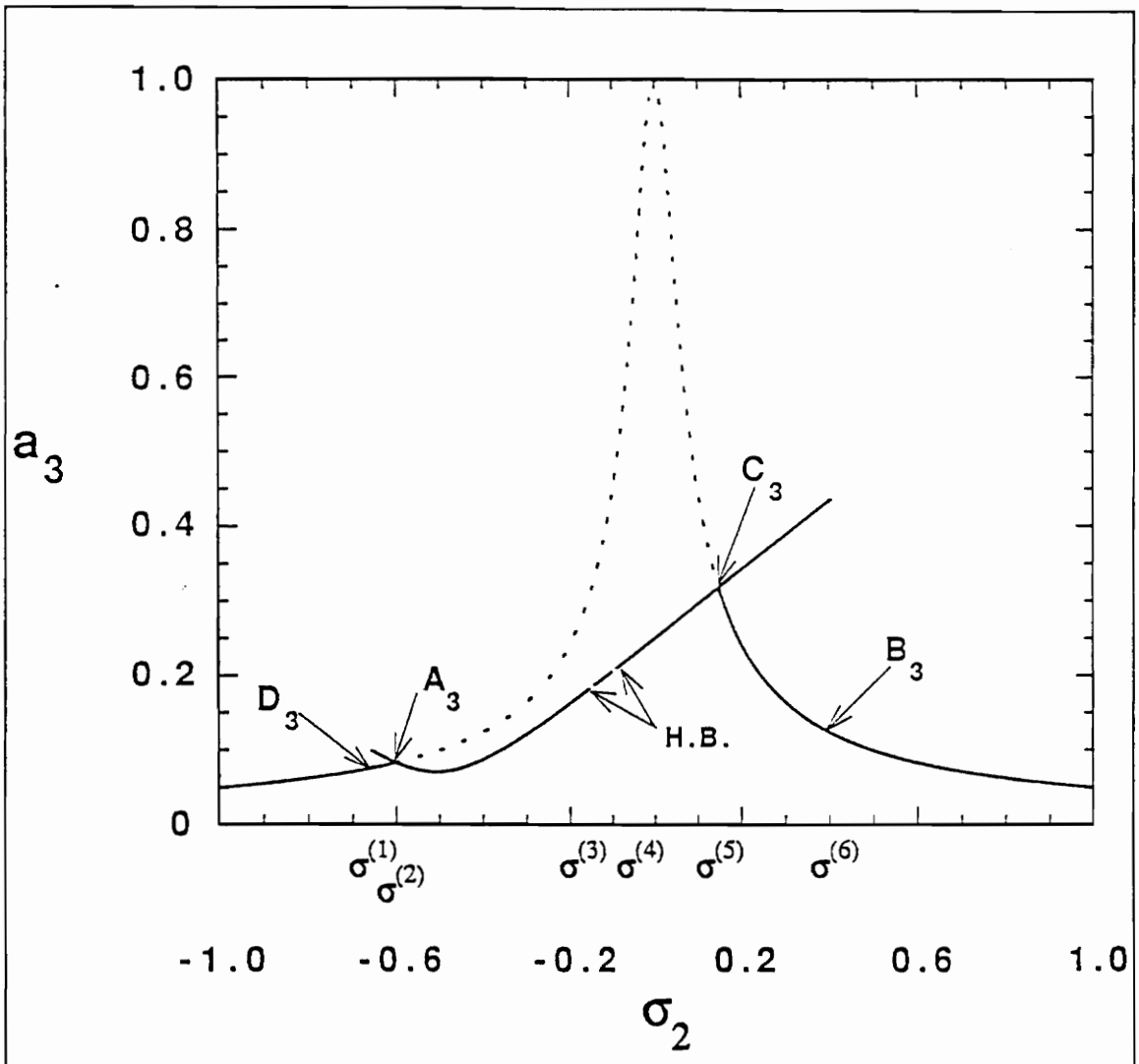

Figure 3.5. **Frequency response of the third mode when $\sigma_1 > 0$:** (...) unstable with real and positive eigenvalues, (---) unstable with a pair of complex conjugate eigenvalues lying in the right half plane, and (___) stable. Here $F = 0.05$, $\sigma_1 = 0.510$, $\mu_1 = 0.05$, $\mu_2 = 0.1$, and $\mu_3 = 0.05$.

the third mode only and is periodic. The amplitude of the third mode increases with increasing σ_2. As σ_2 is increased beyond $\sigma^{(2)}$, the single-mode solution becomes unstable and the amplitude of the third mode ceases to increase and follows branch A_3C_3. The amplitudes of the first two modes a_1 and a_2 jump up to points A_1 and A_2, respectively (Figures 3.3 and 3.4). Here the response becomes two-period quasiperiodic consisting of all three modes. As σ_2 is increased past $\sigma^{(3)}$, the fixed points of the modulation equations undergo a Hopf bifurcation and the amplitudes and phases become modulated. Thus, the response becomes three-period quasiperiodic consisting of all three modes. As σ_2 is increased beyond $\sigma^{(4)}$, the fixed points of the modulation equations undergo a reverse Hopf bifurcation and the response becomes two-period quasiperiodic again consisting of all three modes. As σ_2 is increased beyond $\sigma^{(6)}$, the three-mode solution ceases and the amplitudes of the first two modes jump down to zero (Figures 3.3 and 3.4) while the amplitude of the third mode jumps down to point B_3. As σ_2 is increased further, the amplitude of the third mode decreases.

As σ_2 is decreased from 1.0, the amplitude of the third mode increases (Figure 3.5) while a_1 and a_2 remain zero until σ_2 is decreased beyond $\sigma^{(5)}$. Here, the amplitude of the third mode ceases to increase with decreasing σ_2 and follows branch C_3A_3 and the amplitudes of the first two modes jump up to points C_1 and C_2 (Figures 3.3-3.5). Here the response becomes two-period quasiperiodic consisting of all three modes. As σ_2 is decreased past $\sigma^{(4)}$, the fixed points of the modulation equations undergo a Hopf bifurcation and the response becomes an amplitude- and phase-modulated motion. Here the

response consists of all three modes and is three-period quasiperiodic. As σ_2 is decreased beyond $\sigma^{(3)}$, the fixed points of the modulation equations undergo a reverse Hopf bifurcation and the response becomes two-period quasiperiodic consisting of all three modes (Figures 3.3-3.5). The motion remains two-period quasiperiodic until σ_2 is decreased beyond $\sigma^{(1)}$ where the three-mode solution ceases. The amplitudes of the first two modes jump down to zero and the amplitude of the third mode jumps down to point D_3 (Figures 3.3-3.5). The response is periodic consisting of the third mode only; its amplitude decreases with decreasing σ_2.

We note that the frequency-response curves are bent to the right in Figures 3.3-3.5. Had we used $\sigma_1 = 0$, then the frequency-response curves would have been symmetric. And had we used a negative σ_1, then they would have been bent to the left.

3.3.3 Experiments

A schematic drawing of the experimental setup is shown in Figure 3.6. The instrumentation includes the signal generator, the signal conditioners, and the signal analyzer.

The model shown in Figure 3.7 has two dynamic strain gages attached to it, one on the horizontal beam and one on the vertical beam (both oriented axially). The signal from the axial-strain gage on the horizontal beam is used to measure the response of the structure. From the output signal the

frequency spectra are generated and the amplitudes of the different modes are determined. The strain gage on the horizontal beam is chosen because its signal tends to have a larger amplitude than the other and hence is less susceptible to the ever-present line noise. An accelerometer is mounted on the shaker to measure the table acceleration, as shown in Figure 3.6.

The signal generator is a two-channel, variable-phase wave synthesizer. It is capable of generating a waveform of 0.0001 Hz resolution. It also has an IEEE-488 (GPIB) interface that permits computer control of all its functions. The interface can be used in the feedback-control system depicted in Figure 3.6.

We tuned the model by positioning masses m_2 and m_3 (Figure 3.7) so that the value of $\omega_1 + \omega_2$ is close to ω_3, which produces a so-called internal or autoparametric resonance of the combination type. The measured natural frequencies of the model are $\omega_1 = 4.359\,Hz$, $\omega_2 = 7.828\,Hz$, and $\omega_3 = 12.172\,Hz$.. We show that this autoparametric resonance leads to complicated nonlinear phenomena.

3.3.3.1 Frequency-response curves

The frequency-response curves were produced by sweeping the excitation frequency either up or down while keeping a constant excitation level. By excitation level we mean the root-mean-square (rms) of the shaker base acceleration. Linear theory predicts that the modes of vibration will be uncoupled and that the maximum value on the frequency-response curve will be very close to the third natural frequency. When the amplitude of the

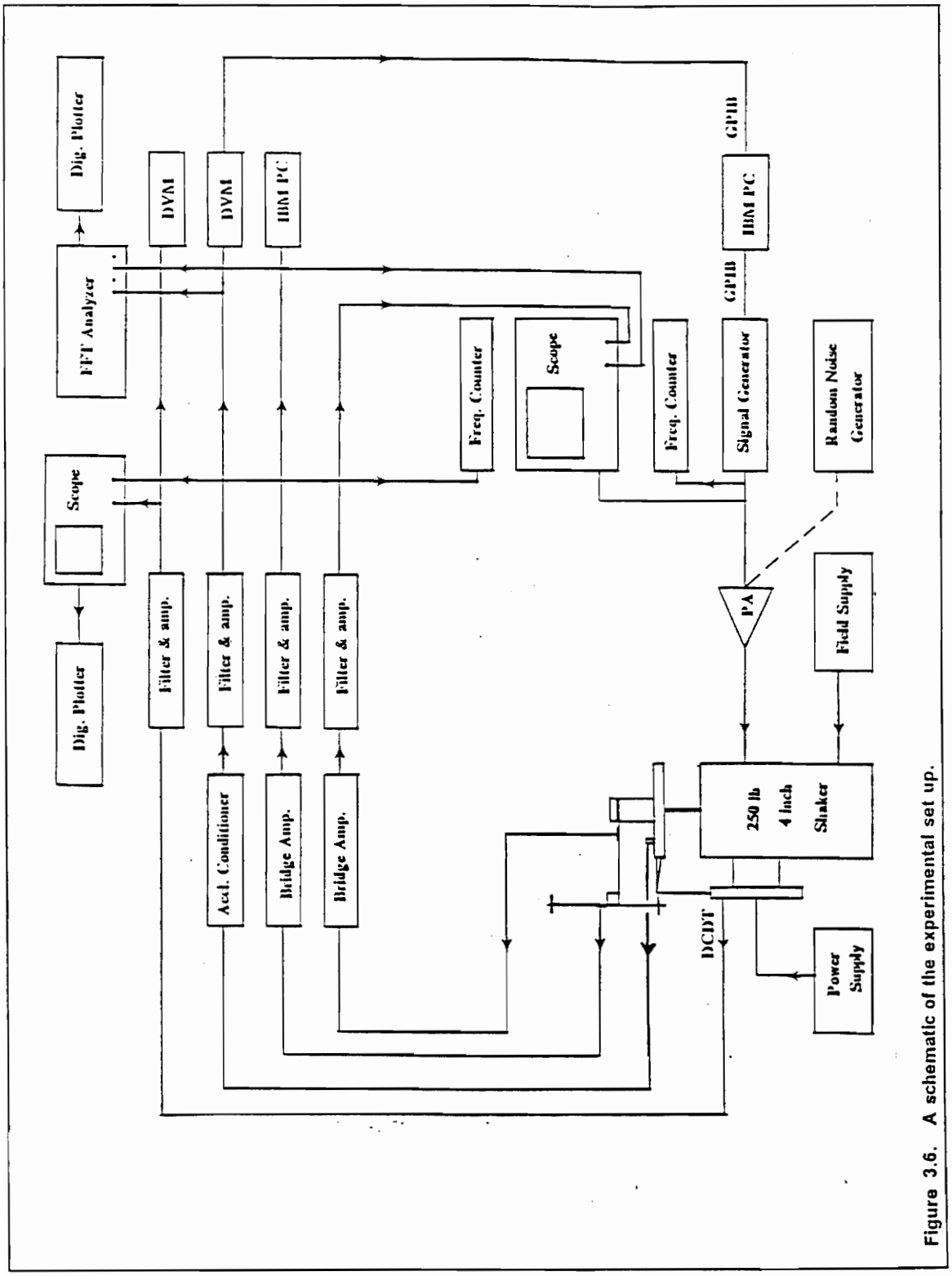

Figure 3.6. A schematic of the experimental set up.

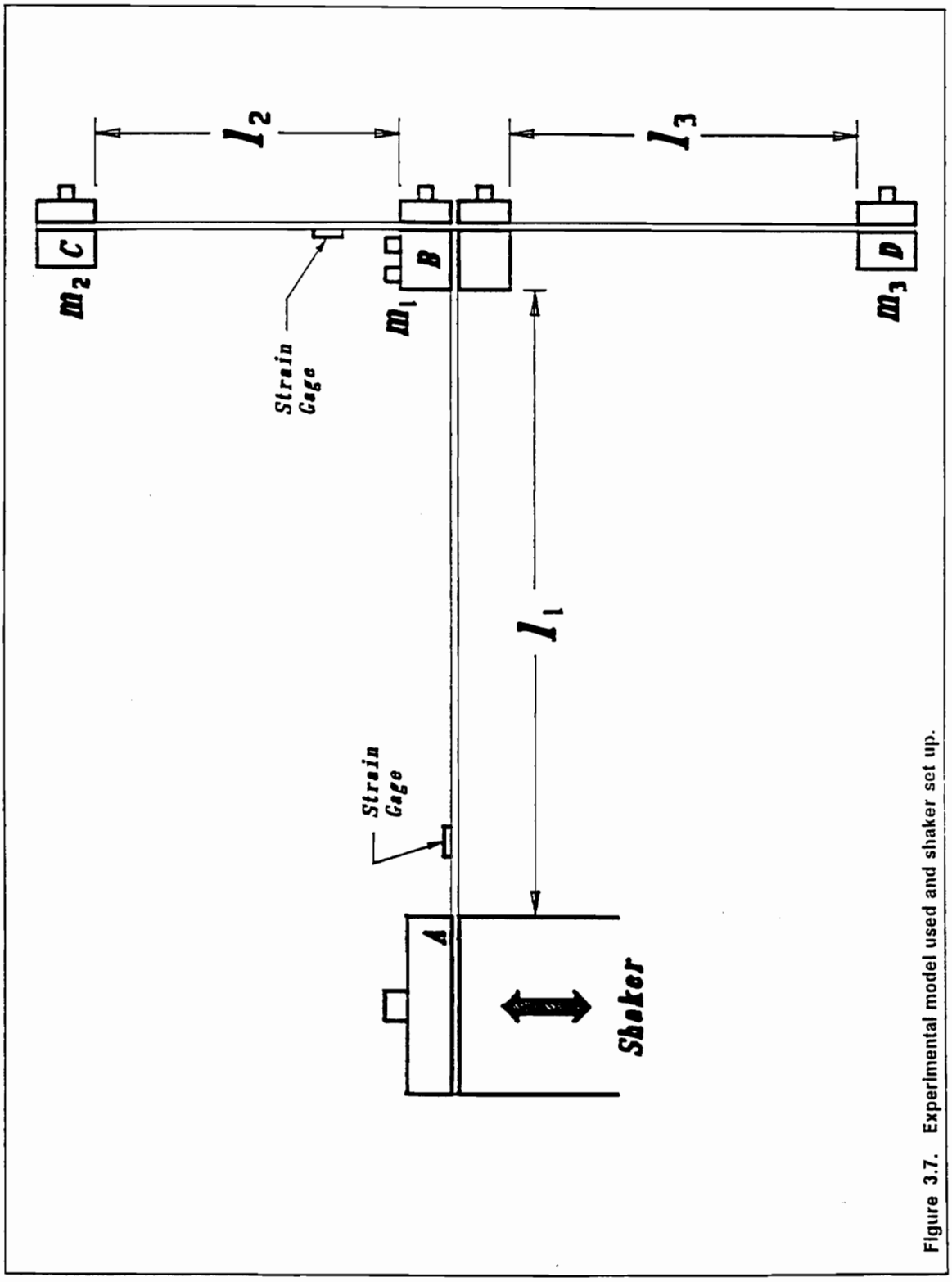

Figure 3.7. Experimental model used and shaker set up.

excitation is small enough, the experimental results do agree with the linear theory.

In this section, we focus on the response when the level of the excitation is large enough to produce nonlinear phenomena in the response. (By "nonlinear phenomena" we mean characteristics or behaviors that can only be predicted by nonlinear equations.) To understand the behavior of the system, we monitor the long-time history and FFT of the strain-gage signal on the horizontal beam, the cross plot of the signals from the vertical and horizontal beams (the so-called pseudo-phase plane), and the Poincaré section of the pseudo-phase plane. The pseudo-phase plane is displayed on a digital oscilloscope and the Poincaré section is generated by inputting the excitation frequency to the digital oscilloscope.

At the beginning of the experiment, the excitation amplitude is set at 58.3 mili-g's and the frequency of the excitation is set at approximately 11.2 Hz. Then, the frequency of the excitation is increased by very small increments, and after each increase the frequency is held constant for a rather long period of time, 40 minutes in some cases. The long-time behavior is recorded and shown in Figure 3.8. Initially, the steady state that develops is in almost perfect agreement with the linear solution: a_1 and a_2 are zero and a_3 is accurately predicted by equation (3.29). The FFT of the strain-gage signal has a single peak at the excitation frequency. Because the displacement of the structure has one frequency, the pseudo-phase plane is a closed curve, which may be a line. Moreover, the Poincaré section consists of one point. The

response continues to closely resemble the linear solution until the frequency of the excitation reaches 12.02 Hz approximately.

At approximately 12.02 Hz, a dramatic change occurs: a_3 begins to decrease (though the frequency of the excitation is still moving toward the third natural frequency) while a_1 and a_2 suddenly increase (i.e., jump up) to very large values. After the jump, the frequency content of the response changes. The FFT of the strain-gage signal exhibits large spikes near the first, second, and third natural frequencies. An example is shown in Figure 3.9 at 12.047 Hz. The last of these spikes is exactly at the frequency of the excitation, and the sum of the frequencies at the first and second spikes is exactly the frequency of the excitation. The lowest and middle frequencies are not commensurable; consequently the response is no longer periodic. A periodic excitation does not produce a long-time periodic response. Such a phenomenon cannot be predicted by linear theory. Because there are only two independent frequencies (Ω and the frequency at either the first peak or the second peak), the response is often described as a two-period quasiperiodic motion. The jump can be easily recognized by the eye without the aid of instrumentation: one can clearly see the increase in amplitude and the decrease in frequency. Because the strain-gage signals consist of two incommensurate frequencies, the pseudo-phase plane does not show a closed curve. Observing it for a short period of time, one sees a tumbling rather than a stationary curve. Moreover, the Poincaré section (Figure 3.10) in this case

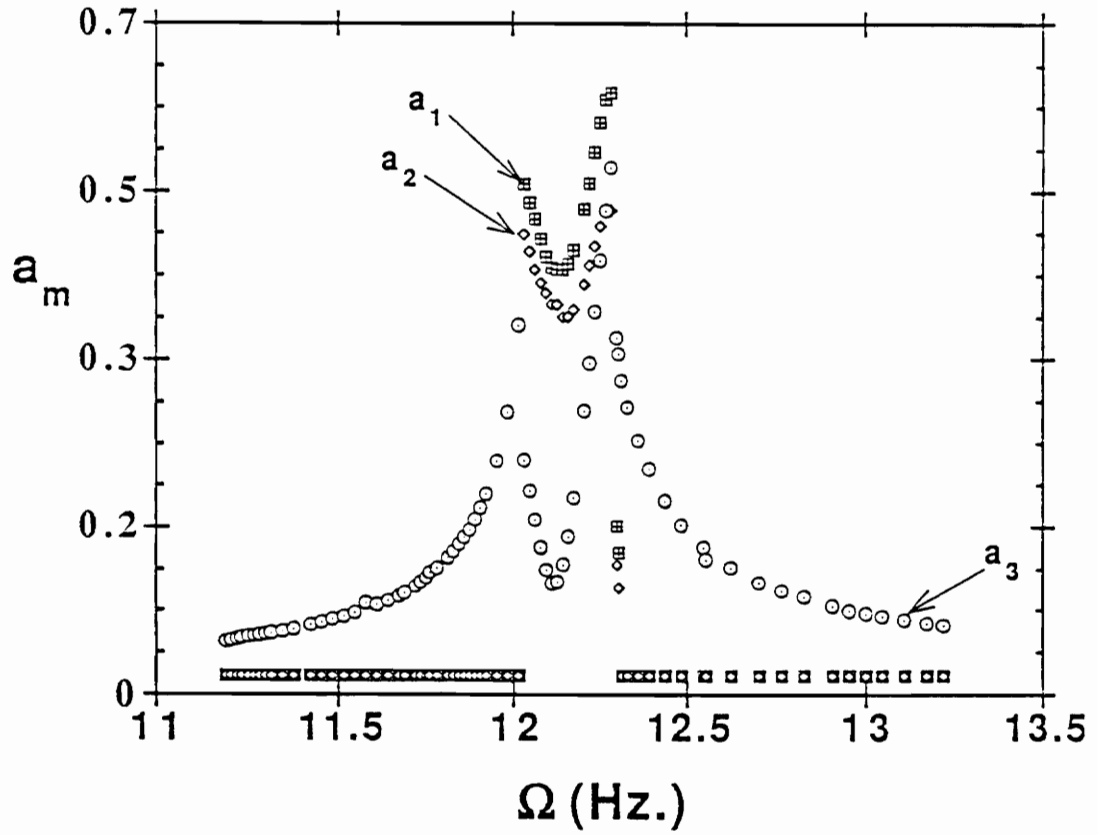

Figure 3.8. Experimentally obtained frequency response curve: frequency is swept up while excitation level is fixed at 350 mill-g's.

is a closed curve rather than a point, confirming the fact that the motion is two-period quasiperiodic.

Further increases in the frequency of the excitation result in decreases in all three modal amplitudes and then increases in all three. The local minima occur when the frequency of the excitation is very near the third natural frequency. It is interesting to see that the smallest amplitudes occur at the frequency for which the linear theory predicts the largest amplitude for a_3. As the frequency of the excitation increases beyond 12.2 Hz, all three amplitudes increase until the frequency reaches 12.3 Hz approximately.

At approximately 12.3 Hz, another dramatic change in the character of the response occurs. The amplitudes of the first and second modes jump down to zero while the amplitude of the third mode jumps down to a value that agrees with the linear theory. This is confirmed by the fact that the FFT consists of a single spike at the excitation frequency, the pseudo-phase plane is a closed curve, and the Poincaré section consists of a single point. Here the transition of the third-mode amplitude from the "nonlinear" value to the "linear" value is not smooth, unlike the transition from the linear to the nonlinear solution that occurred at 12.02 Hz.

For frequencies above 12.3 Hz, the response and the linear theory are in agreement. The behavior of the actual system is in excellent qualitative agreement with the nonlinear theory. There was no attempt to check the quantitative agreement.

By comparing Figure 3.11, which was obtained by sweeping the excitation frequency down, with Figure 3.8 we can see that the steady-state response

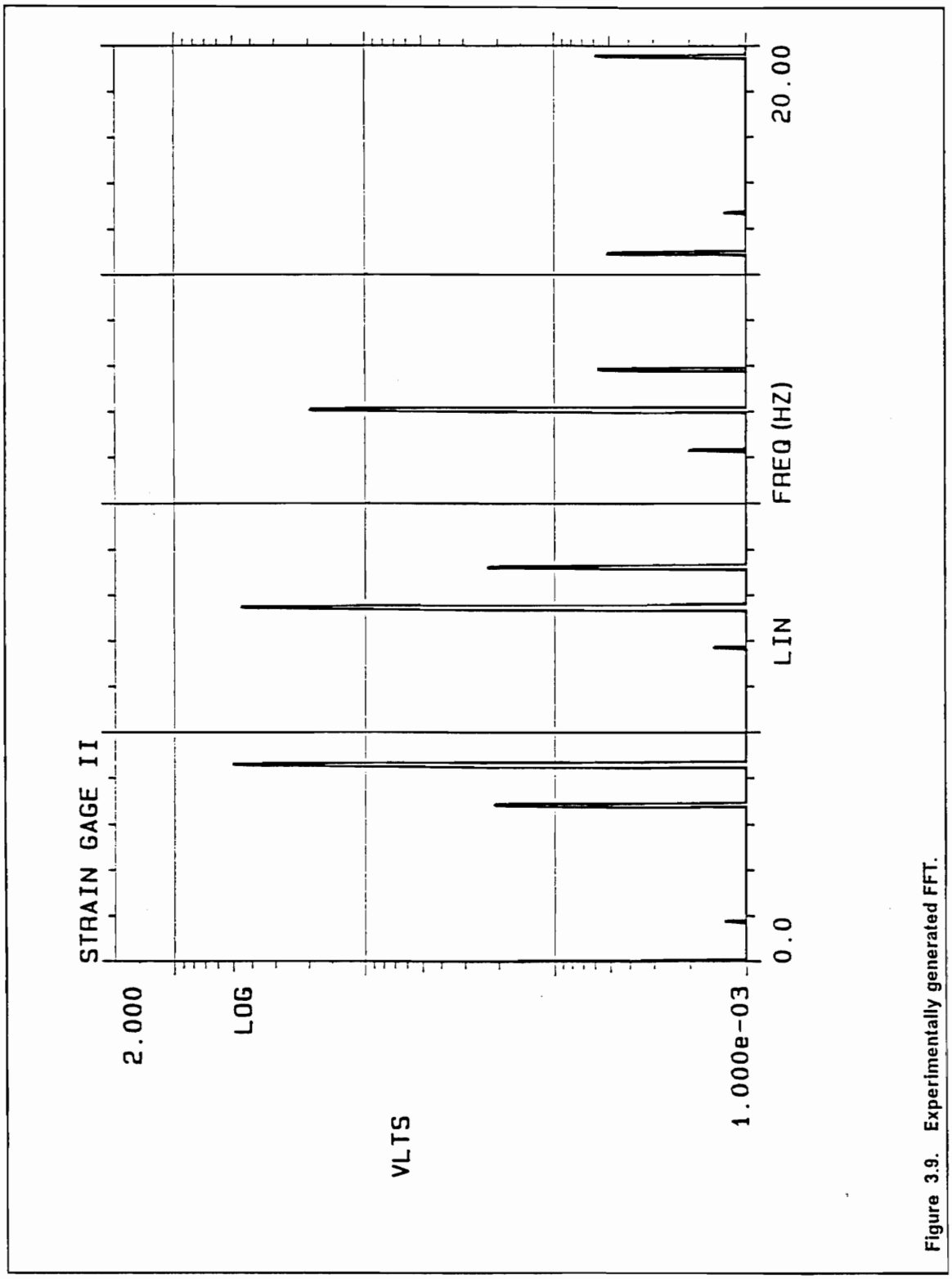

Figure 3.9. Experimentally generated FFT.

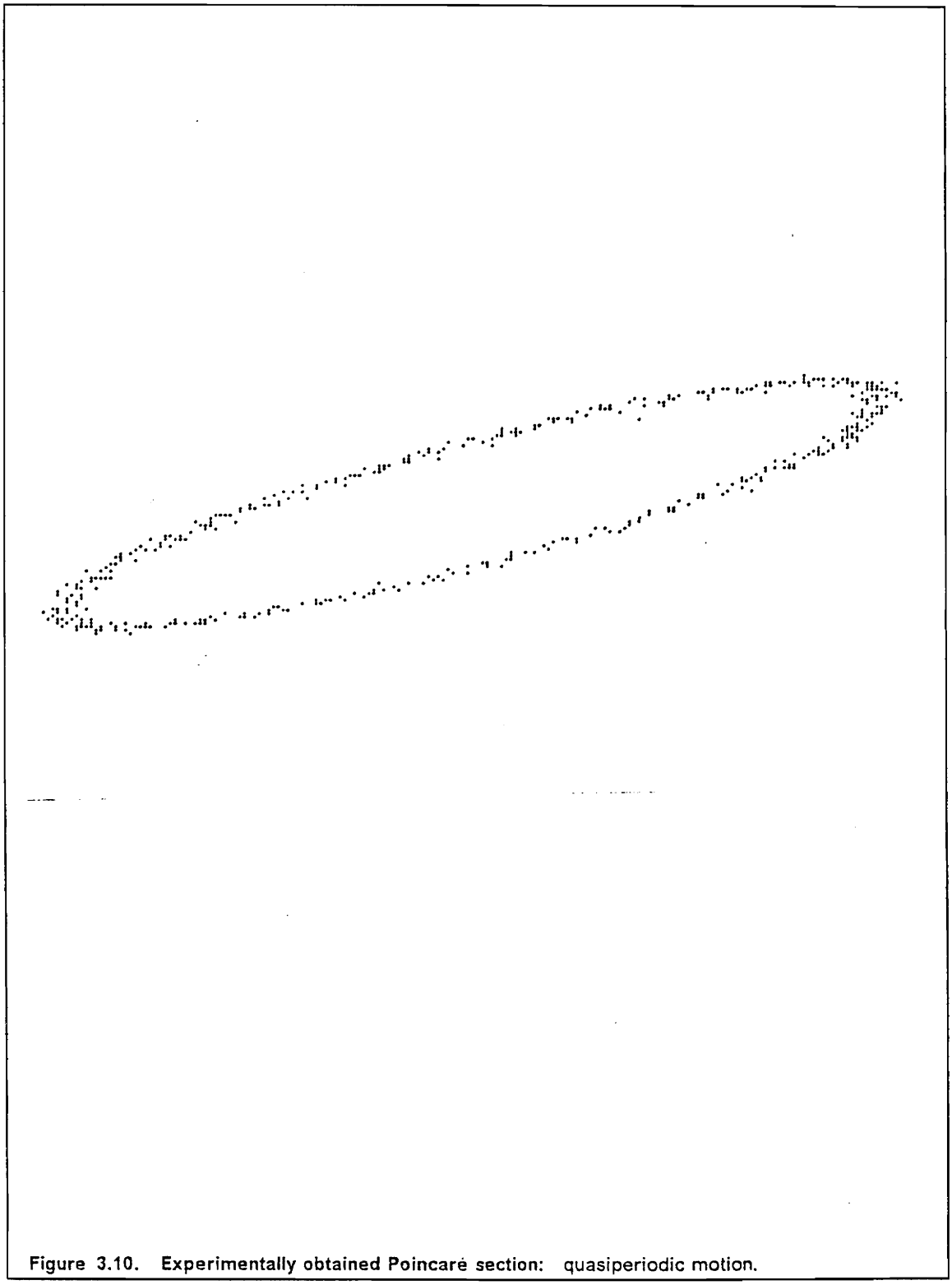

Figure 3.10. Experimentally obtained Poincaré section: quasiperiodic motion.

depends on sweep direction (or equivalently on the initial conditions), a phenomenon that can only be predicted by a nonlinear theory.

3.3.3.2 Amplitude-response curves

Amplitude-response curves (Figures 3.12 and 3.13) were produced by fixing the excitation frequency (in this case at 12.062 Hz) and sweeping the excitation amplitude either up or down. According to linear theory, the response does not depend on the sweep direction, the amplitude of the excited (third) mode is proportional to the excitation amplitude, and the amplitudes of the unexcited (first and second) modes are zero. Again we see an obvious deviation from linear theory. As the excitation amplitude F is swept upwards from zero, a_3 increases linearly with F until a threshold ($F_1 \approx 18$ milli-g's) is reached. Beyond the threshold, a_3 no longer varies linearly with the excitation amplitude but still increases until another threshold ($F_2 \approx 27$ milli-g's) is reached. Beyond this second threshold the response of the excited mode a_3 jumps down and the amplitudes of the other modes a_1 and a_2 jump up from zero. As the excitation amplitude increases, the amplitude of the third mode a_3 remains constant (i.e., saturates). As the excitation amplitude is swept down (Figure 3.13) the amplitude of the excited mode a_3 remains constant until a threshold ($F_3 \approx 17$ milli-g's) is reached. Below F_3 the amplitude of the third mode a_3 increases with decreasing F until F reaches another threshold ($F_4 \approx 11$ milli-g's). Beyond this threshold, a_1 and a_2 jump down to zero and a_3 jumps

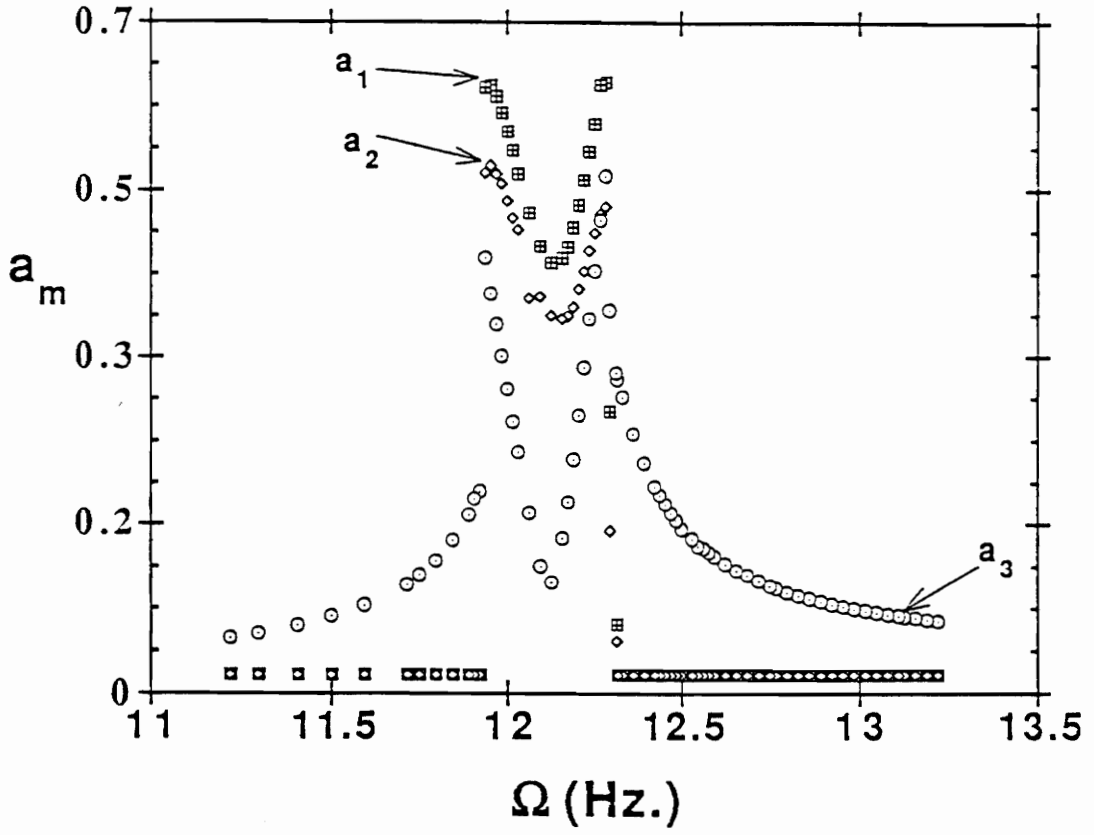

Figure 3.11. Experimentally obtained frequency response curve: frequency is swept down while excitation level is fixed at 350 mill-g's.

down to the linear solution. Furthermore, as the excitation amplitude is further decreased a_3 decreases linearly to zero.

3.4 Limit-Cycle Solutions

In Figure 3.2 we see that as F passes $F = F_3$, the fixed-point solutions undergo a Hopf bifurcation. Thus, when $F > F_3$ the amplitudes and phases become time-varying, and the overall response becomes three-period quasiperiodic.

In Figures 3.14-3.16, we show a typical period-one solution obtained numerically when $F = 0.124$. We use the same shooting method described in Section 2. We searched the region shown in Figure 3.2 and others, but could not find any instabilities of the limit cycle. Hence, the only solution that we could find is the stable period-one solution.

3.5 Conclusions

We study the response of a general three-degree-of-freedom system with the internal resonant condition $\omega_3 \approx \omega_1 + \omega_2$ to a primary resonant excitation of the third mode. The time-averaged-Lagrangian method is used to obtain the equations that govern the amplitude and phases (the modulation equations).

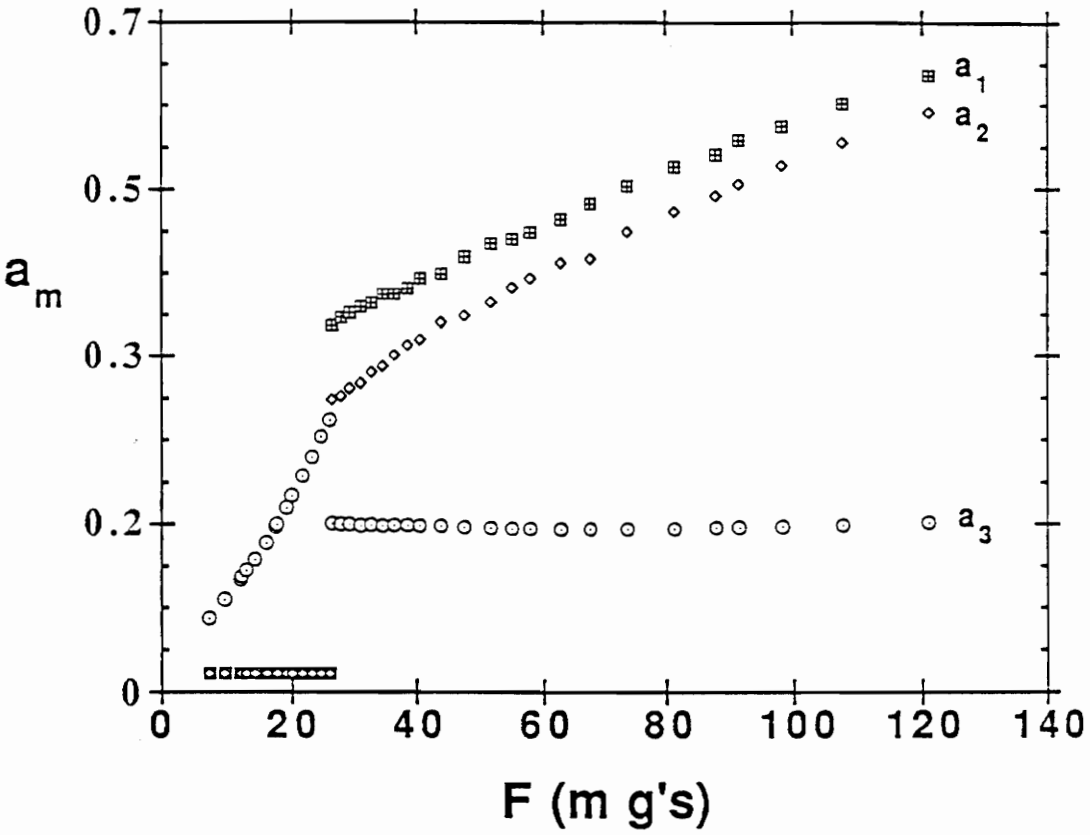

Figure 3.12. Experimentally obtained amplitude-response curve: excitation amplitude is swept up while the excitation frequency is fixed at 12.062 Hz.

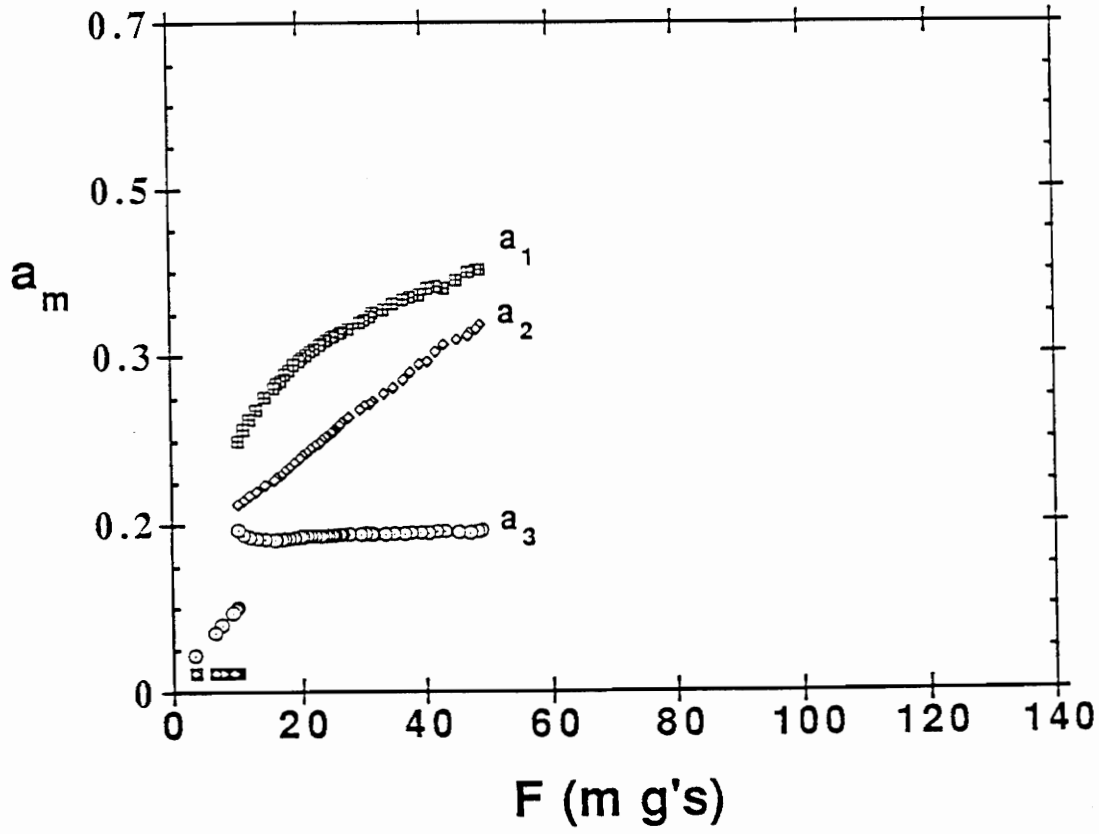

Figure 3.13. Experimentally obtained amplitude-response curve: excitation amplitude is swept down while the excitation frequency is fixed at 12.062 Hz.

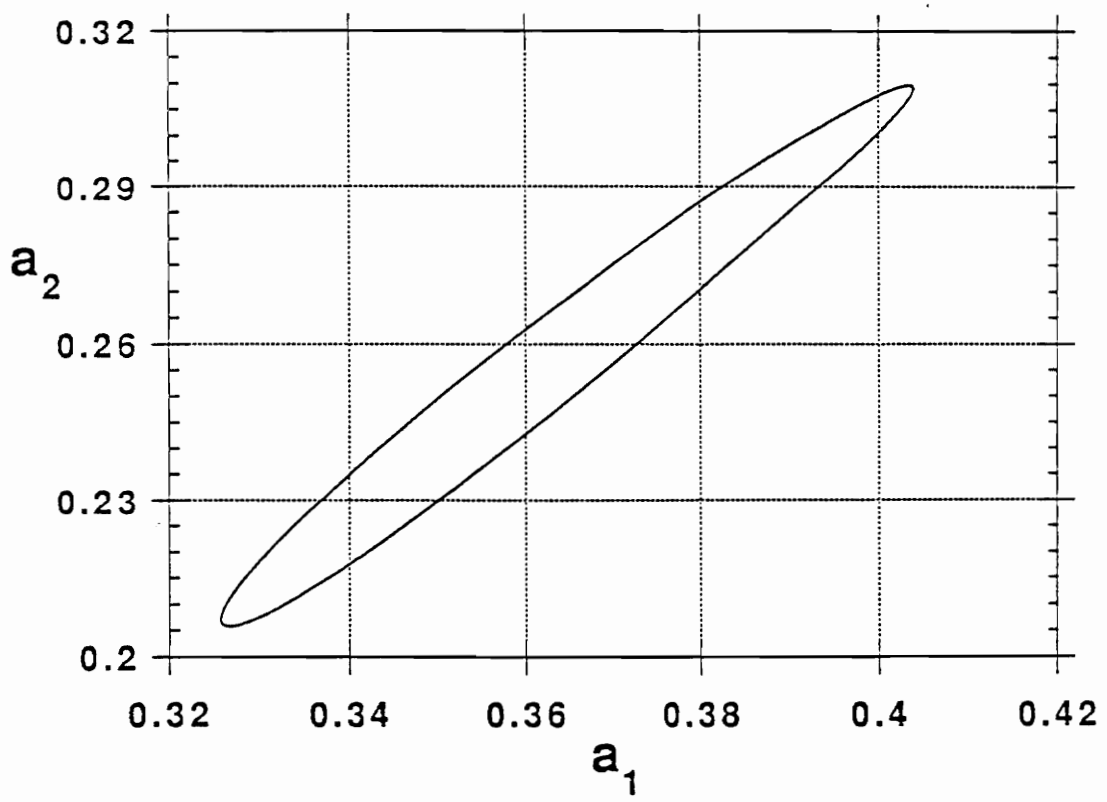

Figure 3.14. A projection of a numerically obtained period-one solution: $F = 0.124$, $\sigma_1 = 0.510$, $\sigma_2 = 0.200$, $\mu_1 = 0.05$, $\mu_2 = 0.1$, and $\mu_3 = 0.05$.

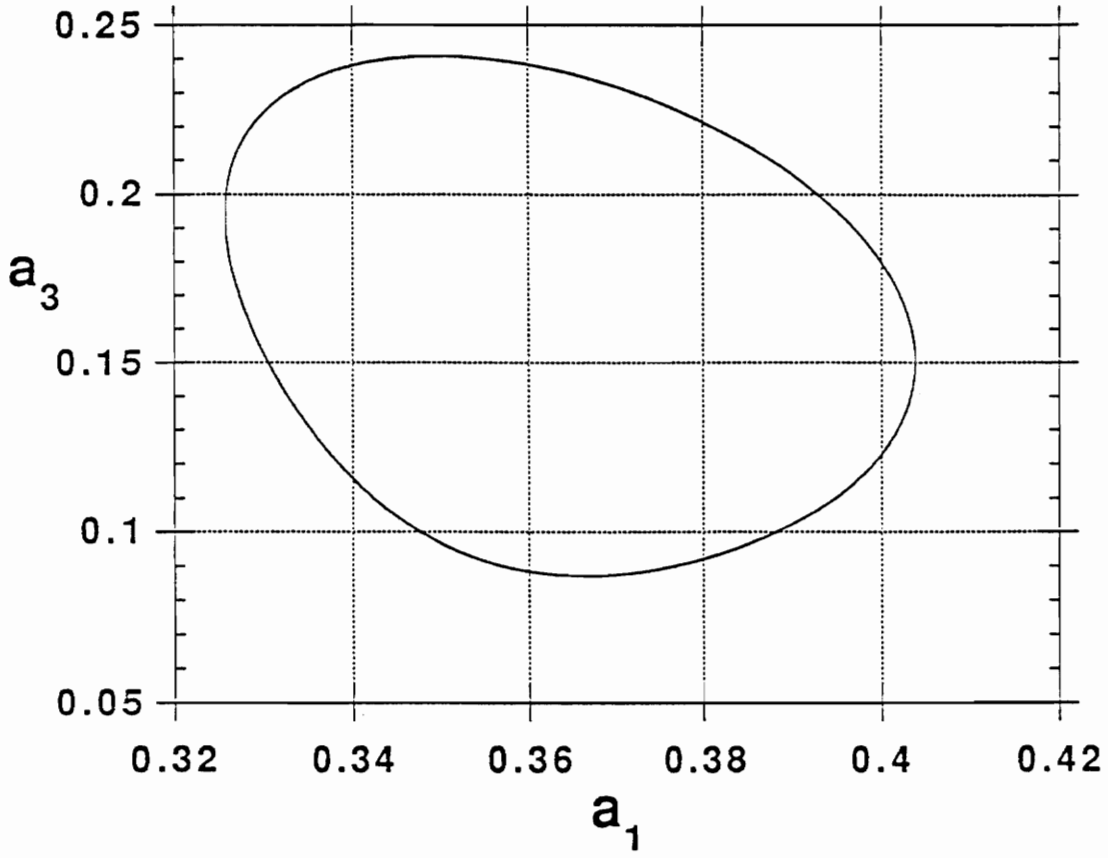

Figure 3.15. A projection of a numerically obtained period-one solution: $F = 0.124$, $\sigma_1 = 0.510$, $\sigma_2 = 0.200$, $\mu_1 = 0.05$, $\mu_2 = 0.1$, and $\mu_3 = 0.05$.

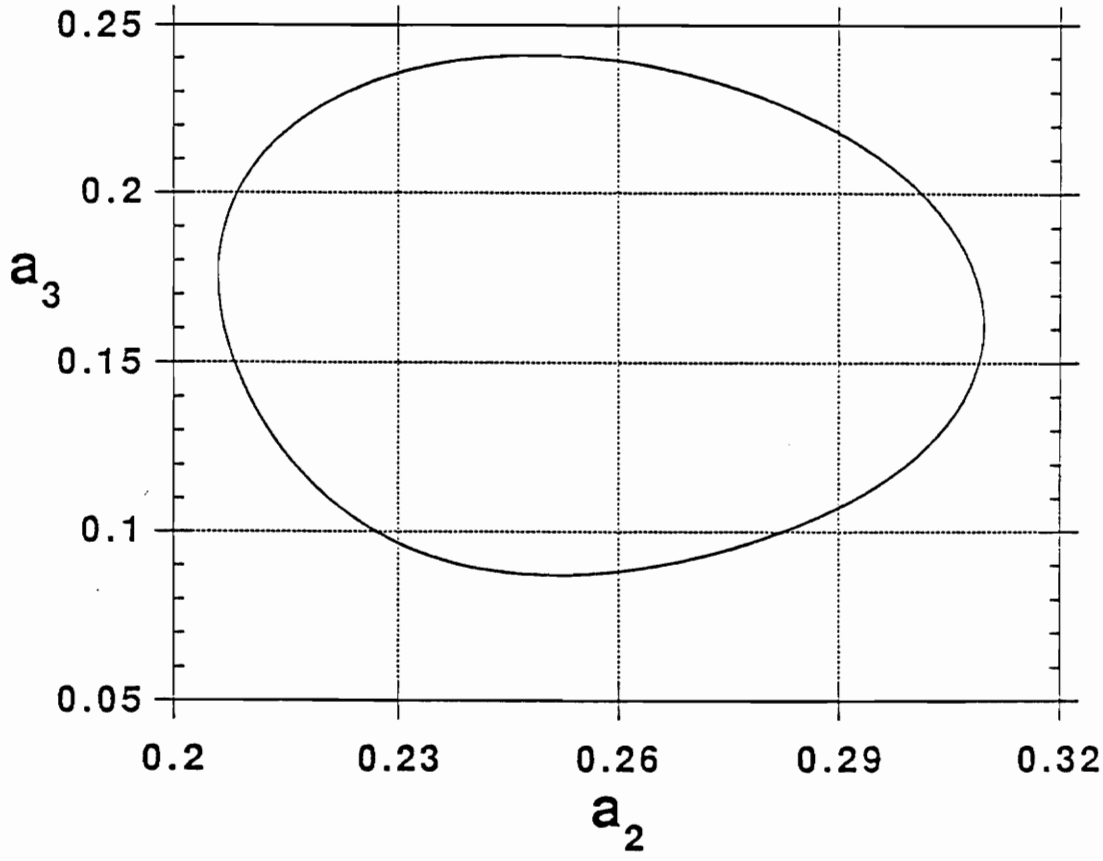

Figure 3.16. A projection of a numerically obtained period-one solution: $F = 0.124$, $\sigma_1 = 0.510$, $\sigma_2 = 0.200$, $\mu_1 = 0.05$, $\mu_2 = 0.1$, and $\mu_3 = 0.05$.

We obtain the fixed points of these equations and study their stability. These fixed points undergo Hopf bifurcations and hence the modulation equations posses limit-cycle solutions. Thus, the system response can be either linear and periodic consisting of the third mode, or nonlinear two-period quasiperiodic consisting of all three modes, or nonlinear three-period quasiperiodic consisting of all three modes. The analytical findings are in qualitative agreement with our experimental results.

CHAPTER 4

Conclusions

4.1 Present Work

We analyze the dynamics of two general three-degree-of-freedom systems with quadratic nonlinearities. The first system has simultaneous two-to-one internal resonances of the type $\omega_3 \approx 2\omega_2$ and $\omega_2 \approx \omega_1$. The second system has a combination internal resonance of the additive type $\omega_3 \approx \omega_1 + \omega_2$. Both systems are subjected to a primary resonant excitation of the third mode (i.e., $\Omega \approx \omega_3$). We investigate the first structure analytically and the second structure both analytically and experimentally.

The method of multiple time scales is used to obtain the equations that govern the amplitudes and phases of the system possessing the simultaneous two-to-one internal resonances (Chapter 2). The fixed points of these

equations are determined and their stability is analyzed. As is typical of nonlinear systems, we find coexistence of multiple fixed-point solutions, and that some of these solutions can undergo Hopf bifurcations. The overall response is found to be periodic (consisting of one, two, or three modes) or amplitude- and phase-modulated (consisting of two or three modes). In the case of three-mode modulated motions the amplitude and phases are found to be periodic, quasiperiodic, or chaotic; thus the resulting overall response can be either periodic or periodically, quasiperiodically, or chaotically modulated.

The time-averaged-Lagrangian method is used to obtain the equations that govern the amplitude and phases of the system possessing the combination internal resonance (Chapter 3). The fixed points of these equations are determined and their stability is analyzed. These fixed points are found to undergo Hopf bifurcations. In this case, the overall response is found to be periodic (consisting of the first mode only), a two-torus (quasiperiodic consisting of all three modes with constant amplitudes and phases), or a three-torus (consisting of all three modes with periodically modulated amplitudes and phases). We are unable to find any regions where the amplitudes and phases are quasiperiodically or chaotically modulated. The fixed points are also obtained experimentally and found to be in good qualitative agreement with the analysis.

4.2 Recommendations for Future Work

The cases in which the first two modes of the systems are excited by a primary resonance (i.e. $\Omega \approx \omega_1$ or $\Omega \approx \omega_2$) need to be studied. Furthermore, cases in which multiple modes are directly excited would most likely lead to interesting if not unusual results.

Cases of simultaneous two-to-one and combination internal resonances need to be explored experimentally. In the case of combination internal resonances, the region between Hopf bifurcation points needs to be analyzed much further. The case of simultaneous two-to-one internal resonances also needs to be explored in detail because it appears to be rich in nonlinear phenomena.

4.3 Closing Remarks

The field of nonlinear dynamics is a relatively unexplored realm. With the advent of new mathematical techniques and high-speed modern computers, a boom in the amount of research in this field has occurred. Yet, there are still many engineers who are unaware of the incredibly fascinating phenomena that exist. In many cases the phenomena are discredited as noise, or as one put it, "a figment of the imagination of mathematicians." Hence, engineers who study nonlinear systems must strive to inform others about their discoveries.

Yet in order to make their discoveries believable engineers need to demonstrate the existence of such complicated nonlinear phenomena through a multitude of experiments.

References

1. Nayfeh, A. H., 'Application of the method of multiple scales to nonlinearly coupled oscillators', in *Lasers, Molecules and Methods,* edited by J. O. Hirschfelder, R. E. Wyatt, and R. D. Coalson, John Wiley and Sons, New York, 1989, 137-196.

2. Nayfeh, A. H. and Balachandran, B., 'Modal interactions in dynamical and structural systems,' *Applied Mechanics Reviews* 42, 1989, 175-201.

3. Froude, W., 'Remarks on Mr. Scott-Russell's paper on rolling', *Transactions of the Institute of Naval Architects* 4, 1863, 232-275.

4. Mettler, E. and Weidenhammer, F., 'Zum problem des kinetischen durchschlangens schwack gekrümmter Stäbe', *Ingenieur Archiv* 31, 1962, 421-432.

5. Sethna, P. R., 'Vibration of dynamical systems with quadratic nonlinearities', *Journal of Applied Mechanics* 32, 1965, 576-582.

6. Haxton, R. S. and Barr, A. D. S., 'The autoparametric vibration absorber', *Journal of Engineering Industry* 94, 1972, 119-125.

7. Nayfeh, A. H., Mook, D. T., and Marshall, L. R., 'Nonlinear coupling of pitch and roll modes in ship motions,' *Journal of Hydronautics* 7, 1973, 145-152.

8. Nayfeh, A. H., **Perturbation Methods,** Wiley-Interscience, New York, 1973.

9. Nayfeh, A. H., **Introduction to Perturbation Techniques,** Wiley-Interscience, New York, 1981.

10. Yamamoto, T. and Yasuda, K., 'On the internal resonance in a nonlinear two-degree-of-freedom system,' *Bulletin of the Japan Society of Mechanical Engineers* 20, 1977, 169-175.

11. Yamamoto, T., Yasuda, K., and Nagasaka, I., 'On the internal resonance in a nonlinear two-degree-of-freedom system (forced vibrations near the higher resonance point when the natural frequencies are in the ratio 1:2)', *Bulletin of the Japan Society of Mechanical Engineers* 20, 1977, 1093-1101.

12. Nayfeh, A. H. and Mook, D. T., **Nonlinear Oscillations** , Wiley-Interscience, New York, 1979.

13. Hatwal, H., Mallik, A. K., and Ghosh, A., 'Nonlinear vibrations of a harmonically excited autoparametric system,' *Journal of Sound and Vibration* 81, 1982, 153-164.

14. Miles, J. W., 'Resonantly forced motion of two quadratically coupled oscillators', *Physica D* 13, 1984, 247-260.

15. Nayfeh, A. H. and Raouf, R. A., 'Nonlinear oscillation of circular cylindrical shells', *International Journal of Solids and Structures* 23, 1987, 1625-1638.

16. Nayfeh, A. H. and Raouf, R. A., 'Nonlinear forced response of infinitely long circular cylindrical shells', *Journal of Applied Mechanics* 54, 1987, 571-577.

17. Nayfeh, A. H., 'On the undesirable roll characteristics of ships in regular seas', *Journal of Ship Research* 20, 1988, 92-100.

18. Hatwal, H., Mallik, A. K., and Ghosh, A., 'Forced nonlinear oscillations of an autoparametric system-part 2: chaotic motions', *Journal of Applied Mechanics* 50, 1983, 663-668.

19. Haddow, A. G., Barr, A. D. S., and Mook, D. T., 'Theoretical and experimental study of modal interaction in a two-degree-of-freedom structure', *Journal of Sound and Vibration* 97, 1984, 451-473.

20. Nayfeh, A. H. and Zavodney, L. D., 'Experimental observation of amplitude- and phase-modulated responses of two internally coupled oscillators to a harmonic excitation', *Journal of Applied Mechanics* 55, 1988, 706-710.

21. Nayfeh, A. H., Balachandran, B., Colbert, M. A., and Nayfeh, M. A., 'An experimental investigation of complicated responses of a two-degree-of-freedom structure', *Journal of Applied Mechanics,* 56, 1989, 960-967.

22. Nayfeh, A.H. and Balachandran, B., 'Experimental investigation of resonantly forced oscillations of a two-degree-of-freedom structure,' *International Journal of Non-Linear Mechanics* 25, 1990, 199-209.

23. Balachandran, B. and Nayfeh, A. H., 'Nonlinear oscillations of a harmonically excited composite structure,' *Composite Structures* 16, 1990, 323-339.

24. Balachandran, B. and Nayfeh, A. H., 'Nonlinear motions of a beam-mass structure,' *Nonlinear Dynamics* 1, 1990, 39-61.

25. Mook, D. T., Marshall, L. R., and Nayfeh, A. H., 'Subharmonic and superharmonic resonances in the pitch and roll modes of ship motions', *Journal of Hydronautics* 8, 1974, 32-40.

26. Mook, D. T., HaQuang, N., and Plaut, R. H., 'The influence of an internal resonance on nonlinear structural vibrations under combination resonance conditions', *Journal of Sound and Vibration* 104, 1983, 229-241.

27. Mook, D. T., Plaut, R. H., and HaQuang, N., 'The influence of an internal resonance on non-linear structural vibrations under subharmonic resonance conditions', *Journal of Sound and Vibration* 102, 1985, 473-492.

28. Balachandran, B. and Nayfeh, A. H., 'Observations of modal interactions in resonantly forced beam-mass structures,' *Nonlinear Dynamics,* 1991, in press.

29. Nayfeh, A. H. and Mook, D T., 'A saturation phenomenon in the forced response of systems with quadratic nonlinearities', *Proceedings of 8th International Conference on Nonlinear Oscillations,* September 11-15, 1978, Prague, Czechoslovakia, pp. 511-516.

30. Ibrahim, R. A. and Barr, A. D. S., 'Autoparametric resonance in a structure containing a liquid, part II: three mode interaction,' *Journal of Sound and Vibration* 42, 1975, 181-200.

31. Ibrahim, R. A., Woodall, T. D., and Heo, H., 'Modal analysis of structural systems involving nonlinear coupling,' *The Shock and Vibration Bulletin* 54, 1984, 19-27.

32. Nayfeh, T. A., Nayfeh, A. H., and Mook, D. T., 'A theoretical-experimental investigation of a three-degree-of-freedom structure,' AIAA Paper No. 90-1081, 1990.

33. Sridhar, S., Mook, D. T., and Nayfeh, A. H., 'Non-linear resonances in the forced responses of plates, part I: symmetric responses of circular plates,' *Journal of Sound and Vibration* 41, 1975, 359-373.

34. Hadian, J. and Nayfeh, A. H., 'Modal interaction in circular plates,' *Journal of Sound and Vibration* 142, 1990, 279-292.

35. Bux, S. L. and Roberts, J. W., 'Non-linear vibratory interactions in systems of coupled beams,' *Journal of Sound and Vibration* 104, 1986, 497-520.

36. Ashworth, R. P. and Barr, A. D. S., 'The resonances of structures with quadratic inertial non-linearity under direct and parametric harmonic excitation,' *Journal of Sound and Vibration* 118, 1987, 47-68.

37. Cartmell, M. P. and Roberts, J. W., 'Simultaneous combination resonances in an autoparametrically resonant system,' *Journal of Sound and Vibration* 123, 1988, 81-101.

38. Ibrahim, G. M., *The Response of Three-Degree-of-Freedom Systems With Quadratic Nonlinearities to a Harmonic Excitation*. Master's thesis, Jordan University of Science and Technology, December 1986.

39. Tadjbakhsh, I. G. and Wang Y., 'Wind-driven nonlinear oscillations of cables,' *Nonlinear Dynamics* 1, 1990. 265-291.

40. Aprille, T. J. and Trick, T. N. 'A computer algorithm to determine the steady-state response of nonlinear oscillators,' *IEEE Transactions on Circuit Theory* CT-19, 1972, 354-360.

41. Parker, T. S. and Chua, L. O. 'Chaos: a tutorial for engineers,' *Proceedings of the IEEE* 75, 1987, 983-1008.

42. Berge', P., Pomeau, Y. and Vidal C., *Order Within Chaos---Towards a Deterministic Approach to Turbulence*, John Wiley and Sons, New York, 1984.

Vita

The author was born in San Bernardino, California on April 4, 1968. He earned the Bachelor of Science degree in Engineering Science and Mechanics at Virginia Polytechnic Institute and State University (Virginia Tech) in 1989. He continued his education at Virginia Tech and earned his Masters degree in Engineering Mechanics in 1991. He will continue his education at the University of Illinois at Urbana-Champaign where he will work towards dual doctorates, one in Mechanical Engineering and the other in Medicine.